Biophysical and Biochemical Characterization of Therapeutical Relevant Membrane Systems

Inaugural-Dissertation

For the attainment of the title of doctor
in the Faculty of Mathematics and Natural Sciences at the
Heinrich-Heine-University Düsseldorf

presented by

Lora Denson
from Neuss, Germany

Düsseldorf, April 2025

From the Institute of Physical Biology at the Heinrich-Heine University, Düsseldorf

Published by permission of the Faculty of Mathematics and Natural Sciences at Heinrich- Heine-University Düsseldorf

Supervisor:

1. Dr. Manuel Etzkorn, Institute for Physical Biology, Heinrich-Heine-University Düsseldorf
2. Prof. Dr. Alexej Kedrov, Synthetic Membrane Systems, Heinrich-Heine-University Düsseldorf

Date of the oral examination: 17th of July 2025

Declaration

I declare under oath that I have compiled this dissertation independently and without any undue assistance by third parties under consideration of the "Fundamental principles for safeguarding good scientific practice at Heinrich-Heine-Universität Düsseldorf". Furthermore, neither this dissertation, nor a similar work, has been submitted to another faculty. I have not made any unsuccessful attempt to obtain a doctorate.

Düsseldorf 22nd of April 2025

Lora Denson

Acknowledgements

First, I would like to express my gratitude to Dr. Manuel Etzkorn for his continuous support and encouragement throughout the past years. I am grateful for the opportunity to be part of his research group.

I would also like to thank Prof. Dr. Alexej Kedrov for kindly taking on the role as second supervisor.

Thanks to Dr. Aldino Viegas for the collaboration project and for giving me the opportunity to visit his laboratory in Lisbon.

I would also like to thank Prof. Dr. Reza Ahmadian for providing the facilities necessary to carry out my cell culture experiments.

I would like to thank all my colleagues and friends at the IPB for their support, and countless moments of motivation throughout my time at the institute. Their presence made the work environment not only productive, but also enjoyable. While I cannot name everyone individually, I would like to especially acknowledge Thomas, Najoua, Bianca, Katharina, and Tina—not only for being great colleagues, but also for the friendships we shared along the way. I truly appreciate the support from Hamed, Fatima, and Ci, who passed on their knowledge to me. I would also like to thank Jessica, Justin and Chris for creating a nice work atmosphere in our group.

A special thank you to our technical staff—Robin, Andrea, and Joana—for their work in keeping the laboratory running smoothly. I am particularly grateful to Joana, whose consistently positive attitude and kindness brightened many of my days.

Lastly, I want to take this opportunity to thank my family for their support.

Table of Contents

List of Tables ..... *- 7 -*

List of Figures *8*

Abbreviations *9*

Summary *11*

Zusammenfassung *12*

1. Introduction *13*

1.1. Membrane Proteins **13**

1.2. G-Protein Coupled Receptor's **14**

1.3. Membrane Mimetics **16**

1.4. Melanocortin System **17**

1.5. Melanocortin Receptors **18**

1.6. Melanocortin Receptor Accessory Proteins (MRAPs) **19**

1.7. Human Norepinephrine Transporter (hNET) **22**

1.8. Challenges of Membrane Protein Expression **24**

1.9. Recombinant Protein Production in Bavulovirus Expression System **24**

2. Aim of this Thesis *27*

3. Material and Methods *28*

3.1. Devices **28**

3.2. Chemicals **29**

3.3 Consumable Material **31**

3.4. Bacterial strains **32**

3.5. Plasmids **32**

3.6. Protein- and DNA standards **33**

3.7. Buffer and solutions **33**

3.8. Metal solution for MRAP *E. coli* Expression **35**

3.9 Methods of Molecular Biology **37**

3.9.1 PCR Polymerase Chain Reaction 37

3.9.2. Agarose gel electrophoresis 38

3.9.3 Transformation of plasmids into chemical competent cells 38

3.9.4 Isolation of plasmid DNA from *E. coli* 38

3.9.5 Sequencing of isolated plasmids 39

3.9.6 Cloning MRAP mutants and MRAPs for *Sf*9 cells. 39

3.9.7 *E. coli* Expression MRAPs 40

3.9.8 MRAP Purification 40

3.9.9 MS1D1 Expression 41

3.9.10 Bacmid isolation 41

3.9.11 Polymerase Chain Reaction (PCR) 42

3.9.12 Baculovirus preparation 43

3.10 Methods of Protein-Biochemistry **44**

3.10.1 Sodium dodecyl-sulfate polyacrylamide gel electrophoresis (SDS-PAGE) 44

3.10.2 Western blot 44
3.10.3 Cell lysis 45
3.10.4 Immobilized metal ion affinity chromatography (IMAC) 45
3.10.5 Affinity chromatography with Strep-tag 46
3.10.6. Ion Exchange Chromatography (IEX) 46
3.10.7 Electronic absorption spectroscopy (EAS) 47
3.10.8 Nanodiscs preparation 47
3.10.9 Size Exclusion Chromatography (SEC) 47
3.10.10 Mass Spectrometry (MS) 48
3.10.11 Bio-Layer Interferometry (BLI) 48
3.10.12 Microfluidic diffusional sizing (MDS) 49

4. Results 50

***4.1.* Recombinant Protein Expression and Purification of MRAPs in *E. coli* 50**

4.2. Optimization of Protein Purification 52

4.3. Metal binding of *E. coli* MRAP and MS Determination 55

4.4. Cloning, Expression and Purification of MRAP Mutants 58

4.5. Recombinant Protein Production of MRAP in *Sf*9 cells 62

4.6. Protein Purification of MRAP2 by Strep-tag 64

4.7. Recombinant Protein Production of hNET in *Sf*9 cells 68

4.8. Nanodiscs – as a platform to study molecular interactions 72

5. Conclusion and Outlook 75

6. Supporting Material 77

7. References 82

List of Tables

Table 1: Overview of GPCR classes. 15
Table 2: List of devices used in this thesis. 28
Table 3: List of chemicals used in this thesis. 29
Table 4: List of consumable material used in this thesis. 31
Table 5: List of the bacterial strains used in this thesis. 32
Table 6: List of plasmids used in this thesis. 32
Table 7: List of Protein- and DNA standards used in this thesis. 33
Table 8: List of buffers and solutions used in this thesis. 33
Table 9: List of buffers and solutions used for MRAP expression. 34
Table 10: List of buffers and solutions used for MSP1D1 expression. 34
Table 11: SBMX stock solution for 500 ml (25x) 35
Table 12: $FeCl_2$ stock solution for 100 ml. 35
Table 13: ,,S'' stock solution for 100 ml. 35
Table 14: ,,TE'' stock solution for 500 ml. 35
Table 15: Vitamin stock solution for 1L. 36
Table 16: Components for 1L M9 Medium. 36
Table 17: Composition of PCR master mix. 37
Table 18: Cycling program. 37
Table 19: Composition of PCR master mix. 39
Table 20: Cycling program for PCR. 39
Table 21: Composition of PCR master mix. 42
Table 22: Cycling program for PCR. 42
Table 23: Primer sequences. 42
Table 24: Transfection conditions. 43
Table 25: Components of a 15 % TRIS-Glycine gel. 44

List of Figures

Figure 1: Overview of different membrane proteins. 13
Figure 2: Timeline of GPCR research. 14
Figure 3: Molecular mechanism of GPCR activation. 15
Figure 4: Nanodiscs Reconstitution. 17
Figure 5: Overview of melanocortin peptides. 18
Figure 6: MC4R and MRAP2 signaling. 20
Figure 7: Schematic representation of MRAP1. 21
Figure 8: Structure of hNET. 22
Figure 9: Workflow of protein production in Baculovirus Expression System. ..25
Figure 10: Expression and Purification of all MRAPs. 51
Figure 11: Detection of MRAP2 by gel electrophoresis and immuned-based detection. 52
Figure 12: Evaluating the protein purity of MRAP2 after IEX chromatography. 53
Figure 13: SEC profile of MRAPs. 54
Figure 14:Electronic absorption spectrum of MRAPs. 56
Figure 15: Results of Mass Spectrometry (MS) measurements. 57
Figure 16: Monitoring E. coli cell growth during MRAP protein expression. 59
Figure 17: Purification of mutant variants of MRAP1/2. 60
Figure 18: Characterization of MRAP electronic absorption spectrum. 61
Figure 19: Design of constructs of MRAP2 for Sf9 insect cells. 62
Figure 20: Microscope images of Sf9 cells during baculovirus infection. 63
Figure 21: Detection of MRAP2 in Sf9 cells. 64
Figure 22: Solubilization of MRAP2. 65
Figure 23: Analysis of MRAP2 from Sf9 cells. 66
Figure 24: Characterization of MRAP2 from Sf9 cells. 66
Figure 25: Bacmid preparation of hNET. 68
Figure 26: Detection of hNET. 69
Figure 27: Structure of hNET. 70
Figure 28: Nanodiscs preparation. 72
Figure 29: Results of nanodiscs DNAzyme interaction study. 73
Figure 30: IC1 inhibits lipid binding of GPX4. 74
Figure 31: Vector map of pFASTBac1. 77
Figure 32: Vector map of pFHMSP-LIC-N. 77
Figure 33: Predicted metal-binding site. 78
Figure 34: DNA Sequence of MRAP2 for Sf9 cell expression. 79
Figure 35: DNA Sequence of MRAP2_C132A_H133A. 80
Figure 36: DNA Sequence of MRAP1_H97A. 81

Abbreviations

2YT	2x Yeast Extract and Tryptone
AcMNPV	Autographa californica multiple-capsid nuclear polyhedrosis virus
ACTH	Adrenocorticotrophin
AGRP	Agouti related protein
APS	Ammoniumperoxidsulfate
Beta 2AR	Human beta 2-adrenergic receptor
BLI	Bio-Layer Interferometry
Bp	Base pairs
BSA	Bovine serum albumin
BVE	Baculovirus Expression System
cAMP	Cyclic adenosine monophosphate
CNS	Central nervous system
CV	Column volumes
DNA	Desoxyribonucleic acid
DMPC	Dimyristoylphosphatidylcholine
DMPG	Dimyristoylphosphatidylglycerol
DTT	Dithiothreitol
EAS	Electronic absorption spectroscopy
EDTA	Ethylenediaminetetraacetic acid
E. coli	Escherichia coli
GDP	Guanosine diphosphate
GHSR1 a	Ghrelin receptor growth hormone secretagogue receptor 1a
GTP	Guanosine triphosphate
GPCR	G-protein-coupled receptors
GPI	Glycosyl-phosphatidylinositol
GuHCl	Guanidinium-Hydrogen chloride
HEPES	4-(2-Hydroxyethyl)-1-piperazin-ethansulfonsäure
His-tag	Histidine tag
hNET	Human Norepinephrine Transporter
IEX	Ion exchange chromatography
IMP	Integral membrane protein
IMAC	Immobilized metal affinity chromatography
IPTG	Isopropyl-beta-D-thiogalactopyranosid
IP3	Inositol 1,4,5-trisphosphate
IFN-ß	Interferon beta

Kb	Kilo basepairs
kDa	Kilo dalton
mAU	Mili absorbance
MWCO	Molecular weight cut off
MT	Mutant
MP	Membrane Protein
MRAP	Melanocortin Receptor Accessory Protein
NE/NA	Norepinephrine/Noradrenaline
MDS	Microfluidic Diffusional Sizing
MSH	Melanocyte stimulating hormones
MSP	Membrane scaffold protein
MCXR	Melanocortin Receptor
OD_{600}	Optical density at 600 nm
PAGE	Polyacrylamide gel electrophoresis
PBS	Phosphate-buffered saline
PCR	Polymerase chain reaction
pI	Isoelectric point
PKC	Protein kinase C
PKR	Prokineticin receptors
PTM	Posttranslational modification
POMC	Pro-peptide proopiomelanocortin
POPG	1-palmitoyl-2-oleoyl-sn-glycero-3-phospho-rac-(1-glycerol)
PMP	Peripheral membrane protein
PVN	Paraventricular nucleus
Rpm	Revolutions per minute
RIPA	Radioimmunoprecipitation Assay
SEC	Size exclusion chromatography
Sf	Spodoptera frugiperda
SDS	Sodium dodecyl sulfate
SUMO	Small ubiquitin-related modifier
TCEP	Tris-(2-carboxyethyl)-phosphine
TEMED	Tetramethylethylendiamine
TEV	Tobacco etch virus
TMD	Transmembrane domain
TRIS	Tris(hydroxymethyl-)aminomethane
T7	Bacteriophage T7
ε	Molar extinction coefficient (M-1 cm-1)

Summary

Membrane proteins (MPs) are one of the most vital components of the cell in living organisms. Thus, well-characterized preparations of purified membrane systems are important for a deeper understanding of MPs, as it allows for detailed studies of their structure and function. One of the largest class of MPs are G-protein-coupled receptors (GPCRs), which include members of the melanocortin system - a network of five receptors, ligands, and two accessory proteins (MRAP1, MRAP2). A dysfunction of the receptors or the accessory proteins can lead to various metabolic diseases. Beyond its physiological and pharmacological significance, the melanocortin system serves as an ideal model for studying membrane proteins and their interactions.

The first part of this thesis focuses on the recombinant expression of MRAP in *E. coli* and the optimization of the protein purification. MRAP plasmids were transformed into the *E. coli* expression strain, purified via affinity chromatography, and analyzed by mass spectrometry (MS). Metal-binding was further assessed by cloning MRAP mutants with alterations in the predicted metal-binding site. Additionally, the MRAPs were expressed and purified from *Sf*9 cells using the Baculovirus Expression System (BVE). The second part of the project involves the recombinant protein production of the human norepinephrine transporter (hNET) in *Sf*9 cells, in collaboration with Dr. Aldino Viegas. hNET plays a key role in norepinephrine recycling, and its dysregulation is associated with cardiovascular diseases. As a final part, membrane binding is investigated. Nanodiscs, serving as membrane mimetics, were purified via size exclusion chromatography (SEC) and subsequently used to study their interactions with DNAzymes through Microfluidic Diffusional Sizing (MDS). Additionally, the potential inhibition of glutathione peroxidase 4 (GPX4) membrane binding by an inhibitory compound (IC1) is studied using Biolayer Interferometry (BLI).

This work presents the recombinant expression of MRAP2 in two systems and a characterization of the metal-binding properties using different biophysical methods. While this study confirms metal-binding characteristics in the MRAP mutant sample, the dedicated mutagenesis and mass spectrometry data, suggests that the metal-binding characteristics are caused by impurities in the sample. Overall, these findings offer valuable insights into components of the melanocortin system and therapeutical relevant membrane systems, contributing to the field of membrane protein research.

Zusammenfassung

Membranproteine (MP) sind eine der wichtigsten Komponenten der Zelle in lebenden Organismen. Daher sind gut charakterisierte Präparate von gereinigten Membransystemen wichtig für ein besseres Verständnis der MP, da sie detaillierte Studien ihrer Struktur und Funktion ermöglichen. Eine der größten Klassen von MPs sind G-Protein-gekoppelte Rezeptoren (GPCRs), zu denen Mitglieder des Melanocortin Systems gehören - ein Netzwerk aus fünf Rezeptoren, Liganden und zwei akzessorischen Proteinen (MRAP1, MRAP2). Eine Funktionsstörung der Rezeptoren oder der akzessorischen Proteine kann zu verschiedenen Stoffwechselkrankheiten führen. Über seine physiologische und pharmakologische Bedeutung hinaus ist das Melanocortin System ein ideales Modell für die Untersuchung von Membranproteinen und deren Wechselwirkungen.

Der erste Teil dieser Arbeit befasst sich mit der rekombinanten Expression von MRAP in *E. coli* und der Optimierung der Proteinreinigung. MRAP-Plasmide wurden in den *E. coli*-Expressionsstamm transformiert, durch Affinitätschromatographie gereinigt und mittels Massenspektrometrie (MS) analysiert. Die Metallbindung wurde ferner durch Klonierung von MRAP-Mutanten mit Veränderungen an der vorhergesagten Metallbindungsstelle untersucht. Außerdem wurden die MRAPs mit Hilfe des Baculovirus-Expressionssystems (BVE) aus *Sf*9-Zellen exprimiert und gereinigt. Der zweite Teil des Projekts umfasst die rekombinante Proteinproduktion des menschlichen Noradrenalin-Transporters (hNET) in *Sf*9-Zellen in Zusammenarbeit mit Dr. Aldino Viegas. hNET spielt eine Schlüsselrolle beim Noradrenalin-Recycling, und seine Dysregulation wird mit kardiovaskulären Erkrankungen in Verbindung gebracht. In einem letzten Teil wird die Membranbindung untersucht. Nanodiscs, die als Membranmimetika dienen, wurden durch Größenausschlusschromatographie (SEC) gereinigt und anschließend zur Untersuchung ihrer Wechselwirkungen mit DNazymen durch mikrofluidische Diffusionsmessung (MDS) verwendet. Darüber hinaus wird die potenzielle Hemmung der Membranbindung von Glutathionperoxidase 4 (GPX4) durch einen Inhibitor (IC1) mit Hilfe der Biolayer-Interferometrie (BLI) untersucht.

In dieser Arbeit wird die rekombinante Expression von MRAP2 in zwei Systemen und eine Charakterisierung der Metallbindungseigenschaften mit verschiedenen biophysikalischen Methoden vorgestellt. Während diese Studie die Metallbindungseigenschaften in der MRAP-Mutantenprobe bestätigt, deuten die speziellen Mutagenese- und Massenspektrometriedaten darauf hin, dass die Metallbindungseigenschaften durch Verunreinigungen in der Probe verursacht werden. Insgesamt bieten diese Ergebnisse wertvolle Einblicke in Komponenten des Melanocortin Systems und therapeutisch relevante Membransysteme und leisten einen Beitrag zur Erforschung von Membranproteinen.

1. Introduction

1.1. Membrane Proteins

Membrane proteins (MPs) are essential components of the cell membrane and take part in a variety of processes in the cell, such as cell communication, chemical transport and signal transduction.[1] They represent 30 % of the human proteome.[1,2] MPs are responsible for the transport of molecules across the bilayer and are among the most common targets for therapeutic drugs.[3,4]

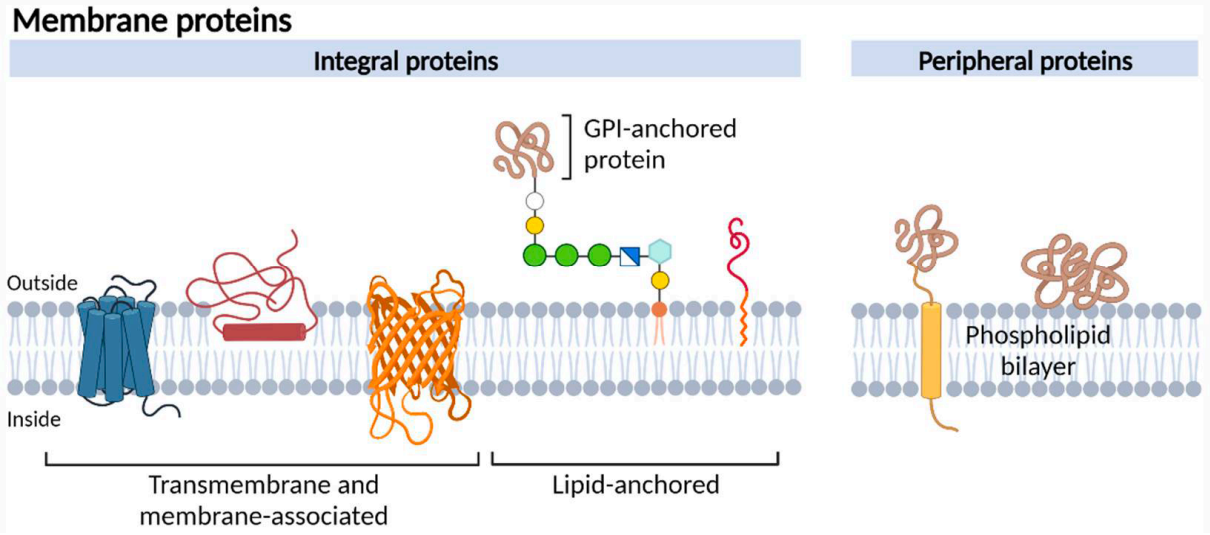

Figure 1: Overview of different membrane proteins. Figure taken by Jong and Kocer et al., 2023. [5]

MPs can be divided into two main classes: peripheral membrane proteins (PMPs) and integral membrane proteins (IMPs).[6] PMPs are associated with the cell membrane surface via non-covalent interactions like electrostatic and hydrophobic interactions.[3] Moreover, they can directly interact with the membrane through a covalent linkage such as glycosyl-phosphatidylinositol (GPI).[2,6] The association of peripheral membrane proteins (PMPs) with the cell membrane can be reversible, whereas integral membrane proteins (IMPs) are permanently embedded within the membrane.[6] IMPs are amphipathic proteins and consist of single or multiple membrane-spanning domains (transmembrane domains).[3,6] Transmembrane domains (TMs) are composed of hydrophobic stretches of nonpolar amino acids. As a result, an increase in the number of TMs generally enhances the overall hydrophobic character of a membrane protein.[2] One of the most extensively studied proteins of IMPs are the G protein-coupled receptors (GPCR). A timeline of key GPCR research milestones is shown in Figure 2.

1.2. G-Protein Coupled Receptor's

G protein-coupled receptors (GPCR) belong to the largest integral membrane protein family and are involved in a wide range of physiological processes such as signal transduction, immune response and neurotransmission.[7,8] More than 800 genes belong to the GPCR family.[9] Their most important role is to transduce extracellular signals and the regulation of intracellular second messengers through coupling to heterotrimeric G-proteins.[10] GPCR's are highly dynamic structures. Their function depends on their ability to go through different conformational changes.[11] They exist in different conformational state, depending on the absence or presence of an agonist (ligand). The receptor remains in its inactive state when no ligand is bound, with the G-protein tightly associated with the receptor. Upon ligand binding to the extracellular binding site, the receptor undergoes a conformational change, transitioning into its active state. This conformational change allows the G-protein to bind more effectively to the intracellular loops, which leads to the exchange of GDP for GTP on the Gα subunit, activating the G-protein and initiating downstream signaling cascades.[12]

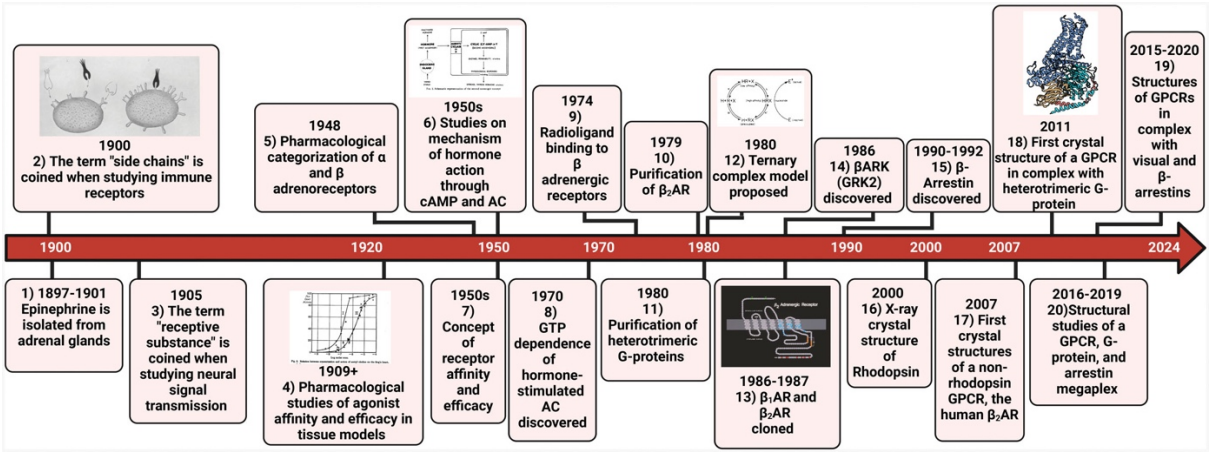

Figure 2: Timeline of GPCR research. This timeline outlines key milestones in GPCR research, starting with the purification of epinephrine, a ligand of β-adrenergic receptors, which belong to the GPCR family. The first crystal structure of a GPCR (human ß2-AR) was solved by Rosebaum et al. in 2007. Taken from Liu et al., 2024. [13]

The ability of GPCRs to transmit a signal across the cell membrane is depending on the receptor's ability to change shape.[11] If an extracellular ligand (e.g., hormones, chemokines) binds to the extracellular site of the GPCR, the receptor undergoes conformational changes that facilitate the binding of G-proteins and other signaling proteins to its intracellular surface (Figure 3).[11] G-Proteins are the largest family of GPCR signaling transducers and consist of a complex of Gα, Gβ, and Gγ subunits.[13]

When the receptor is activated, guanosine diphosphate (GDP) is released for guanosine triphosphate (GTP). The Gα-GTP subunit is then released from the complex and the units can now interact with a wide range of effectors to regulate second messenger.[13] The process of activation and inactivation of a GPCR is depicted in Figure 3.

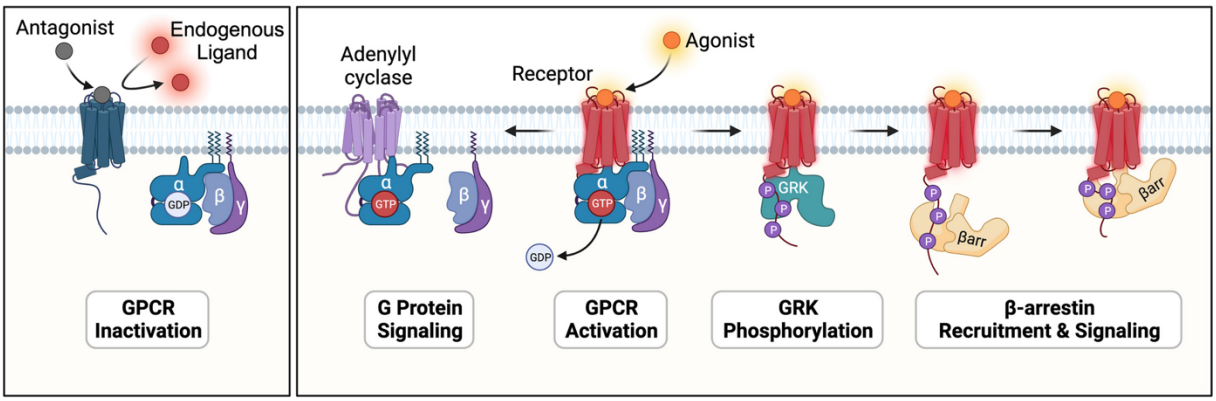

Figure 3: Molecular mechanism of GPCR activation. When an agonist binds to the receptor pocket, heterotrimeric G-proteins (Gα, Gβ, and Gγ) are recruited. The Gα-GTP subunit dissociates from the Gβγ transducer, and both signal to diverse downstream effectors. GRKs (GPCR kinases) phosphorylate the intracellular domains of the GPCR, which promote tight binding of β-arrestin. Taken from Cheng et al., 2023. [14]

GPCR's can be divided in to 6 different classes of receptors: Class A (rhodopsin-like receptors), Class B (the secretin family), Class C (metabotropic glutamate receptors), Class D (fungal mating pheromone receptors), Class E (cyclic adenosine monophosphate (cAMP) receptors), and Class F (Frizzled and Smoothened receptors).[7] Class A GPCR's can be further divided into "rhodopsin GPCRs" and "nonrhodopsin GPCRs".[7] An overview of the function of the different GPCR classes are listed in the table 1.

Table 1: Overview of GPCR classes.

GPCR class	Biological function
Class A	Transduction of extracellular signals through interaction with G-protein
Class B	Activation of adenyl cyclase and phosphatidyl-inositol-calcium pathway
Class C	Involved in cognitive functions and pain perception
Class D	Involved in response to mating factors
Class E	Regulation of expression of developmentally-regulated genes
Class F	Part of developing processes (e.g., cell proliferation)

The receptor structure is highly conserved across different types of GPCR. All GPCR's have seven transmembrane domains (7TM) connected by three extracellular loops and three intracellular loops.[7,9] The extracellular loops and the N-terminus, which contain the ligand-binding site, are crucial for ligand recognition, while the intracellular loops and the C-terminal are involved in interacting with G proteins, arrestins, and GPCR kinases.[7]

GPCR's are also involved in many diseases and are therefore of high interest for the pharmacological industry as 40% of the available drugs target them.[8,15] The melanocortin system, composed of five GPCR receptor's, is a promising therapeutic target for treating various metabolic disorders such as obesity.[16] As mentioned above, GPCR's are integral membrane proteins, therefore they need their natural environment for functioning. To extract them from the cell membrane, detergents are needed for instance.[7] Therefore, to gain more insights to GPCRs and furthermore for the development of drug target, it is important to obtain the structure of the receptors.[11] Especially activation and receptor dynamics are still not fully understood.[17]

1.3. Membrane Mimetics

To understand the biological function of MP, it is important to study the membrane-protein complex. However, overexpression and purification of the proteins and finally obtain these complexes is a challenge.[18] Most MP lose their activity or are denatured when they are removed from the native cell membrane.[19] A suitable tool for studying membrane proteins in a close to native environment are membrane mimetics such as nano discs. Nano discs are disc-shaped, nanoscale (7-17nm), phospholipid bilayers surrounded by two molecules of an amphipathic alpha-helical protein called membrane scaffold protein (MSP), which is a truncated version of Apolipoprotein-10.[20] The great advantage of nanodiscs is, that the assembled protein-nanodiscs complex does not contain detergent, making them a suitable tool for creating a native-like environment for the membrane proteins. [21]

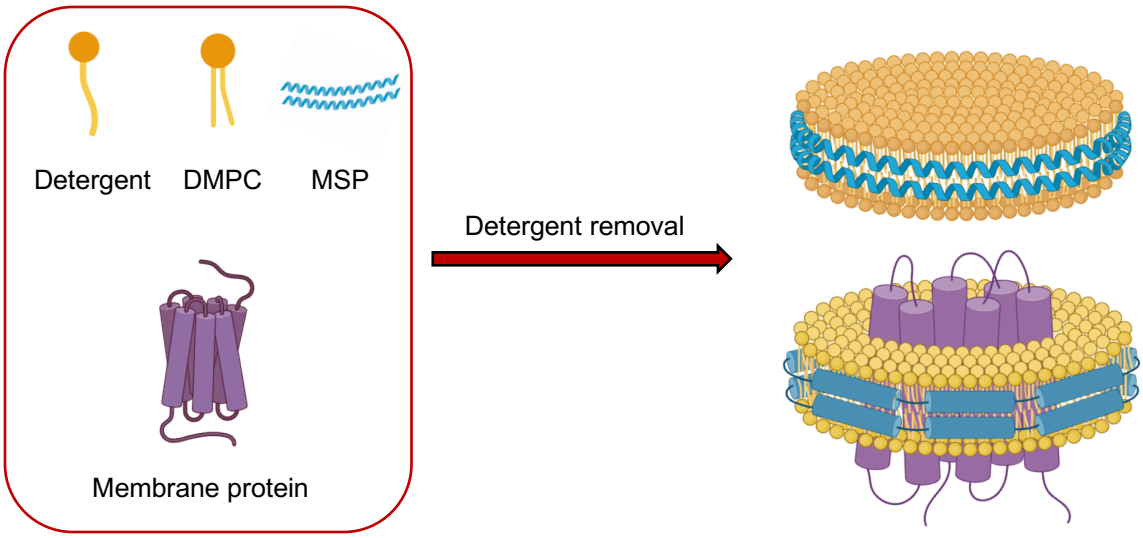

Figure 4: Nanodiscs Reconstitution. The nanodisc is composed of two alpha helical molecules of membrane scaffold protein (MSP, blue), phospholipids (yellow) and the embedded membrane protein (MP, purple). Figure created with *BioRender.*

Nano discs have the ability to self-assemble. This is caused on one hand because of the strong tendency of phospholipids to form bilayers and on the other hand on the stability of the amphipathic helix structure of the MSP.[19] They provide a stable tool compared to other membrane mimetics, due to the strong interaction of the scaffold protein and the phospholipids.[19] Nanodiscs are assembled from a detergent solubilized mixture of MSP, phospholipids by removing the detergent through adsorption with hydrophobic beads or by dialysis.[20,22,23] The length of MSP determines the diameter of the resulting nanodiscs.[19]

1.4. Melanocortin System

The melanocortin system is one of the best studied network of endocrine and neuropeptide signaling pathways.[24] It is involved in various physiological processes such as melanogenesis, pigmentation and energy homeostasis.[25,26] It consists of melanocortin peptides, five Melanocortin Receptors (MC1R-MC5R) endogenous antagonists and two receptor accessory proteins, MRAP1 and MRAP2.[24,27] The endogenous antagonists are one of the unique components of the melanocortin system.[28]

The melanocortin peptides derive from the pro-peptide proopiomelanocortin (POMC) through proteolysis (Fig. 5).[27,29] POMC is converted into the melanocyte stimulating hormones, α-MSH, β-MSH and γ-MSH, and adrenocorticotrophin (ACTH).[24,29] The

melanocortin agonist peptides mediate their function through interaction with the melanocortin receptors (MCRs).[27]

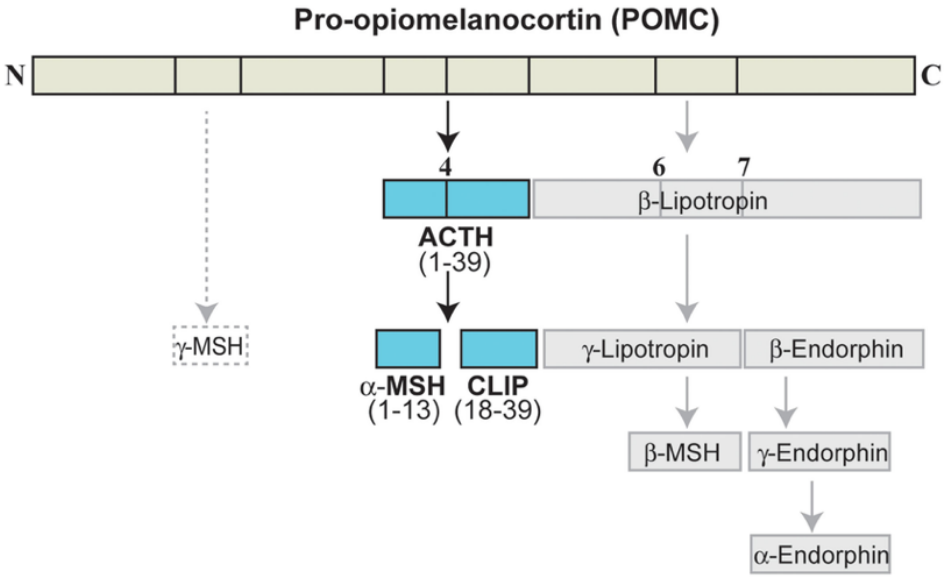

Figure 5: Overview of melanocortin peptides. ACTH, adrenocorticotropic hormone; CLIP, corticotropin-like intermediate lobe peptide; MSH, melanocyte-stimulating Hormone. Figure taken from Ross et al., 2013. [30]

1.5. Melanocortin Receptors

Following the cloning of the first melanocortin receptor in 1992 by Wikberg et al. and Mountjoy et al., our understanding of the melanocortin system's function has advanced significantly.[29] Cloning of the Melanocortin Receptors (MCRs) have provided the framework for understanding their function and their respective agonists/antagonist, which is the basis for the development of drug targets.[31] Today, the melanocortin system is one of the best described and studied physiological system. Since the MCR family contributes to a wide range of physiological function, it is also involved in several disease processes and therefore of high interest for therapeutic drugs.[32]

The MCRs are G-protein-coupled receptors (GPCRs) with seven transmembrane segments.[25] There are several structural features, which are conserved in GPCRs.[26] Like other G-protein-coupled receptors, they generate cAMP through a stimulatory G protein (G_s) and adenylate cyclase.[31] This then activates protein kinase C (PKC) and leads to an influx of extracellular Ca^{2+} and inositol 1,4,5-trisphosphate (IP3) is activated, which activates the MAPK and JAK-STAT pathway. [33]

Five subtypes of the receptors have been identified including, MC1R, MC2R, MC3R, MC4R and MC5R.[25,27] MC1R receptor is expressed in different cytotypes (e.g., melanocytes) and is involved in melanogenesis by activating the enzyme tyrosinase. The receptor's function is mediated through the melanocortins ACTH and alpha-MSH.[25] The function of MC2R is also mediated by ACTH and is found in the adrenal cortex and adipocytes, where it plays a role in steroid synthesis.[25] MC3R is expressed in several tissue e.g., in the gut, heart and in central nervous system (CNS). MC4R is expressed mainly in the CNS and regulates food intake and is overall involved in energy homeostasis. Lastly, MC5R, can be found in several tissues and contributes to immunomodulation of B/T lymphocyte and the control of exocrine glandular secretion. The melanocortin system has a unique feature, the paracrine signaling molecules agouti and agouti-related protein (AgRP). They act as endogenous antagonist for 3 MCRs. [24,28,31] Agouti was first described as an antagonist for MC1R and AgRP is a natural inverse agonist for MC4R.[24] Generally, an inverse agonist reduces the activity of the receptor it binds to, producing the opposite effect of an agonist.[34]

The MCRs have different affinities for their respective melanocortin peptides and their endogenous antagonists, agouti and AgRP.[31] While MC1R shows equal affinity for α-MSH and ACTH, MC2R binds only ACTH.[33] MC3R binds all melanocortins equally and MC4R has similar affinity to ACTH, α-MSH, and β-MSH, while MC5R has a higher affinity to α-MSH, a lower affinity to ACTH and no affinity to γ-MSH.[33]

1.6. Melanocortin Receptor Accessory Proteins (MRAPs)

Melanocortin Receptor Accessory Proteins (MRAPS) are small single transmembrane proteins, that are important for receptor trafficking, signaling and ligand specificity.[35,36] The MRAP family is composed of two members, MRAP1 and MRAP2.[36] MRAP1 forms a complex with MC2R (ACTH receptor) and is essential for surface expression and signaling of the receptor in the adrenal gland.[35,37,38] Mutations in MRAP1 result in a loss of function of MC2R.[35] MRAP1 is important for binding of ACTH to the receptor.[35,37] MRAP2 and MC2R can form a complex, but the affinity of ACTH for this receptor is lower.[37] ACTH signaling is essential for glucocorticoid synthesis, and as a result, a mutation in MRAP1 is associated with familial glucocorticoid deficiency type-2. [39] MRAP2 is expressed in several tissues including the brain and is involved in the regulation of energy homeostasis.[40] MRAP2 is primarily expressed in the paraventricular nucleus (PVN) of the hypothalamus, a key region involved in the

regulation of food intake.[41,42] In the PVN, MRAP2 is co-expressed with MC4R.[41] It was shown, that MRAP2 is essential for MC4R trafficking, since mutations in MRAP2 lead to increase in food intake and obesity in MRAP2 knockout mice.[35,40,43]

MRAP2 targets other receptors like prokineticin receptors (PKRs) and regulates their activity. It acts like an endogenous inhibitory protein of PKR2.[41] PKR2 is important for regulation of food intake as well as energy.[44,45] Moreover, MRAP2 is involved in ghrelin signaling through the ghrelin receptor growth hormone secretagogue receptor 1a (GHSR1a).[41] Additionally, MRAP2, regulates energy homeostasis through melanin-concentrating hormone receptor 1 (MCHR1).[41] MRAP2 can also form higher-order oligomers.[42]

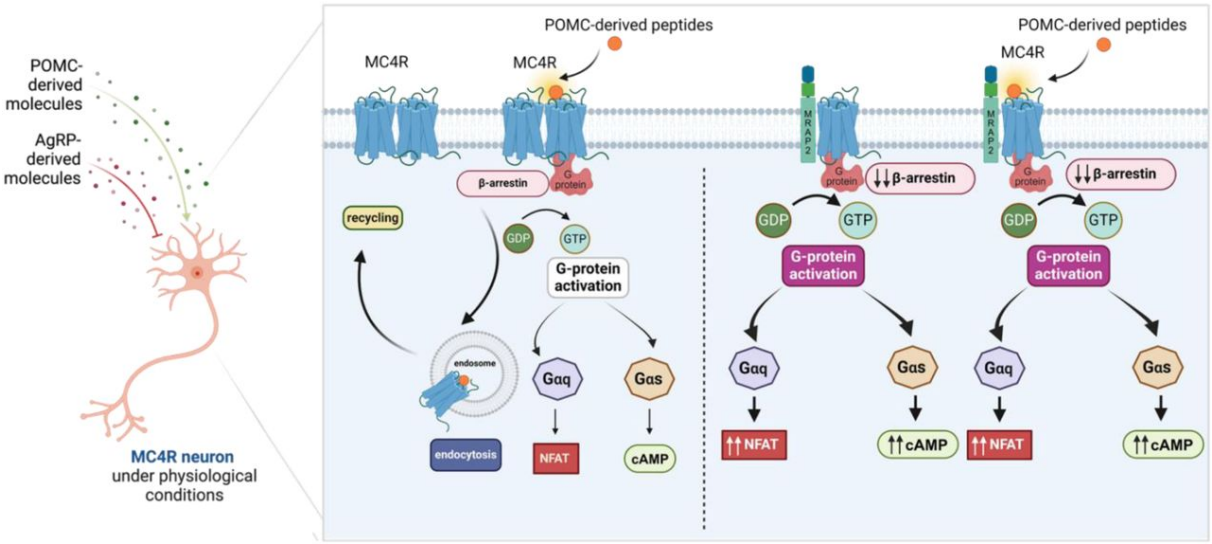

Figure 6: MC4R and MRAP2 signaling. Like all GPCRs, MC4R is a 7 TM protein embedded in the membrane and carries out its effect by coupling to a G-protein. MC4R is activated by α-MSH (alpha-melanocyte-stimulating hormone, POMC-derived peptides) and further modulated by AgRP-derived peptides, which act as inverse agonists.[34] α-MSH binds to MC4R, which activates a downstream signaling pathways through G-proteins (Gαs and Gαq). This leads to elevated cAMP levels. MRAP2 is important for cell surface expression, stability and enhances MC4R activity. Figure taken from Sohail et al., 2024.[46]

The most interesting feature of the MRAPs is their dual topology, depicted in Figure 7. Both proteins can form an antiparallel homodimer in the cell membrane, with N_{in}/C_{out} and N_{out}/C_{in} orientations.[35] It has been shown, that the orientation of the proteins is fixed in the membrane. The unusual structure of the MRAPS was studied by Sebag and Hinkle et al., 2007 where the group inserted biotin ligase acceptor peptides at the *N*- or C-terminal ends of MRAP.[37] Subsequently, they carried out the expression of the modified proteins in mammalian cells with cytoplasmic or endoplasmic reticulum-targeted biotin ligase. The data demonstrates the dual topology of MRAPs and shows that both proteins maintain a fixed orientation throughout receptor trafficking. The

MRAPs contain a single glycosylation site in the N-terminus. Experiments have shown, that half of MRAP undergoes glycosylation at the single predicted site for *N*-linked glycosylation.[37] This glycosylation is also important for MRAPs antiparallel insertion into the membrane.[39]

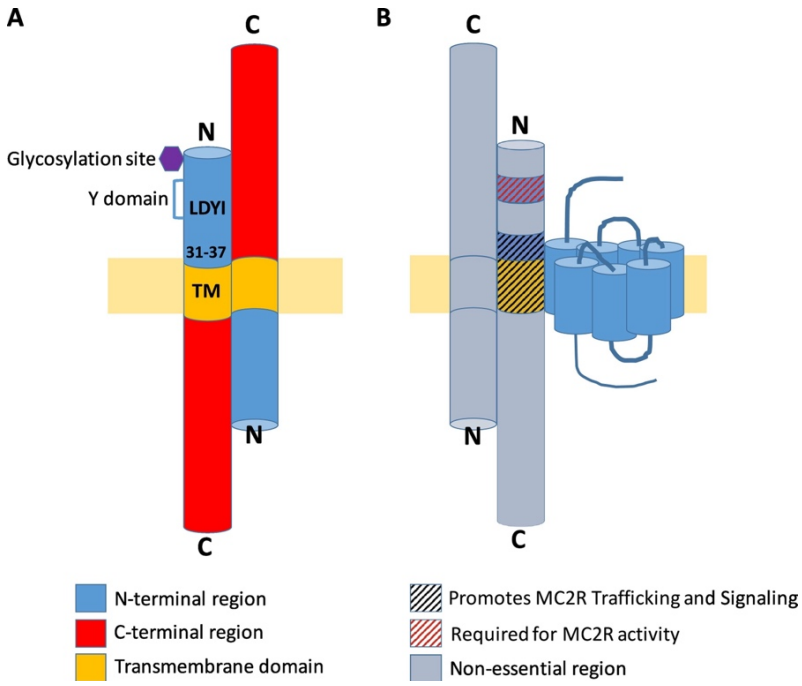

Figure 7: Schematic representation of MRAP1. (**A) MRAP1 as antiparallel homodimer. (B) Schematic function of MRAP1.** Taken from Rouault et al., 2017. [35]

While the sequence features, that are important for MRAP2 membrane orientation are unknown, MRAP1 contains a short polybasic segment, 31–37 sequence (LKANKHS), adjacent to the transmembrane domain in the N-terminal domain.[35,39,42] It was shown that the amino acids 31- 37 (LKANKHS) are essential for the orientation of MRAP1 in the cell membrane and mutation lead to N_{out}/C_{in} orientation of MRAP1.[35] Furthermore, amino acids 18-21 (LDYI) are important for MRAP1-mediated MC2R receptor trafficking. The amino acids 18-21 (LDYI) of the transmembrane (TM) domain is not required for the orientation of MRAP1 in the membrane, but it was shown that alteration in the TM amino acid sequence lower MC2R function. Moreover, The N-terminal and transmembrane regions of MRAP1 are well conserved, while the C-terminal region is extremely variable. Additionally, the C-terminus of MRAP1 is not required for the dual topology of MRAP1, since truncation does not affect the topology or function of the protein.

Interestingly, MRAP2 contains the polybasic segment, but unlike MRAP1, it does not affect the insertion of the protein into the membrane.[42] Another structural difference

to MRAP1 is that, the LDYI motif is missing in MRAP2, resulting in MRAP2 being able of MC2R receptor trafficking but not signaling.

1.7. Human Norepinephrine Transporter (hNET)

The human Norepinephrine Transporter (hNET) gene (SLC6A2) was isolated and cloned in 1991 by Pacholczyk et al.[47] Since then, extensive research has been carried out on the transporter, as the protein serves as an important drug target. The human Norepinephrine Transporter (hNET) is responsible for the recycling of norepinephrine/noradrenaline (NE/NA) in the synaptic cleft.[48,49] A dysfunction of the transporter, leads to elevated NE levels and is linked to cardiovascular diseases like high blood pressure.[48] hNET is responsible for the sodium-dependend reuptake of extracellular norepinephrine (80 % - 90 % of all transmitted NE). NE (main neurotransmitter) stimulates the activity of the cardiovascular system. High levels of norepinephrine (NE) can result in elevated blood pressure, and dysfunction of the norepinephrine transporter (NET) is associated with neuropsychiatric and cardiovascular diseases.

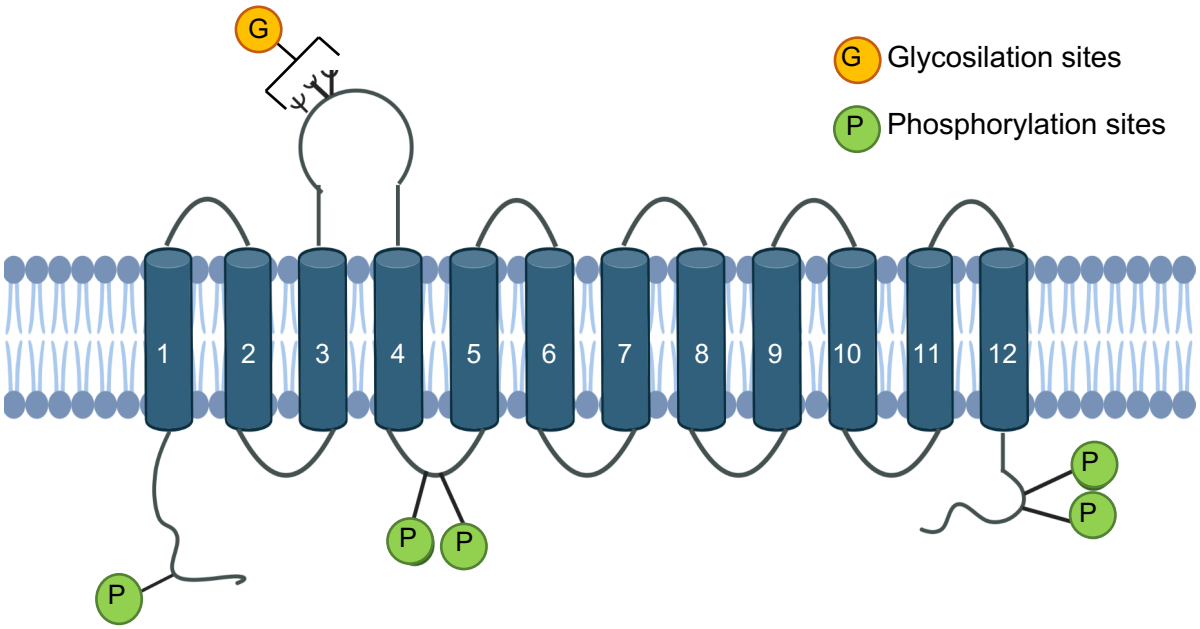

Figure 8: Structure of hNET. The figure shows all 12 TM domains of hNET embedded in the phospholipid bilayer. Figure created with *BioRender.*

hNET is a 12-transmembrane protein with different glycosylation and phosphorylation sites (Figure 8).[50] These sites for PTM are conserved among different species, which suggest an essential role for the modification sites.[51,52] hNET is synthesized as a

glycoprotein and undergoes post translational N-glycosylation between TMD3 and TMD4 in the second extracellular loop EL2.[53,54] Sequence analysis of the isolated hNET cDNA predicted a 69 kDa protein with three N-glycosylation sites, N184, N192, N198, which are important for surface trafficking, hNET stability and transport activity, but do not affect ligand recognition.[51,53,55,56] The role of N-glycosylation was assessed in different cell lines transfected with the hNET cDNA. Site-directed mutagenesis was utilized to mutate the three n-glycosylation sites of the transporter in HeLa cells. Changes in protein expression, protein stability, surface expression and ligand recognition of the hNET-mutant and hNET-wild-type were compared.[51,56] Results showed that catecholamine uptake was reduced, but ligand recognition was not affected. Furthermore, the hNET-mutant expressed an isoform of the transporter which appeared to be less stable with a 50% reduced half-life compared to the wildtype.[51] The important role of the N-linked carbohydrates was supported by results that showed, that even the addition of a carbohydrate at a single site can significantly increase the transport activity of hNET. This underlines the importance of the of N-glycosylation sites for the Norepinephrine (NE) uptake.[56] To determine the cellular localization of the transporter protein immunofluorescences microscopy was used of cells that contained glycosylated and non-glycosylated forms of hNET. Results revealed a reduction in surface expression and an increase of mutated hNET intracellular localized.[56] This supports the findings in other studies that poorly glycosylated protein remains in the cytoplasm and is not functional, while glycosylated forms are directed to the cell surface and are functional.[51] Taken together these findings state the essential role of N-glycosylation of hNET regarding to protein expression, stability and overall transporter activity.

Phosphorylation sites may act as central molecular switches for the modulation of protein function and trafficking by kinases and phosphatases.[52]

Phosphorylation sites of NET are targeted by casein kinase II and protein kinase C (PKC) and are depicted in Figure 8.[47,53] The phosphorylation-dependent regulation of NET by PKC has been studied in COS-7 cells by Bonisch et al., 1997.[52] These fibroblast-like cell line was transfected with hNET cDNA and changes in the function of hNET were monitored. It was shown that hNET activity is reduced through phosphorylation by PKC, which most likely reduces surface expression of hNET.[52,57] Furthermore, a downregulation and endocytosis of NET was demonstrated in placental trophoblasts upon the activation of PKC.[58]

The several PTMs of hNET highlight, that choosing a suitable expression system for mammalian proteins is essential. The Baculovirus-Expression System (BEV) is a common system for expressing mammalian proteins and was selected for the recombinant protein expression of hNET in this thesis.

1.8. Challenges of Membrane Protein Expression

Expression and purification of membrane proteins is a challenging task compared to soluble proteins.[59,60] The *E. coli* expression system is the first choice, for the recombinant production of simple membrane proteins, that do not require post-translational modifications.[59] The prokaryotic expression system is cost efficient enables rapid cell growth, and no specific cell equipment is needed.[61] There are different *E. coli* cell strains for protein expression. The *E. coli* BL21 (DE3) strain is one of the most widely used strains for protein expression.[62] Additionally, the *E. coli* Rosetta (DE3) strain is frequently employed for this purpose. Studies have demonstrated that using the Rosetta strain instead of the BL21 (DE3) strain can significantly enhance protein production. The Rosetta strain is specifically designed to compensate for rare codons such as AGA, AGG, CUA, AUA, CCC, and GGA, which enhances protein expression.[63]

To solubilize MPs, detergents or other membrane mimetics are used. They adhere to the hydrophobic regions of a membrane protein, which results in soluble protein/detergent complex that can be purified.[61,64]

1.9. Recombinant Protein Production in Baculovirus Expression System

The Baculovirus Expression System (BVES) is a widely used tool for producing recombinant proteins in insect cells.[65,66] The system is also commercially used for the production of viral vaccines.[67] The BVE system was also successful utilized in producing functional GPCRs such as the human beta 2-adrenergic receptor (beta 2AR).[68]

It is based on the ability of the baculovirus to infect insect cells.[65] The virus is engineered to carry and express foreign genes. The insect cell lines most commonly used for recombinant protein expression are derived from Lepidoptera (moths and butterflies) and Diptera (flies).[66] The first study of utilizing a baculovirus to

recombinantly express a foreign protein was reported by Smith et al. in 1983, where the human IFN-ß protein was produced.[69] Baculoviruses are rod-shaped and belong to a large group of DNA viruses that infect insect cells.[70] Autographa californica multiple-capsid nuclear polyhedrosis virus (AcMNPV) is the most commonly used baculovirus which infects *Spodoptera frugiperda* (Sf).[71] It has a large genome of approximately 130 kb and can carry large amount of foreign DNA.[72] To produce the baculovirus the gene is first cloned into a transfer vector.[72] The virus attaches through surface receptors to the insect cells and is taken up by endocytosis. [73] The circular baculovirus DNA initiates a replication cycle in transfected insect cells.[74] The baculovirus vector can be either produced by co-transfection of the insect cells or using a baculovirus shuttle vector (bacmid) developed by Luckow et al.[74,75] The bacmid can replicate in *E. coli* and infect insect cells. The work flow of the BVE used in this thesis is depicted in Figure 9.

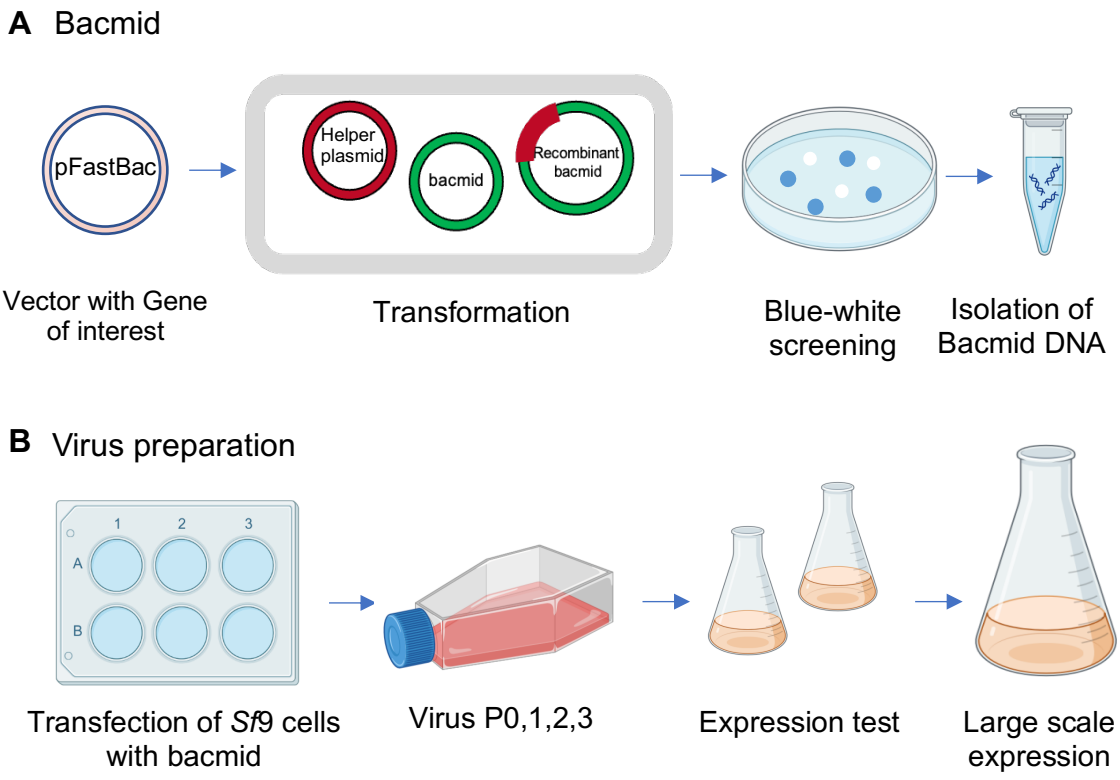

Figure 9: Workflow of protein production in Baculovirus Expression System. (A) Bacmid preparation. The bacmid is prepared by chemical transformation of the vector, containing the gene of interest, with *E. coli* DH10Bac chemical competent cells. The recombinant bacmid plaques (white plaques) were identified by using a blue-white screening. Upon disruption of the lacZ gene by DNA insertion, the gene can not produce β-galactosidase. The agar plates

used for the screening contain a chromogenic substrate like 5-bromo-4-chloro-3-indolyl-β-D-galactopyranoside (X-gal). In presence of this substrate the enzyme produces a blue color.[76,77] After isolation of the Bacmid DNA the virus was prepared. **(B) Virus preparation.** The cells were first transfected with the bacmid and the baculovirus prepared followed by recombinant protein production using *Sf*9 insect cells as host cells. Figures created with *BioRender*.

The great advantage of using insect cells is that the system is capable of producing correctly folded proteins with post-translational modifications.[67,78] Another advantage is the high biosafety of the baculovirus, since it does not replicate in mammalian cells.[70] The baculovirus system is also capable of expressing higher yields of recombinant protein.[79] Given its advantages the system is limited by proteolysis.[78] In this thesis the commercial Bac-to-Bac system is employed, which generates recombinant baculoviruses by site-specific transposition in E. coli (DH10bac). The Competent cells exhibit bacmid with a lacZ-mini-attTn7 fusion for the transposition between the vector and the bacmid.

2. Aim of this Thesis

The aim of the thesis is to achieve a better characterization of membrane proteins using appropriate biochemical and biophysical methods. The focus is particularly on the Melanocortin Receptor Accessory Proteins (MRAPs), which are part of the melanocortin system, besides various receptors (MCXRs) and ligands. For that, the MRAP proteins are produced in different expression systems, purified via affinity tags and characterized by mass spectrometry (MS) and electronic absorption spectroscopy (EAS).

Following objectives were set for this work:

- Recombinant production of the MRAP proteins in *E. coli* and the purification by affinity chromatography.
- Evaluation of the reported metal-binding of MRAP.
- Establishing eukaryotic expression of membrane systems including MRAP2 and hNET.
- Exploration of the nanodiscs system in combination with suitable biophysical techniques to investigate membrane binding interactions.

Taken together, these studies aim to advance the characterization of membrane proteins by optimizing established biochemical and biophysical methods.

3. Material and Methods

3.1. Devices

Table 2: List of devices used in this thesis.

Device	Manufacturer
Agarose gele chamber system	Bio-Rad Laboratories GmbH, Munich
ÄKTA prime	GE Healthcare, Sweden
ÄKTA Start	GE Healthcare, Sweden
Analytical balance	Satorius AG, Göttingen
Autoclave VX-150	Systec GmbH, Linden
Cell Disruptor	Constant Systems LTD, Northans UK
Centrifuge Avanti J-26S XP	Beckmann Coulter GmbH, Krefeld
CLARIOStar Plus Plate Reader	BMG Labtech, Ortenberg
Electrophoresis power supply 3501XL	Fisher Scientific UK Ltd, Loughborough
Desk centrifuge 5415 R	Eppendorf GmbH, Hamburg
Drying chamber T 5050	Heraeus, Hanau
Gel documentation systems	Bio-Rad Labratories GmbH, Munich
Incubation shaker Infors HT Multitron	Infors AG, Bottmingen
Incubation shaker New Brunswick innova 40	New Brunswick Scientific Co Inc, Enfiled, CT, USA
Incubation shaker New Brunswick innova 44	New Brunswick Scientific Co Inc, Enfiled, CT, USA
Magnetic stirrer C-MAG HS7	IKA Werke GmbH & Co KG, Staufen
Microcentrifuge 5415R	Eppendorf AG, Hamburg
Milli-Q	Merck Millipore, Merck KGaA, Darmstadt
NanoDrop2000	Thermofisher Scientific, Schwerte
pH Meter	Satorius AG, Göttingen
Pipettes	Eppendorf, Hamburg
Rotor JA-20	Beckmann Coulter GmbH, Krefeld
Rotor JLA 10.500	Beckmann Coulter GmbH, Krefeld
Scale	Satorius AG, Göttingen
Sonicator device sonopuls	Bandelin electronic GmbH & Co KG, Berlin

Sonotrode VS-70T	Bandelin electronic GmbH & Co. KG, Berlin
Spectrophotometer Agilent Cary 60	Agilent CA, USA
Thermocycler compact	Eppendorf, Hamburg
Vortexer	VWR International GmbH, Darmstadt

3.2. Chemicals

Table 3: List of chemicals used in this thesis.

Chemicals	Manufacturer
Acetic acid, puriss p.a., ACS, reag. ISO, >99.8%	Sigma-Aldrich Chemie GmbH, Steinheim
APS, >98%, p.a., ACS	Carl Roth GmbH & Co. KG, Karlsruhe
Ampicillin sodium salt	Sigma-Aldrich Co., St. Louis, MO, USA
cOmplete Tablets, EDTA-free EASY pack protease inhibitor	Roche Deutschland Holding GmbH, Grenzach-Wyhlen
Coomassie Brilliant Blue R 250	SERVA Electrophoresis GmbH, Heidelberg
DTT, >99% p.a	Carl Roth GmbH & Co. KG, Karlsruhe
D-Glucose Monohydrate	Fisher Scientific UK Ltd, Loughborough
di-Potassiumhydrogenephosphate-Trihydrate, >99%, p.a.	Carl Roth GmbH & Co. KG, Karlsruhe
di-Sodiumhydrogenephosphate-Dihydrate, >99.5%, p.a.	Carl Roth GmbH & Co. KG, Karlsruhe
DMPG	Avanti Polar Lipids, USA
DMPC	Avanti Polar Lipids, USA
EDTA-Disodiumsalt-Dihydrate	AppliChem GmbH, Darmstadt
GelRED Nucleic Acid Stain, 10000x in H_2O	Biotium Inc. Fremont, CA, USA
HCl	Merck KGaA, Darmstadt

Imidazole 99%	Acros Organics, Thermo Fisher Scientific Inc., New Jersey, USA
Isopropanol, HPLC grade	Fisher Scientific GmbH, Schwerte
IPTG, 99%	Carbolution Chemicals GmbH, St. Ingbert
Magnesium sulfate Heptahydrate puriss. p.a.	Sigma-Aldrich Chemie GmbH, Steinheim
Potassium chloride, AnalaR NORMAPUR	VWR International GmbH, Darmstadt
Potassiumdihydrogenephosphate, Analytical grade	Fisher Scientific GmbH, Schwerte
POPG lipid stock	Avanti Polar Lipids, USA
Rotiphorese Gele 30 (37, %:1) Acrylamid-Bisacrylamid-*Stocksolution*	Carl Roth GmbH & Co. KG, Karlsruhe
Sodium chlorid >99.5%, p.a., ACS, ISO	Carl Roth GmbH & Co. KG, Karlsruhe
SDS granulated pure	AppliChem GmbH, Darmstadt
TB-Medium	AppliChem GmbH, Darmstadt
TEMED, >99%, p.a.	Carl Roth GmbH & Co. KG, Karlsruhe
TRIS, 99.8% for analysis	Acros Organics B.V.B.A., Thermo Fisher Scientific, Waltham, MA USA
Tris-HCl Buffer, >99%, p.a.	Carl Roth GmbH & Co. KG, Karlsruhe
2YT Media powder (Broth for Molecular biology)	Carl Roth GmbH & Co. KG, Karlsruhe
HEPES, fine white crystals	Fisher Scientific GmbH, Schwerte
10x Tris/Glycine/SDS Electrophoresis buffer	Bio-Rad Laboratories GmbH, Feldkirchen
Acetic acid, puriss p.a., ACS, reag. ISO, >99.8%	Sigma-Aldrich Chemie GmbH, Steinheim
APS, >98%, p.a., ACS	Carl Roth GmbH & Co. KG, Karlsruhe
Ampicillin sodium salt	Sigma-Aldrich Co., St. Louis, MO, USA

3.3 Consumable Material

Table 4: List of consumable material used in this thesis.

Consumable Material	Manufacturer
Amicon Ultra-15 centrifugal filter units, 3K and 10K	Merck KGaA, Darmstadt
Bio-Beads SM-2 Adsorbent Media	Bio-Rad Laboratories GmbH
Biosphere Filter tips	SARSTEDT AG & Co. KG, Nürmbrecht
Filtropurs S 0.2	SARSTEDT AG & Co. KG, Nürmbrecht
Laboratory bottles with PP screw cap	VWR International GmbH, Darmstadt
High performance transfer pipettes	VWR International GmbH, Darmstadt
HiLoad™ 16/600 Superdex 200 pg	GE Healthcare Life Sciences
Protino Ni-NTA column, 5ml	MACHEREY-NAGEL GmbH & Co. KG, Düren
Protino Ni-NTA Agarose Resin	MACHEREY-NAGEL GmbH & Co. KG, Düren
Quartzcuvettes with PE stopper	Hellma GmbH & Co. KG, Mühlheim
SafeSeal reaction tubes 1.5ml	Sarstedt AG & Co. KG, Nümbrecht
SafeSeal reaction tubes 2ml	Sarstedt AG & Co. KG, Nümbrecht
Schikane Kolben 100,250,2	DWK Life Sciences GmbH, Werheim/Main
Serologische Pipetten	Sarstedt AG & Co. KG, Nümbrecht
SnakeSkin 3.5K and 10K MWCO, 16mm dry I.D., 35 feet dialysis tube	Fisher Scientific GmbH, Schwerte
Amicon Ultra-15 centrifugal filter units, 3K and 10K	Merck KGaA, Darmstadt
Bio-Beads SM-2 Adsorbent Media	Bio-Rad Laboratories GmbH

3.4. Bacterial strains

Table 5: List of the bacterial strains used in this thesis.

Bacterial strains *E. coli*	Strain name
XL1-blue competent cells	endA1 gyrA96(nalR) thi-1 recA1 relA1 lac glnV44 F'[::Tn10 proAB+ lacIq Δ(lacZ)M15] hsdR17(rK- mK+)
BL21 (DE3)	*E. coli* str. B F– ompT gal dcm lon hsdSB(rB– mB–) λ(DE3 [lacI lacUV5-T7p07 ind1 sam7 nin5]) [malB+]K-12(λS)
Rosetta™ (DE3) competent cells	F^- *ompT hsdS*$_B$(r_B^- m_B^-) *gal dcm* (DE3) pRARE (Cam^R)
Stellar™ competent cells	F-, endA1, supE44, thi-1, recA1, relA1, gyrA96, phoA, Φ80d lacZΔ M15, Δ(lacZYA-argF) U169, Δ(mrr-hsdRMS-mcrBC), ΔmcrA, λ-

3.5. Plasmids

Table 6: List of plasmids used in this thesis.

Construct	Plasmid
pET28a_ MRAP1	*E. coli* Melanocortin Receptor Accessory Protein 1
pET28a_ MRAP2	*E. coli* Melanocortin Receptor Accessory Protein 2
pET28a_ MRAP2_MRAP2	*E. coli* Melanocortin Receptor Accessory Protein 2 (2 copies of gene)
pET28a_MSP1D1	*E. coli* Membrane Scaffold Protein
pET28a_ MRAP1_C96A	*E. coli* Mutant Melanocortin Receptor Accessory Protein 1
pET28a_ MRAP1_C96A_H97A	*E. coli* Mutant Melanocortin Receptor Accessory Protein 1
pET28a_ MRAP2_C132A	*E. coli* Mutant Melanocortin Receptor Accessory Protein 2
pET28a_ MRAP2_C132A_H133A	*E. coli* Mutant Melanocortin Receptor Accessory Protein 2

pFASTBac_MRAP2	*Sf*9 Melanocortin Receptor Accessory Protein 2
pFASTBac_MRAP2_MRAP2	*Sf*9 Melanocortin Receptor Accessory Protein 2 (2 copies of gene)
pFHMSP_LIC_N_hNET	*Sf*9 human Norepinephrine Transporter
pET28a_ MRAP1	*E. coli* Melanocortin Receptor Accessory Protein 1

3.6. Protein- and DNA standards

Table 7: List of Protein- and DNA standards used in this thesis.

Standard	Manufacturer
DNA Ladder *GeneRuler* 1 kb	Thermo Fisher Scientific, Schwerte
PageRuler Plus Prestained Protein Ladder	Thermo Fisher Scientific, Schwerte
Spectra Multicolor Low Range	Thermo Fisher Scientific, Schwerte

3.7. Buffer and solutions

Table 8: List of buffers and solutions used in this thesis.

Buffer and solutions	Composition
Ampicillin stock	100 mg/ml
Coomassie-brilliant blue staining	0.05 % (m/v) Coomassie brilliant blue R-250; 25 % (v/v) isopropanol, 10 % (v/v) acetic acid
IPTG	0.5 M
Kanamycin stock	50 mg/ml
Laemmli sample buffer (4x)	10 % (w/v) SDS, 6 % 10 mM β mercaptoethanol, 20 % (v/v) glycerol, 0.05 % Bromphenol-Blue, 200 mM Tris-HCl, pH 6.8
$NiSO_4$	0.1M

PBS (1 liter)	NaH_2PO_4 (10mM), KH_2PO_4 (1.8mM), KCl (2.7mM), NaCl (140mM), pH 7.3
Running SDS-gele buffer	1.5 M Tris/HCl, pH 8.0
Stacking SDS-gele buffer	0.5 M Tris/HCl, pH 6.0
Ampicillin stock	100 mg/ml
Coomassie-brilliant blue staining	0.05 % (m/v) Coomassie brilliant blue R-250; 25 % (v/v) isopropanol, 10 % (v/v) acetic acid
IPTG	0,5 M
Kanamycin stock	50 mg/ml
Laemmli sample buffer (4x)	10 % (w/v) SDS, 6 % 10 mM β mercaptoethanol, 20 % (v/v) glycerol, 0.05 % Bromphenol-Blue, 200 mM Tris-HCl, pH 6.8
$NiSO_4$	0.1M
PBS (1 liter)	NaH_2PO_4 (10mM), KH_2PO_4 (1.8mM), KCl (2.7mM), NaCl (140mM), pH 7.3
Running SDS-gele buffer	1.5 M Tris/HCl, pH 8.0

Table 9: List of buffers and solutions used for MRAP expression.

Buffer and Solutions	Composition
NaPi Buffer A	NaPi 20 mM, NaCl 5mM, pH 7.4
NaPi Buffer B	NaPi 20 mM, NaCl 5mM, Urea 6 M
NaPi Elution Buffer	NaPi 20 mM, NaCl 5mM, Urea 6 M, Imidazole 10 mM – 300 mM, pH 7.4

Table 10: List of buffers and solutions used for MSP1D1 expression.

Buffer	Composition
Buffer A	Tris-HCl 50 mM, NaCl 500 mM, Urea 6 M
Buffer B	Tris-HCl 50 mM, NaCl 500 mM, Triton X-100 1%

3.8. Metal solution for MRAP *E. coli* Expression

Table 11: SBMX stock solution for 500 ml (25x)

M9 Medium (1 liter)	Composition
K_2HPO_4	87.5 g
KH_2PO_4	16.15 g
NaCl	18.25 g

Table 12: $FeCl_2$ stock solution for 100 ml.

Component	Composition
HCl	10 ml
$FeCl_2$	5 g
$CaCl_2$	184 mg
H_3BO_3	64 mg
MnCl	40 mg
$CoCl_2$	18 mg
$CuCl_2$	4 mg
$ZnCl_2$	340 mg
Na_2MoO_4	605 mg

Table 13: ,,S'' stock solution for 100 ml.

Component	Composition
K_2SO_4	4.8 g

Table 14: ,,TE'' stock solution for 500 ml.

Component	Composition
$MgCl_2$ $6H_2O$	28.8 g
$FeCl_2$ stock solution	10 ml

Table 15: Vitamin stock solution for 1L.

Component	Composition
Biotin (Vitamin B7)	2.2 mg
Folic acid (Vitamin B9)	2.2 mg
PABA (para-aminobenzoic acid)	220 mg
Riboflavin (Vitamin B2)	220 mg
Pantothenic acid (Vitamin B5)	440 mg
Pyridoxine HCl (Vitamin B6)	440 mg
Thiamine (Vitamin B1)	440 mg
Niacinamide (Vitamin B3)	440 mg

Table 16: Components for 1L M9 Medium.

M9 Medium (1 L)	Composition
SBMX stock solution	40 ml
S stock solution	1 ml
TE stock solution	2 ml
Thiamine	1 ml
Vitamin stock solution	1 ml
Glucose	2 g
NH_4Cl	1 g
ddH_2O	940 ml

3.9 Methods of Molecular Biology

3.9.1 PCR Polymerase Chain Reaction

To verify the presence of the gene of interest in the recombinant bacmid Polymerase Chain Reaction was employed using components and cycling steps in the table below. After PCR, the PCR product was analyzed by agarose gel electrophoresis. Recombinant bacmid DNA is greater than 135 kb in size. As restriction analysis is difficult to perform with DNA of this size, use PCR analysis to verify the presence of the gene of interest in the recombinant bacmid.

Table 17: Composition of PCR master mix.

Component	Volume
Rekombinant Bacmid DNA 100ng	1 µl
10X PCR Buffer	5 µl
10 mM dNTPs	1 µl
50 mM MgCl2	1.5 µl
M13/pUC Forward/Reverse Primer (10	1.25 µl of each primer
Platinum™ Taq polymerase	0.5 µl
Milli-Q water	38.5 µl Rest

Table 18: Cycling program.

Step	Temperature	Duration (min)
Initial denaturation	95 °C	03:00
Denaturation	95 °C	00:45 (25x-35x)
Annealing	55 °C	00:45
Elongation	72 °C	05:00
Final elongation	72 °C	07:00

3.9.2. Agarose gel electrophoresis

To verify the presence of the correct amplified vector Agarose gel electrophoresis was performed. For preparation of 1% agarose gel, 50 ml of TAE Buffer or LiAc Buffer were added to 0.5 g agarose and heated to obtain a homogenous solution. Subsequently, 3 µl of Gelrad Biostain were added poured into the provided aperture. After polymerization of the gel, 5µl of each sample were mixed with 1µl of 6 x Agarose loading dye and loaded onto the gel. As a standard 3 µl of 1kb DNA ladder were used. For TAE gel the max. voltage and running time was 120 V (constant volt) and 45 minutes and for the LiAc Buffer the max. voltage and running time was 240V and 20 minutes. After the completed run, the bands were visualized by using the gel documentation system (Bio-Rad Laboratories GmbH, München).

3.9.3 Transformation of plasmids into chemical competent cells

For transformation of the modified vector into cells the chemical competent XL1-Blue cells oder stellar-cells were chosen. For that, 50 µl of chemical competent cells were thawed on ice for 10 minutes and mixed. Subsequently, 10 ng of plasmid were added and incubated for an additionally 10 minutes on ice. For heat shock, the reaction mixture was incubated for 60 seconds and 800 rpm at 42 °C mixed gently and incubated on ice for 2 minutes. Subsequently, 450 µl of 2YT medium were added and incubated for 1 hour at 37 °C and 800 rpm. After incubation, cells were centrifuged, 350 µl of the supernatant discarded, the cell pellet resuspended in the remaining buffer and plated out on an agar plate containing LB medium and antibiotic. The agar plate was incubated over night at 37 °C. The next day, the agar plate was examined, to see if colonies had grown. Colonies were picked and used for plasmid isolation.

3.9.4 Isolation of plasmid DNA from *E. coli*

To isolate the plasmid DNA, single colonies were picked from the agar plate to inoculate 5ml of 2xYT medium supplemented with 100 mg/ml of antibiotics. The culture was incubated for 16 h at 37°C and 160 rpm. Plasmid isolation was carried out by using the NucleoSpin Plasmid DNA purification – Kit from Macherey-Nagel.
Concentration of the obtained plasmid DNA was measured by using the NanoDrop200 (Thermofisher Scientific, Schwerte).

3.9.5 Sequencing of isolated plasmids

The plasmid DNA was sequenced by sanger sequencing at Microsynth Seqlab Göttingen, Germany. For sequencing 12 µl of the Plasmid DNA with a concentration between 50 to 100 ng/µl was transferred to an Eppendorf tube. As a primer, the standard primer T7 promotor provided by Microsynth Seqlab was added. The results were analyzed by using SnapGene ® Viewer 6.0.

3.9.6 Cloning MRAP mutants and MRAPs for *Sf*9 cells.

For generation of the MRAP mutants, forward and reverse primer were designed to introduce a single amino acid into the potential metal binding site of MRAP1 and MRAP2. The components of the PCR mastermix and the PCR cycler program are depicted in the list below.

Table 19: Composition of PCR master mix.

Component	Volume
PCR reaction mix	12.5 µl
Forward/Reverse Primer (10 µM)	1 µl of each primer
Plasmid (1.3 ng/µl)	1 µl
Milli-Q water	Rest

Table 20: Cycling program for PCR.

Step	Temperature	Duration (min)
Initial denaturation	95 °C	03:00
Denaturation	95 °C	00:45 (25x-35x)
Annealing	55 °C	00:45
Elongation	72 °C	05:00
Final elongation	72 °C	07:00

The PCR product was evaluated by agarose gel electrophoresis and the according band cut out of the gel and vector purified using the NucleoSpin Gel and PCR Clean-up by Macherey-Nagel. For the In-Fusion cloning the In-Fusion® Snap Assembly Master Mix by Takara Bio Inc. (Japan) was used to fuse plasmids and the gene of

interest. The PCR reaction was carried out for 15 minutes at 37 °C followed by 15 minutes at 50 °C in a PCR cycler. The resulting In-Fusion products were then used to transform chemically competent cells, and the sequences were validated by Sanger sequencing. The plasmids obtained were subsequently used for recombinant protein expression.

3.9.7 *E. coli* Expression MRAPs

For MRAP expression, chemically competent *E. coli* rosetta (DE3) were thawed on ice and transformed with 100 ng of pET28a-MRAP(1-22) plasmid. After transformation, a starting culture of 50 ml of 2YT medium, supplemented with 50 µg/ml kanamycin, was inoculated with a single colony. The flask was incubated o/n at 37°C at 160 rpm. The next day, 1 L of 2YT medium, supplemented with 2 ml of metals and 50 ug/ml kanamycin was inoculated 1:10 with the starting culture and incubated at 37°C, at 140 rpm, until an OD_{600} between 0.8-1 was reached. Subsequently, gene expression was induced by adding 1 mM of IPTG to the culture. The culture was incubated o/n at 27°C and 140 rpm and harvested the next day by centrifugation at 6000 xg for 10 min at 4°C using the JLA10500 rotor.

3.9.8 MRAP Purification

For MRAP purification, 1 g of cell pellet were resuspended in 10 ml of NaPi Buffer (20 mM NaCl, 50 mM NaPi, pH 7.4) and lysed by sonification using the *sonicator device sonopuls.* After sonication, the lysate was centrifuged for 45 min at 40.000 xg using the JASCO Avanti J-26S XP centrifuge and the JA-20 rotor to remove cell debris. For solubilization of the membrane protein, the cell pellet was resuspended in NaPi buffer, with 6 M of urea (20 mM NaCl, 50 mM NaPi,6 M urea pH 7.4) and centrifuged again for 30 min at 40000 xg. The supernatant was loaded onto a column, containing previously equilibrated Protino Ni-NTA Agarose from Macherey & Nagel. Subsequently, several washing steps followed with NaPi buffer, containing 10 mM, 20 mM and 30 mM of imidazole, to remove unspecific binding proteins. The target protein was eluted from the column using 5 CV of NaPi buffer, containing 300 mM of imidazole. After purification, dialysis was performed to remove excess imidazole. The sample was transferred into a SnakeSkin dialysis tube (10 K MWCO, Fisher Scientific GmbH, Schwerte), placed into a beaker with 1 Liter of NaPi buffer and stirred over night at 4 °C. The next day the protein was concentrated in an Amicon® Ultra-15 Centrifugal

Filter Unit with a 10 kDa molecular weight cut off (MWCO) and the samples stored at -80 °C until further use.

3.9.9 MS1D1 Expression

The cell pellet from 1L of cell culture was resuspended in buffer A (50 mM Tris/HCl, 500 mM NaCl, pH 8.0) + 6 M GuHCl (Guanidinium-HCl) and one tablet of EDTA-free protease inhibitor. Cells were lysed using the *sonicator device sonopuls* (amplitude: 50%, pulse on: 2s, pulse off: 5 s, 10-15 cycles on ice). The lysate was centrifuged for 40 min at 40.000 xg at 4°C using the JASCO Avanti J-26S XP centrifuge and the JA-20 rotor. The supernatant was incubated over night with equilibrated Protino Ni-NTA Agarose from Macherey & Nagel at 4°C. The next day, the mixture was loaded onto a gravity flow column and the column washed with 10CV of buffer A, 10 CV of buffer A + 1% Triton X-100, 10 CV of buffer A + 60 mM NaCholate, 10 CV of buffer A, 10 CV of buffer A + 20 mM imidazole, 10 CV of buffer A + 50 mM imidazole. MSP1D1 was eluted from the column, using buffer A + 500 mM imidazole. Dialysis was performed overnight in Tris Buffer (50 mM Tris-HCl, 100 mM NaCl, pH 7.4). The sample was concentrated in a Amicon® Ultra-15 Centrifugal Filter Unit with a 10 kDa molecular weight cut off (MWCO) and the purified MSP1D1 was stored at -80 ℃ until further use.

3.9.10 Bacmid isolation

First, the bacmid had to be prepared. For that, 1ng plasmid of the hNET or MRAP2, were transformed with DH10Bac TM competent cells and incubated for 30 min on ice. Heat shock was performed for 45 seconds at 42 °C and the cell transferred to ice for 2 min. Subsequently, 900 µl of 2 YT medium was added and the reaction mixture and everything incubated at 37 °C, 300 rpm for 4 h. Then, cells were plated out onto a LB agar plate, supplemented with different antibiotics for blue-white screening of the recombinant bacmid. Plates were incubated for 48 hours at 37 °C and checked for white colonies. The white colonies were picked from the agar plate and re-streaked and the plates incubated again for 48 h at 37 °C. After incubation singe white colonies were picked and the recombinant bacmid DNA isolated. 5ml of 2 YT medium were inoculated with a single white colony and the bacmid DNA isolated using NucleoSpin Plasmid DNA purification – Kit from Macherey-Nagel.

3.9.11 Polymerase Chain Reaction (PCR)

To verify the presence of the gene of interest in the recombinant bacmid Polymerase Chain Reaction was employed using components and cycling steps in the table below. After PCR, the PCR product was analyzed by agarose gel electrophoresis. Recombinant bacmid DNA is greater than 135 kb in size. As restriction analysis is difficult to perform with DNA of this size, use PCR analysis to verify the presence of the gene of interest in the recombinant bacmid

Table 21: Composition of PCR master mix.

Component	Volume
Rekombinant Bacmid DNA 100ng	1 µl
10X PCR Buffer	5 µl
10 mM dNTPs	1 µl
50 mM MgCl2	1.5 µl
M13/pUC Forward/Reverse Primer (10	1.25 µl of each primer
Platinum™ Taq polymerase	0.5 µl
Milli-Q water	38.5 µl Rest

Table 22: Cycling program for PCR.

Step	Temperature	Duration (min)
Initial denaturation	95 °C	03:00
Denaturation	95 °C	00:45 (25x-35x)
Annealing	55 °C	00:45
Elongation	72 °C	05:00
Final elongation	72 °C	07:00

Table 23: Primer sequences.

Primer name	Sequence
M13/pUC Forward	5’-CCCAGTCACGACGTTGTAAAACG-3’
M13/pUC Reverse	5’-AGCGGATAACAATTTCACACAGG-3’

3.9.12 Baculovirus preparation

After bacmid isolation, the next step was to prepare the baculovirus. For that, the *Sf*9 cells were transfected with the bacmid DNA using the Fugene HD transfection reagent from promega. The composition of the transfection reaction is depicted in the table below. The reaction mixture was incubated at RT for 30 min and subsequently the cells were incubated for 3-4 day at 27 °C.

Table 24: Transfection conditions.

Component	Amount
*Sf*9 cells	$1x10^6$ cells
Medium	3 ml
Bacmid DNA	7 µg
Transfection Reagent	5 µl

After transfection, the medium containing the virus is transferred to a sterile 15 ml falcon tube and centrifuged at 500 xg for 5 min. The supernatant, containing the P0 virus, was transferred to a fresh 15 ml falcon tube. For preparation of the P1 virus, 80 % of *Sf*9 cells were seeded to a T75 flask and incubated at 27 °C for 30 min, for the cells to attach to the flask. 1 ml of P0 virus is added to the flask and the cells incubated for 3 days at 27 °C. These steps are repeated to prepare the P1 and P2 virus. For the P3 virus, 200 ml of *Sf*9 cells (2x10^6 cells/ml) are added to a 1 L Erlenmeyer flask and 2 ml of P2 virus added. The culture was incubated at 27 °C, at 110 rpm for 3 days. Cells are harvested at 800 xg for 5 min and the cell pellet checked for the target protein. For this purpose, the cell pellet was washed with 1x PBS and resuspended in RIPA Lysis Buffer (150 mM NaCl, 50 mM Tris/HCl, 0,5 % sodium deoxycholate, 1% Triton-X100, 0,1 % SDS, pH 8.0). Everything was incubated on ice for 15 min and subsequently centrifuged at 14000 xg, 4°C for 15 min. Samples were prepared for Western blot analysis. After detection of the target protein, larger scale expression of the recombinant protein was carried out by adding 5 ml of P3 virus to 500 ml of *Sf*9 cells and incubated at 27 °C, at 110 rpm for 3 days. After incubation, the cells were lysed using the RIPA lysis buffer or by sonication. Subsequently, protein purification was carried out using the appropriate purification method.

3.10 Methods of Protein-Biochemistry

3.10.1 Sodium dodecyl-sulfate polyacrylamide gel electrophoresis (SDS-PAGE)

To evaluate the purity of the isolated proteins, gel electrophoresis was performed. A standard 15 % TRIS-Glycine gel was used, consisting of a running, - and stacking gel. The composition of both gels is listed in the table below. For analysis, samples were diluted 3:1 with 5x Laemmli-SDS Buffer, supplemented with 2 mM of DTT. Subsequently, 3 µl of the protein standard *PageRuler Plus Prestained* and 10 µl of each sample were loaded onto the gel. The SDS-PAGE was carried out with a constant current of 20 mA per gel in 1xTGS buffer. After the completed run, the gel was stained with Coomassie Brilliant Blue for 20 min and destained for 1 hour with 10 % acetic acid. All gels were imaged by a gel documentation system (Bio-Rad Laboratories GmbH, Munich).

Table 25: Components of a 15 % TRIS-Glycine gel.

Component	Stacking gel 2 % (ml)	Running gel 15 % (ml)
H_2O	1.488	1.1
TRIS 0.5 M, pH 6.8	0.625	-
TRIS 1.5 M, pH 8.8	-	1.3
Acrylamide/Bisacrylamide stock solution (37.5:1)	0.335	2.5
SDS (w/v, 10 %)	0.025	0.05
APS (w/v, 10 %)	0.025	0.05
TEMED	0.0025	0.005

3.10.2 Western blot

To detect the presence of the target protein, Western blot analysis was performed. In preparation for the Western blot, gel electrophoresis with the analytes was performed and the SDS-Page not stained, but directly transferred onto a PVDF-membrane. The membrane was previously activated with 100% of EtOH. The membrane is placed between Watman-paper, which was soaked in Towbin buffer (100 ml 10xTGS buffer, 200 ml of 100% of EtOH, 700 ml Milli Q water) and placed into the the Bio-Rad Universal Hood III documentation system (Bio-Rad Laboratories GmbH, München) (25 V, 1.0 A, 30 min). After transfer, the membrane is placed in a fresh falcon and 5ml of

blocking solution (5% milk powder blotting grade) added and incubated for 1 h at RT. Subsequently, the blocking solution was discarded and the primary antibody added (His-tagged antibody (mouse), 1:1000) and everything incubated o/n at 4 °C. Followed by that, the primary antibody is removed from the falcon and the membrane washed 3x with 1xTBS-T buffer, before the secondary antibody is added (Anti-His GamPo (mouse) 1:10000). The membrane is incubated for 1 h with the secondary antibody at RT and afterwards washed again 3x with 1x TBS-T. Afterwards, the membrane is ready to be visualized by mixing 1:1 super signal peroxidase and enhancer solution and incubating the membrane for 5 min with the solution. The membrane is imaged using the gel documentation system (Bio-Rad Laboratories GmbH, Munich).

3.10.3 Cell lysis

Cell lysis was performed by cell disruption with *the Constant Systems LTD Cell disruptor* or by sonification using the *sonicator device sonopuls*. For both methods, the cell pellet was resuspended in the appropriate lysis buffer. Subsequent, one tablet of protease inhibitor and 20 ng/µl of DNase were added and the mixture incubated for 15 min at 4 °C. For cell disruption, the system was washed at 0.44 bar with 0.5 M NaOH and H_2O. Cell disruption was then performed at 2.9 bar. For ultra-sonification, the VS70/T sonotrode was used. Sonication was performed according to the requirements of the target protein. The lysate was clarified by centrifugation for 30 min at 40000 xg and 10 °C using the JASCO Avanti J-26S XP centrifuge and the JA-20 rotor. The supernatant was transferred to a fresh falcon and kept on ice for protein isolation.

3.10.4 Immobilized metal ion affinity chromatography (IMAC)

Isolation of His-tagged proteins was performed by immobilized metal ion affinity chromatography (IMAC) using a Ni-NTA Protino column. The tagged protein binds to the nickel ions in the column and thus can be separated from other proteins in solution. Prior to use the chromatography system ÄKTA start (GE Healthcare, Sweden) was washed with water and the washing buffer (50 mM Tris/HCl, 150 mM NaCl, pH 7.6) and then equilibrated with 6 CV of washing buffer at a flow rate of 3 ml/min and 0.3 MPa. Next, the cell lysate was injected into the system and the column washed with the washing buffer and with 10% of the elution buffer (50 mM Tris/HCl, 150 mM NaCl, 250 mM Imidazole), to remove unspecific binding proteins. All fractions were collected during each step. The target protein was eluted with 100 % of elution buffer and

collected in 2 ml fractions. To remove the imidazole from the eluted sample, a dialysis was performed overnight. The collected fractions containing the target protein were pooled and transferred into a *SnakeSkin* dialysis tube (10 K MWCO, Fisher Scientific GmbH, Schwerte), placed into a beaker with 1 Liter of dialysis buffer (10 mM Tris/HCl, 150 mM NaCl, pH 7.6) and stirred over night at 4 °C. The next day the sample was concentrated in a Amicon® Ultra-15 Centrifugal Filter Unit with a 10 kDa molecular weight cut off (MWCO) and stored at -80 °C for further analysis.

3.10.5 Affinity chromatography with Strep-tag

MRAP2 expressed in *Sf*9 cells was purified by affinity chromatography using the Twin-Strep-Tag and gravity flow. All solutions were used from *iba-lifescience*. For purification the IBA Lifesciences Strep-Tactin™ Sepharose™ Resin was used and equilibrated prior with the Strep-Tactin ® wash buffer (100 mM Tris/HCl, 150 mM NaCl, 1 mM EDTA, pH 8.0) and the sample loaded. The column was then washed with 5CV of was buffer and the target protein MRAP2 eluted from the column, using the Strep-Tactin ® elution buffer (100 mM Tris/HCl, 150 mM NaCl, 1 mM EDTA, 2.5 mM desthiobiotin, pH 8.0). The different fractions were then pooled and dialysis performed o/n in wash buffer. The sample was then concentrated in a Amicon® Ultra-15 Centrifugal Filter Unit with a 10 kDa molecular weight cut off (MWCO) and stored at -80 °C for further analysis.

3.10.6. Ion Exchange Chromatography (IEX)

Ion exchange chromatography (IEX) was additionally utilized for the protein purification. This method is based on the attraction of oppositely charged molecules.[80] The matrix of the IEX column is composed of a positively or negatively charged ligand that is immobilized, where the protein can bind to. Above its pI, the protein is negatively charged and binds to an anion exchanger, which carries a positive charge. Below its pI, the protein is positively charged and binds to a cation exchanger, which carries a negative charge. The binding of a protein is then achieved at low and elution at high salt concentration. Prior to protein purification, the ÄKTA start system (GE Healthcare, Sweden) was equilibrated and washed with buffer containing 20 mM Tris/HCl, pH 8.0. Subsequently, the protein was loaded onto the IEX column. The protein was eluted with a high salt buffer containing 20 mM Tris/HCl and 1 M NaCl, pH 8.

3.10.7 Electronic absorption spectroscopy (EAS)

For determination of the protein concentration the absorbance at 280 nm was measured using the Cary Win 60 Spectrophotometer (Agilent CA, USA). As reference a buffer containing 50 mM Tris/HCl and 150 mM NaCl was measured followed by the protein sample. With the value at 280 nm the protein concentration was calculated using the Lambert-Beer law A=ε*c*d (A=absorbance, ε=molar extinction coefficient [M^{-1} cm^{-1}], c=concentration [M], d= path length of the light beam [cm]). EAS was also used to characterize the electronic spectrum of the MRAPS.

3.10.8 Nanodiscs preparation

In this thesis different types of nanodiscs were prepared, comprised of Dimyristoylphosphatidylglycerol lipid (DMPG), Dimyristoylphosphatidylcholine (DMPC) or 1-palmitoyl-2-oleoyl-sn-glycero-3-phospho-rac-(1-glycerol) (POPG). Prior to preparation, the amount of lipids that needed to be weighted had to be calculated. The appropriated amount of lipids was weight and dissolved in lipid resuspension buffer, Subsequently, the lipids were mixed with the previously purified scaffold proteins MSP1D1 in a 1:80 ration and the mixture incubated for 30 min at RT, 500rpm shaking. After that, 40 % w/v of Bio-Beads were added to the solution and incubated for 2 h or o/n at RT, 500rpm shaking. The Bio-Beads were previously washed and equilibrated with methanol, MQ water and MSP1D1 buffer. After the incubation time, the bio-beads were removed and 20 % w/v of biobeads added and everything incubated for for 2 h or o/n at RT, 500rpm shaking. The nanodiscs were purified by SEC using 16/600 Hi-flow column. After purification, the fractions containing the nanodiscs were pooled and concentrated using an Amicon® Ultra-15 Centrifugal Filter Unit with a 10 kDa molecular weight cut off (MWCO). The nanodiscs were stored for short-term storage at 4°C and for long-term storage at -20°C.

3.10.9 Size Exclusion Chromatography (SEC)

For SEC, the Hi-load Superdex 200 16/600 pg column from *GE Healthcare* was used and the ÄKTA pure™ chromatography system from *Cytiva Life Science* was used. First, the system was washed with MQ water and the appropriate buffer. The SEC column was then equilibrated with buffer at a at a flowrate of 0.5 ml/min at 4 °C, followed by loaded the sample onto the column. After the run, the system and column were again washed with MQ water and the column stored in 20 % of ethanol. All

solution and buffers were filtered and degassed, prior to using it with the chromatography system.

3.10.10 Mass Spectrometry (MS)

Mass spectrometry measurements were kindly carried out by Ian Gering at the Institute of Biological Information Processing (IBI, Research Center Jülich) and by Dr. Anja Stefanski at the Molecular Proteomics Laboratory (MPL) at Heinrich-Heine-University, Düsseldorf. The gel samples were cut into pieces and destained with 200 µl of 100 mM NH_4HCO_3, 20 % ACN at 37°C. The sample was then reduced with 50 µl of 100 µM of DTT at 60 °C for 10 min. Alkylation was performed by addition of 3 µl of Iodoacetamide (10 mg/ml) and incubated for 20 min at RT. 2 µl of Trypsin is added to each sample and incubated at 30 °C o/n. The Data was processed by *Agilent BioConfirm 10.0 software*, FlagPipe and the online database *Uniprot*.

3.10.11 Bio-Layer Interferometry (BLI)

Bio-Layer Interferometry (BLI) was carried out by using the BLItz™ device from avantor™ and the high precision streptavidin Octet® SAX biosensors. All steps were performed at room temperature. For this measurement, nano discs compromised of negatively charged POPG lipids were used as well as a potential GPX4 inhibitor. The protein was immobilized onto the streptavidin-coated biosensors, following the association and dissociation with the respective interaction partner monitored in real time. Prior to use, the biosensor was hydrated for 20 minutes in sodium phosphate buffer (20 mM sodium phosphate, 50 mM sodium chloride pH 7.4). After hydration, the initial baseline was measured for 30 seconds. Subsequently, the lysate, containing the biotin-tagged protein, was immobilized on the tip of the biosensor by loading 4 µl of the lysate onto the drop holder of the BLI device. Loading of the protein to the sensor was then measured for 300 seconds and the sensor placed back into sodium phosphate buffer for a second baseline measurement. Next, 4 µl of POPG nano discs or the nanodiscs- inhibitor mixture was loaded onto the drop holder and association monitored for 180 seconds. Afterwards, dissociation was performed for 240 seconds by placing the sensor into a fresh tube of sodium phosphate buffer. Different dilutions of the respective interaction partner were measured. A negative control was carried out by using buffer. Data was processed using baseline compensation to matching start values and linear compensation to compensate for evaporation effects. Control

measurements show contributions of unspecific interactions (not shown), complicating data analysis and preventing extraction of the exact association rates of GPX4 binding to the respective nanodiscs or nanodiscs- inhibitor mixtures.

3.10.12 Microfluidic diffusional sizing (MDS)

For interaction between nanodiscs and DNAzymeCy5, MDS using the Fluidity One-M was used. Fluidity One-M measures molecular size (hydrodynamic radius) of a sample by evaluating its diffusion in a microfluidic chamber (fluidic.com). First the nanodiscs were incubated together with the Cy5' labeled DNAzyme for 30 min on ice. Subsequently, 4 µl of each sample were loaded in duplicates onto a cassette and placed into the Fluidity One-M device. After the fluorescence reached an appropriate intensity, the hydrodynamic radius of the sample was measured.

4. Results

4.1. Recombinant Protein Expression and Purification of MRAPs in *E. coli*

Melanocortin receptor accessory proteins (MRAPs) are critical regulators of the melanocortin receptor (MCR) family, a group of G protein-coupled receptors (GPCRs) involved in various physiological processes such as energy homeostasis, pigmentation and adrenal gland function.[81,82] MRAPs modulate expression, trafficking, and activity of the melanocortin receptors.[83] A dysfunction of MRAP2 impacts appetite and energy balance by modulating MC4R signaling, which has been associated with obesity in rodent studies. Therefore, MRAPs represent a promising target for developing therapies for metabolic diseases.[45,84]

Previously in studies of our group, a metal-binding site in both, MRAP1 and MRAP2, was identified. To validate and investigate this feature of the accessory proteins, the initial approach involved the recombinant production of the wild-type MRAP proteins. For this purpose, all MRAP plasmids were newly transformed into chemically competent cells, and the correct sequence was verified by sanger sequencing. After transformation into the appropriate *E. coli* strain for protein expression, all three MRAP constructs were expressed, and the target proteins were purified. Subsequently, the proteins were analyzed using electronic absorption spectroscopy (EAS) and mass spectrometry (MS). All constructs were expressed under identical conditions in 2YT medium, supplemented with $FeCl_2$, 50 µg/ml kanamycin, and 35 µg/ml chloramphenicol. Protein purification was carried out using affinity chromatography followed by size-exclusion chromatography (SEC).

To solubilize the target proteins buffers with 6 M urea were used. Urea disrupts the hydrophobic interactions between the protein and the lipid membrane. Additionally, urea helps prevent protein aggregation, a common issue encountered with membrane proteins. [85–87] The purity of the isolated proteins was analyzed by gel electrophoresis, and an electronic absorption (EAS) spectrum was recorded. The presence of the correct target proteins was confirmed through gel electrophoresis and Western blot analysis.

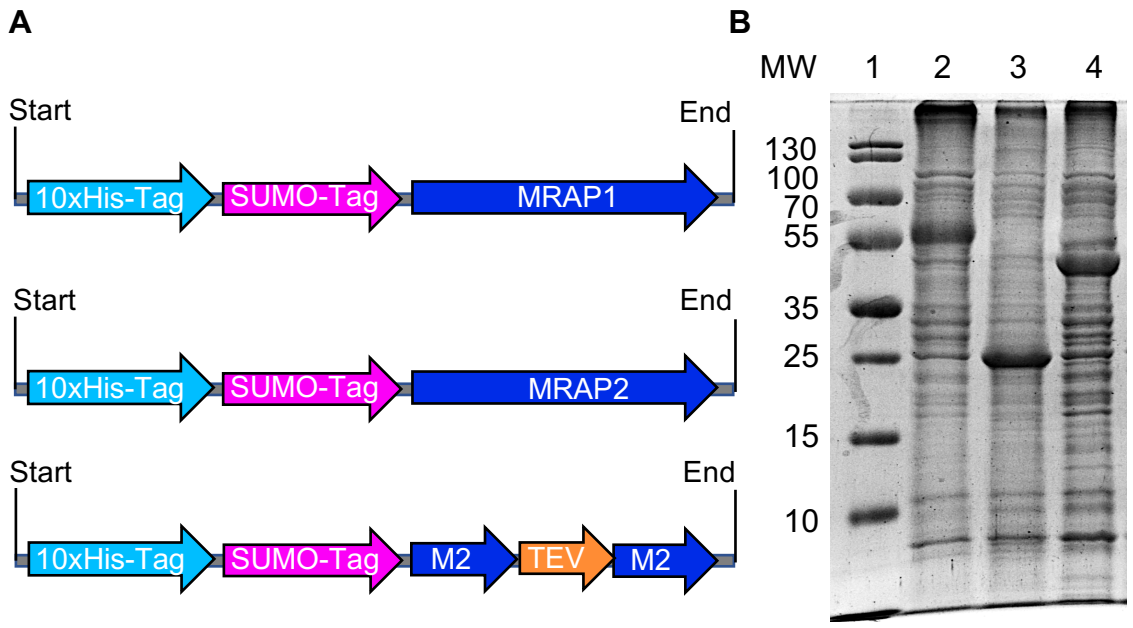

Figure 10: Expression and Purification of all MRAPs. (A) Overview of the MRAP constructs. Depicted are the different parts of the MRAP-SUMO-Fusion constructs. All constructs contain a 10x Histidin-tag (light blue), followed by the SUMO-tag (pink) and the MRAP1/MRAP2 gene (blue). The MRAP2_2 construct contains two copies of the MRAP2 gene, with a TEV cleavage site located between them. **(B) SDS-PAGE of purified MRAPs.** The image shows the SDS-PAGE of all MRAP samples purified by IMAC (yellow arrows). All constructs were expressed and isolated under the same conditions. The molecular weight of the marker ranges from 10 kDa to 130 kDa in this figure. 1: Marker *PageRuler Plus Prestained*, 2: MRAP2_2 55 kDa, 3: MRAP1 32 kDa, 4: MRAP2 36 kDa.

After purifying the MRAP proteins, SDS-PAGE analysis of MRAP2 was performed to verify the presence of the target protein in the eluted sample (Figure 10B). However, additional protein bands, beside MRAP, were detected in the purified samples.

MRAP1 (band 3), with a molecular weight of 32 kDa, is observed at approximately 25 kDa, which is lower than the expected molecular weight. MRAP2 (band 4), with a molecular weight of 36 kDa, is detected at approximately 45 kDa, above the expected molecular weight. Figure 11A shows the different steps involved in MRAP2 purification, suggesting that the protocol could be further optimized to obtain a purer protein sample. Nevertheless, presence of MRAP2 could be confirmed via Western blot (Figure 11B). To enhance protein purity, various chromatography methods were applied.

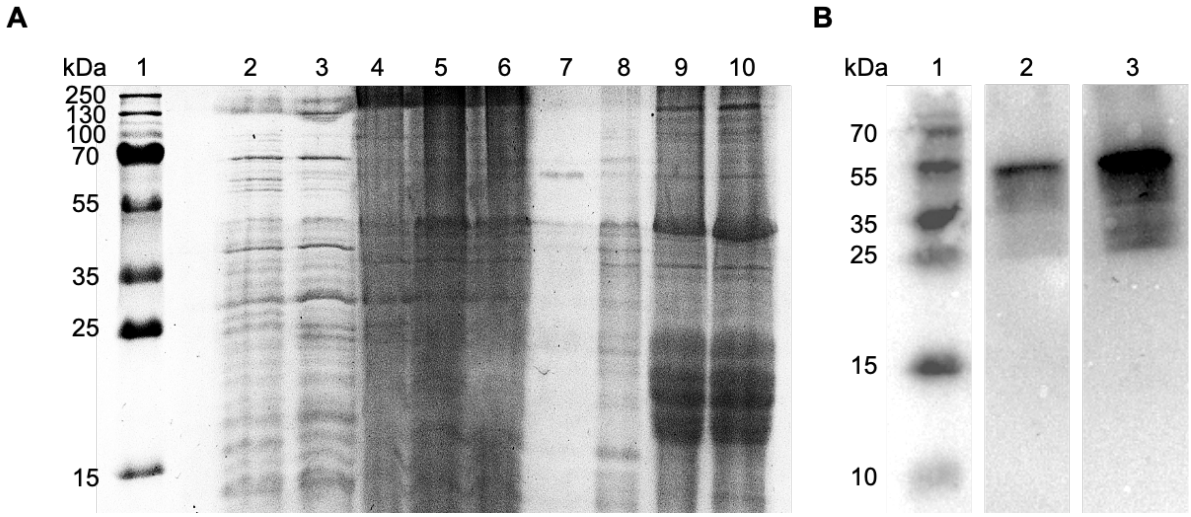

Figure 11: Detection of MRAP2 by gel electrophoresis and immuned-based detection. (A) SDS-PAGE of native MRAP2. The presence and purity of the isolated protein was analyzed by SDS-PAGE using a 15% TRIS-Glycine gel. During protein purification different samples were collected and loaded onto the SDS-PAGE. 1: Marker *PageRuler Plus Prestained*, 2: *E. coli* cells before IPTG, 3: *E. coli* cells after IPTG, 3: cell pellet after second lysis, 5: lysate after second lysis 6: flow through, 7: wash fraction 1 with 10mM Imidazole, 8: wash fraction 2 with 20mM Imidazole, 9-10: elution fractions with 300 mM Imidazole. The molecular weight of the marker ranges from 15 kDa to 250 kDa in this figure. **(B) Western blot of the isolated protein**. To confirm the presence of the correct target protein Western blot analysis was performed. Primary antibody: anti-His antibody, secondary antibody: GAMPO antibody. 1: Marker *PageRuler Plus Prestained*, 2: MRAP2, 3: MRAP2.

4.2. Optimization of Protein Purification

To specifically remove contaminants that bind to the nickel resin similarly to the target protein, ion exchange chromatography (IEX) was employed. The sample was loaded to an anion exchange column, due to the target protein's isoelectric point (pI) of 5.23. Elution was carried out using a high-salt buffer containing 20 mM Tris/HCl and 1 M NaCl at pH 8. The results of the IEX chromatography are presented in Figure 12A. While the target protein remains present in the eluted fraction, the SDS-PAGE analysis reveals, the elution fraction still contains several other proteins.

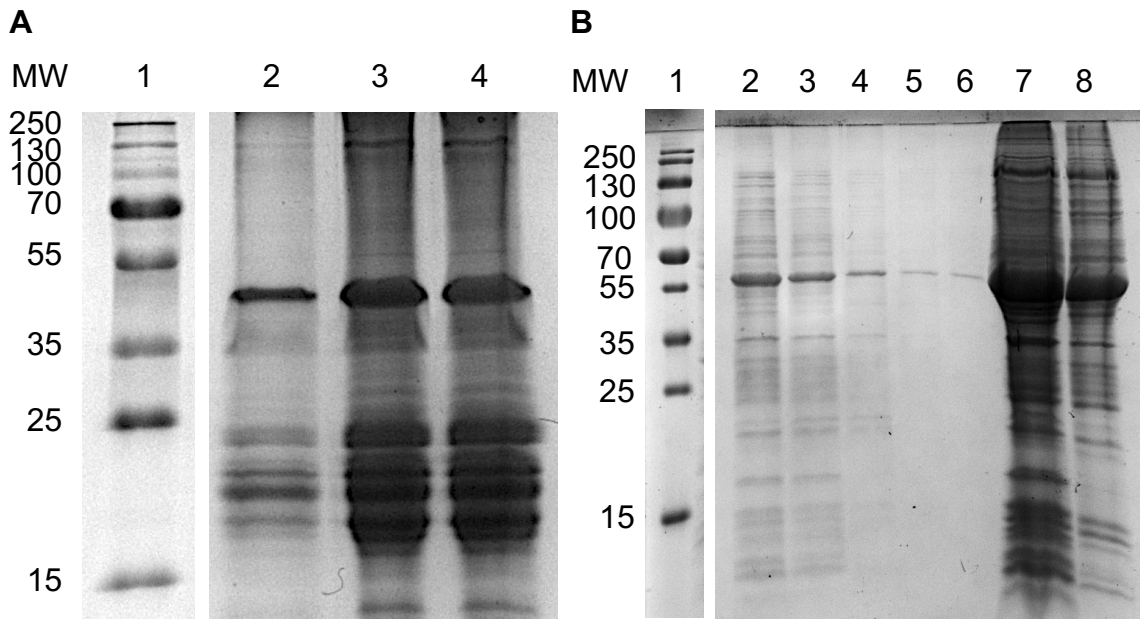

Figure 12: Evaluating the protein purity of MRAP2 after IEX chromatography. (A) SDS-PAGE of MRAP2 after IEX purifcation. The protein purity was evaluated by gel electrophoresis. During protein isolation different samples were collected and loaded onto the SDS-PAGE. 1: Marker *PageRuler Plus Prestained*, 2: wash fraction, 3: elution fraction 1, 4: elution fraction 2. **(B) SDS-PAGE of MRAP2 after IMAC purification and SEC.** The gel electrophoresis analysis shows the elution fractions (2-6) of MRAP2 after the protein was purified by gravity flow using Ni-NTA Agarose. Band 7 shows the concentrated MRAP2 after IMAC, while band 8 shows MRAP2 after SEC. The molecular weight of the marker ranges from 15 kDa to 250 kDa in both images.

While IEX chromatography was utilized to remove contaminants, such as additional proteins in the sample, based on their charge, SEC was performed to separate MRAP2 from other proteins in the sample based on their molecular weight (Figure 12B). The SDS-PAGE shows the direct comparison between the purification of MRAP2 by IMAC (bands 2-7) and after subsequent SEC (band 8). Especially the comparison between the concentrated MRAP2 sample after IMAC (band 7) and the MRAP2 sample after the SEC shows, that the SEC was more effective than IEX in removing additional proteins in the MRAP2 sample. The SEC profile of all MRAPS is shown in Figure 13. All MRAP samples elute at the same volume, between 40 ml and 50 ml. MRAP1 elutes at 49 ml, MRAP2 at 45 ml and MRAP2_2 at 42 ml from the SEC column. The chromatogram indicates multiple additional peaks in intensity for all MRAP samples.

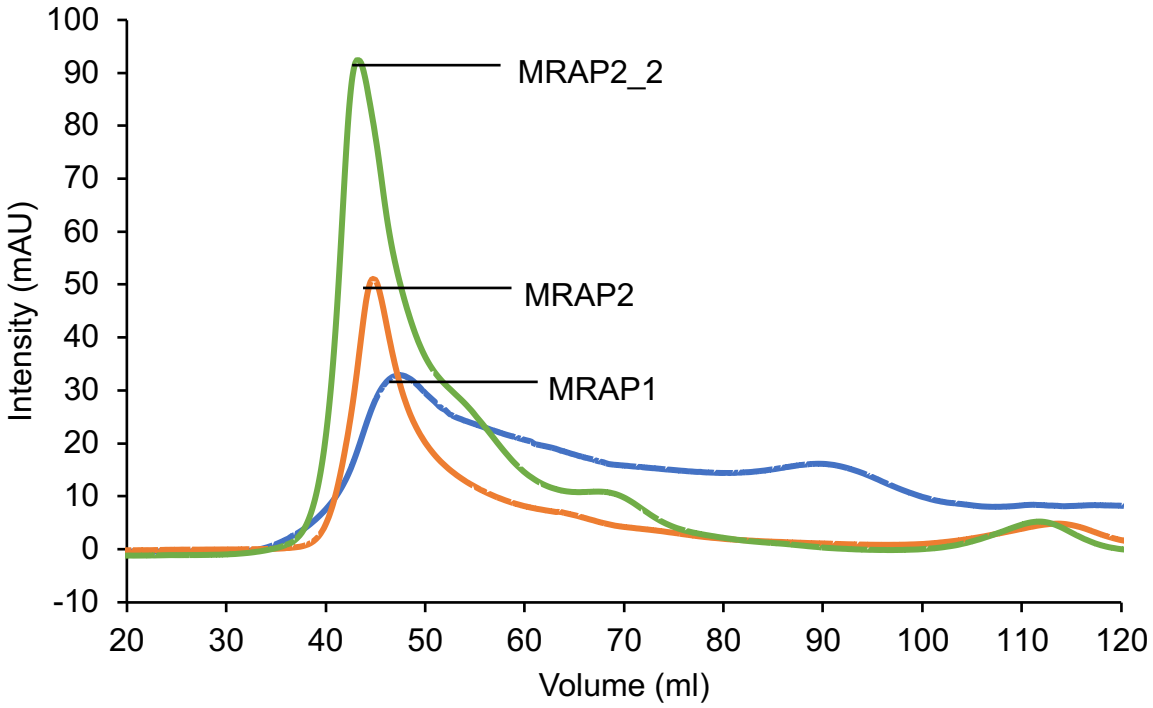

Figure 13: SEC profile of MRAPs. The intensity (mAU) is plotted against the elution volume (ml). MRAP1 (blue) is eluted from the column between 48 – 53 ml, while MRAP2 (orange) and MRAP2_2 (green) are eluted between 42 – 49 ml from the column. All samples show addition peaks/shoulders in the chromatogram. MRAP1 has broad shoulder between 53 - 69 ml and a peak in intensity at 90 ml. MRAP2 shows an additional intensity peak at 115 ml. MRAP2_2 has an absorbance shoulder between 52 – 66 ml and two peaks in intensity at around 69 ml and 112 ml. SEC of all MRAPS was performed using the ÄKTA pure™ chromatography and a Hi-load Superdex 200 16/600 pg column. Samples were injected manually and a flow rate of 0.5 ml was used. The run was performed at 7 °C.

In conclusion, all MRAPs were successfully purified. However, despite employing various additional purification methods, further improvement in protein purity was not achieved. Strong additional bands, particularly in the range between 15 kDa and 25 kDa, remain present in the samples. These proteins elute at the same time with the target protein and cannot be separated from it by either IMAC or IEX chromatography (Figure 11A/12A).

After applying SEC, many different proteins are still present in the sample. A major issue with the MRAP SEC profile is, that the MRAP proteins elute in the void volume of the HiLoad Superdex 200 16/600 pg column, which is at 40 ml. Despite the usage of 6 M of urea in the buffer. This can indicate, that the protein is too large and does not enter the pores of the column matrix. The protein may be forming oligomers or aggregates, which can be also seen in the SDS-PAGE, where the MRAP protein samples often remain gel pockets. Large aggregates elute early from the column, since they do not enter the pores of the column matrix. A possible solution would be to add

reducing agents like DTT to the protein sample or to the buffers used. Still after the addition of DTT, the SEC profile remained unchanged, and the MRAP samples still eluted in the void volume of the column (Figure 13). As mentioned, the SEC profile shows additional intensity peaks for all MRAPs besides the target protein peak. This could be caused by protein instability or proteolysis, leading to smaller protein fragments that elute later from the column. Additionally, non-specific interactions with the column may also contribute to these late eluting peaks.

Overall, the MRAP proteins exhibit an unusual or unfavorable SEC profile, suggesting that the protein samples do not properly enter the SEC column matrix. As a result, the MRAP proteins in the applied sample could not be effectively separated by size from other proteins present. This might explain why the purified SEC sample does not show a significant difference compared to the IMAC sample in the gel electrophoresis analysis (Figure 12B, Band 7/8).

Ultimately, the MRAP proteins were successfully purified, and the presence of the correct target protein was confirmed by Western blot, making the protein sample suitable for further characterization.

4.3. Metal binding of *E. coli* MRAP and MS Determination

To determine whether the purified MRAPs exhibit the spectral characteristics of a metalloprotein, as previously demonstrated by our group, EAS spectra were recorded for all isolated MRAP samples. All spectra displayed a peak at
410 nm, a feature commonly associated with Fe-binding proteins or metalloproteins. (Figure 14). The Figure shows two EAS of each MRAP construct, one MRAP sample without DTT and the other measured sample with 2 mM of DTT. It can be seen, that adding DTT to the sample shifts the spectrum and the absorbance peak at 410 nm to 420 nm. Taken together, the results show and confirm the presence of the metal characteristic feature in the recorded EAS.

Following these experiments, mass spectrometry was conducted on MRAP1 and MRAP2 to analyze their composition (Figure 15). This step was particularly important because the purified samples still displayed multiple bands, representing other proteins on the SDS-PAGE after applying various chromatography methods.

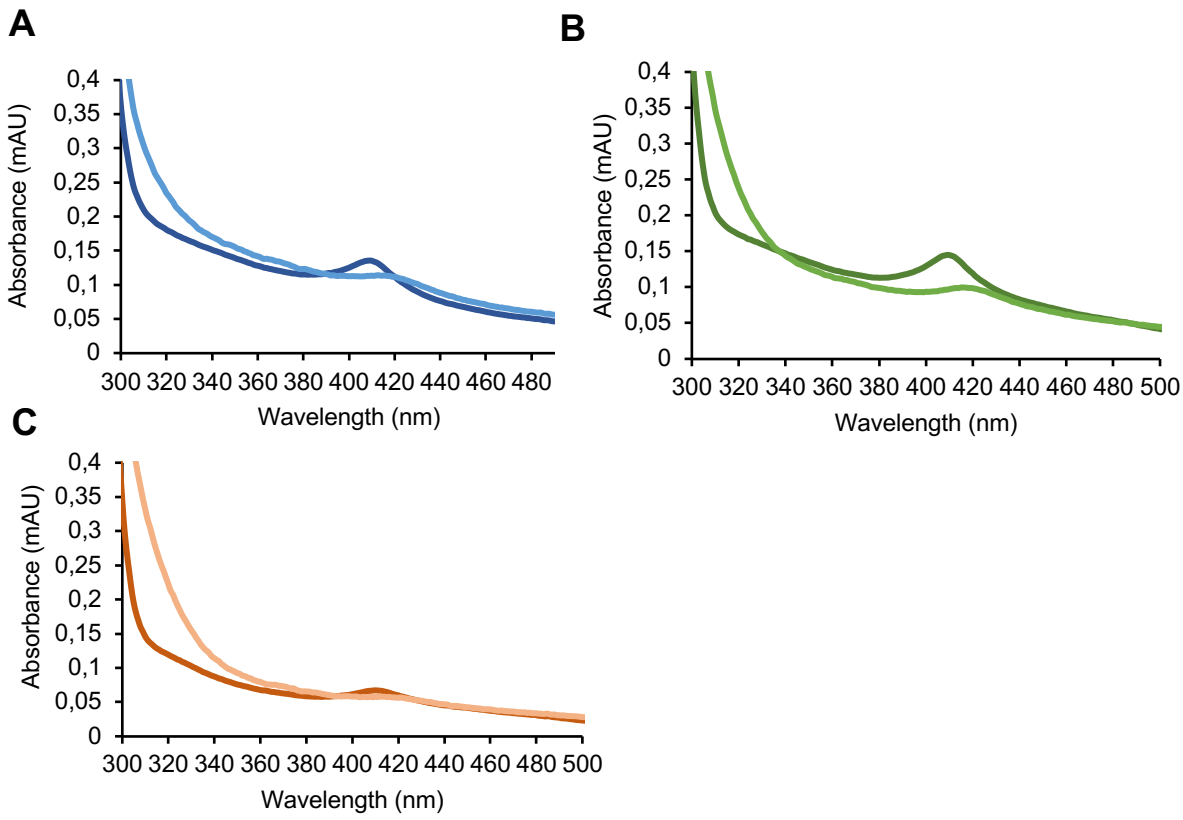

Figure 14: Electronic absorption spectrum of MRAPs. Plotted is the absorbance (mAU) against the wavelength (nm). All spectra were recorded at RT using the AGILENT Cary 60 Uv-Vis Spectrophotometer. As baseline, buffer containing 20 mM NaPi, 50 mM NaCl and 6 M Urea was used. For each protein, a spectrum was recorded in buffer both with and without DTT. **(A) EAS of MRAP1. (B) EAS of MRAP2. (C) EAS of MRAP2_2.** All proteins show a similar EAS. Proteins in buffer without DTT (dark blue, dark green, dark orange), show an absorbance peak at 410 nm, while DTT addition causes a shift in the EAS to 420 nm (light blue, light green, light orange).

Mass spectrometry (MS) measurements were performed by the proteomics laboratory at Heinrich Heine University in Düsseldorf and at Forschungszentrum Jülich. Different samples (gel extraction or in solution) were prepared and given to MS analysis. Figure 15A illustrates the analysis of MRAP1 and MRAP2 after IMAC purification. The analysis of both MRAP samples confirms sequence coverage after alignment with the *UniProt database*. However, the MRAP2 sequence coverage is higher compared to the sequence coverage of MRAP1. While the sequence coverage for MRAP2 aligns over 80% with the sequence from the database in both analyzed samples (solution and gel), MRAP1 sequence coverage is only at 37.5% in the solution sample and 27.2% in the gel sample. As noted earlier, multiple additional bands were observed on the SDS-PAGE of the purified MRAP samples. Figure 15B shows the results of the MS analysis

for the IMAC purified MRAP2 sample and shows, that several other proteins also have high sequence coverage.

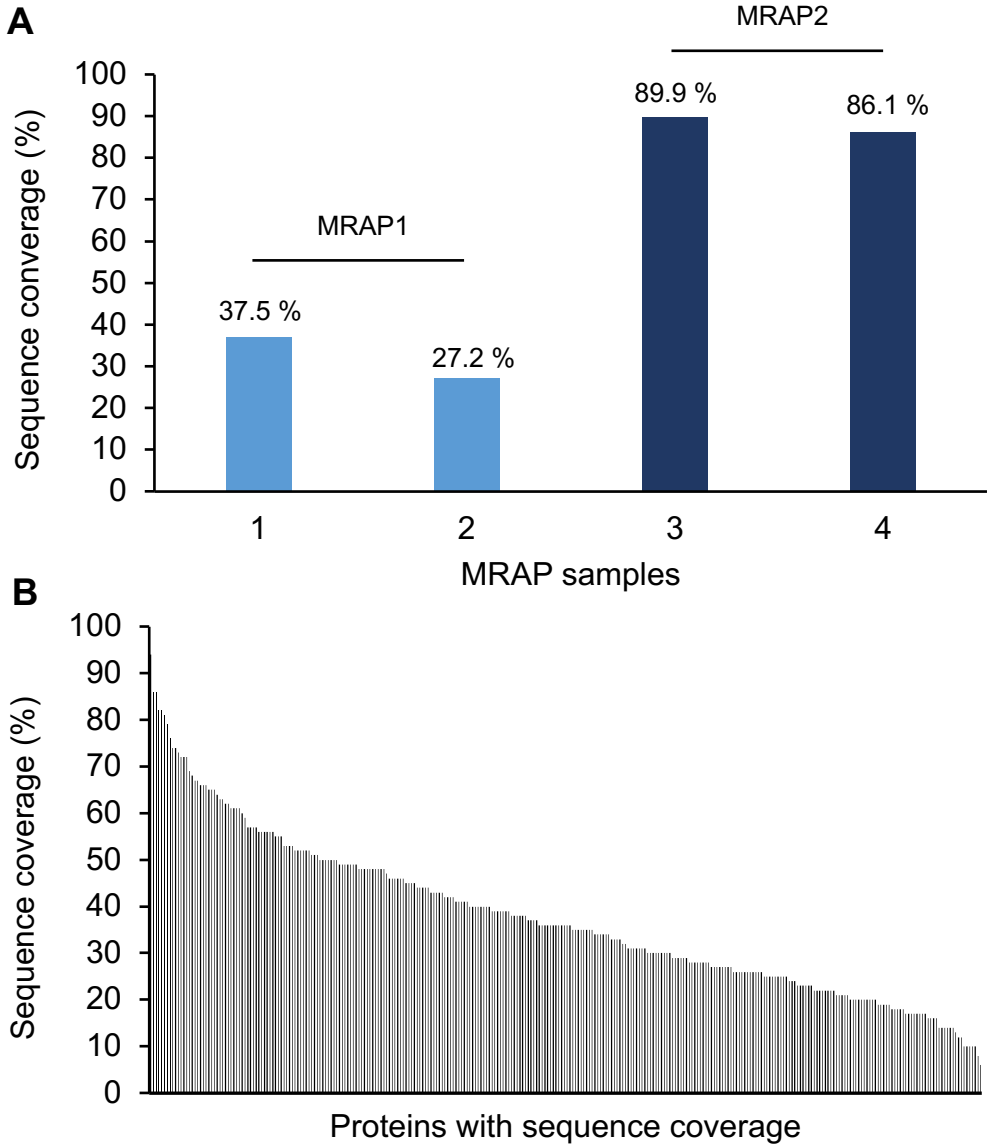

Figure 15: Results of Mass Spectrometry (MS) measurements. Depicted is the sequence coverage of the respective analyzed sample in %. **(A) MS analysis of MRAP1 and MRAP2**. The samples were measured in solution and as a gel sample. Based on a comparison with the sequence of the respective MRAP proteins and the comparison to the UniProt database, MRAP1 sequence coverage of the soluble sample was at 37.5% (1) and at 27.2% of the gel sample (2), while the sequence coverage of MRAP2 was at 89.9% of the soluble sample (3) and 86.1% of the gel sample (4). **(B) MS analysis of IMAC purified MRAP2 sample.** MRAP2 was analyzed, and the results were compared to protein sequences from the *UniProt* database.

The MS analysis results for MRAP2, shown that although the sequence of several other proteins aligns with the MRAP2 sequence, the sequence coverage of the target protein itself has still a high coverage, with a sequence coverage of approximately over

80% (Figure 15A). The results indicate, that the metal binding feature, seen in the electronic absorption spectrum of the MRAPs, could be influenced by other proteins in the sample, especially since there are metalloproteins or proteins that transport electrons present in the purified sample. NADH-quinone oxidoreductase subunit F for instance, which had a sequence coverage of 76%, binds NADH and is associated with an Fe-S-center.[88] Another example is the citrate synthase, which is capable of binding divalent metal ions and had a sequence coverage of 56%. Consequently, it appears possible that the EAS of MRAP2 is influenced *E. coli* proteins present in the sample.
To further analyze this outcome and determine whether MRAP2 is responsible for the characteristic Fe absorption peak at 410 nm in the spectrum, various MRAP1 and MRAP2 mutants were generated. In the predicted metal-binding site of MRAP1 and MRAP2, the potentially coordinating amino acids cysteine and histidine were substituted with alanine. This modification aimed to assess, whether the characteristic absorption peak would remain detectable in the EAS.

4.4. Cloning, Expression and Purification of MRAP Mutants

In metalloproteins, cysteine and histidine are known as key amino acids for coordinating metals.[89] Therefore, the approach involved replacing these amino acids in the predicted metal-binding sites of MRAP1 and MRAP2 with alanine, a residue that does not coordinate metals.
For this purpose, six different constructs were designed, each with a single cysteine or histidine replaced by alanine, or both amino acids substituted. After successful cloning and sequence validation via Sanger sequencing, the substitution of histidine by alanine was unsuccessful. Therefore, experiments were conducted with the MRAP Cys and Cys-His mutants (M1_C96A, M2_C132A, M1_C96A_H97A, M2_C132A_H133A), leading to a total of four different constructs. All constructs were expressed under the same conditions as the native MRAPS in *E. coli* Rosetta cell strain. Cell growth was monitored by measuring the OD_{600} every 30 minutes to determine potential differences between the wild-type forms of MRAP1 and MRAP2 and their respective mutants. After protein expression, all proteins were purified using IMAC. Protein purity was analyzed by SDS-PAGE, and the presence of the target protein was confirmed through Western blot analysis. Finally, the EAS spectra of all isolated proteins were recorded.

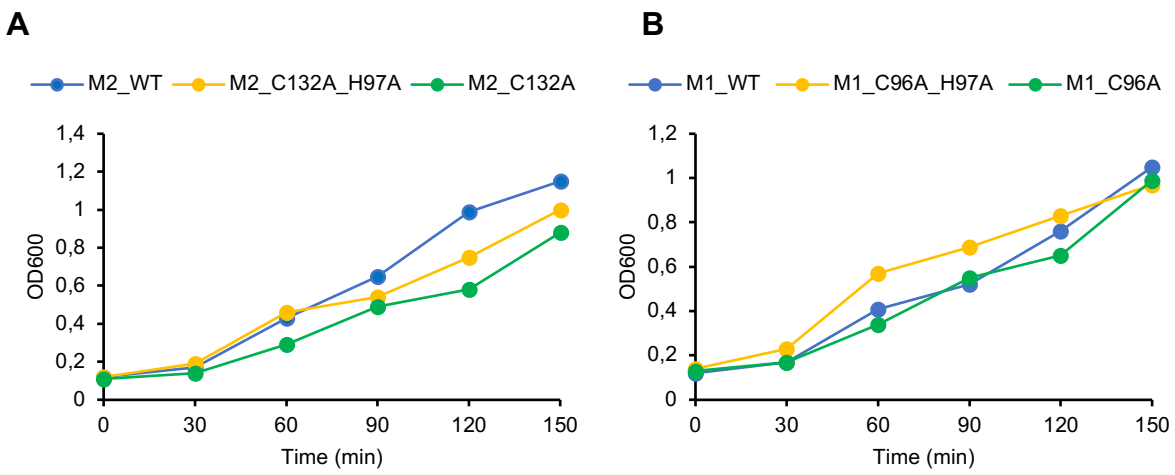

Figure 16: Monitoring *E. coli* cell growth during MRAP protein expression. The cell growth was monitored by measuring the optical density at 600 nm (OD_{600}) every 30 minutes for 150 minutes. Cells were grown in 2YT medium, supplemented with $FeCl_2$ and 50 µg/ml kanamycin at 37 °C and 120 rpm. MRAP protein overexpression was induced using 1 mM IPTG after an OD_{600} of around 1 was reached and the cell culture incubated at 27 °C o/n. The figure illustrates the cell growth of wild-type MRAP1/2 (blue), the cysteine-histidine mutant of MRAP1/2 (M1_C96A_H97A, M2_C132A_H133A), and the cysteine mutant of MRAP1/2 (M1_C96A, M2_C132A). **(A) *E. coli* growth curve of all MRAP1 proteins.** The cell growth of all proteins starts at the same OD_{600} and reach an optical density of 1 after 150 min. **(B) *E. coli* growth curve of all MRAP2 proteins.** Cell growth starts at an OD_{600} of 0.11 for all cell cultures. After 150 min, M2_WT reaches an OD_{600} of 1.2, M2_C132A_H133A an OD_{600} of 1 and M2_C132A OD_{600} of 0.8.

Since alteration were introduced in the metal binding site of MRAP1 and MRAP2, the cell growth was monitored, because the modification might result in slower cell growth. Figure 16A shows the *E. coli* cell growth for MRAP1, while Figure 16B illustrates the growth for MRAP2. For MRAP1, all constructs started with the same OD_{600} of 0.19. During the cell growth process, all constructs had a similar growth pattern. However, the growth of M1_C96A_H97A is faster in the beginning compared to the M1_WT and M1_C96A. In the end, for M1_WT, a cell pellet of 8.2 g was harvested, for M1_C96A_H97A, a cell pellet of 6.1 g, and for M1_C96A, a cell pellet of 9.6 g was obtained.

The growth curve for the MRAP2 constructs show a slightly different behavior between the three constructs. M2_WT shows a faster cell growth in the exponential phase (Figure 16B), compared to the mutants. In the end for M2_WT a cell pellet of 5.8 g, for M2_C132A_H133A a cell pellet of 4.4 g, for M2_C132A 7.3 g was harvested.

After cell harvest, the target proteins were successfully purified by IMAC under the same conditions. As an example, the results of the purified cysteine mutants can be seen in Figure 17. The SDS-PAGE (Figure 17A) displays the elution fractions of the target proteins. M1_C96A, which has a molecular weight of 32 kDa, is observed in the elution fractions (bands 2-6) around 40 kDa. In this analysis, MRAP1 appears at the expected molecular weight on the SDS-PAGE, indicating that MRAP1 was not successfully isolated in the first purification shown in Figure 10B, where it was observed at a lower molecular weight.
M2_C132A has a molecular weight of 36 kDa and runs on the SDS PAGE at 55 kDa. The Western blot the presence of both target proteins in the elution fractions.

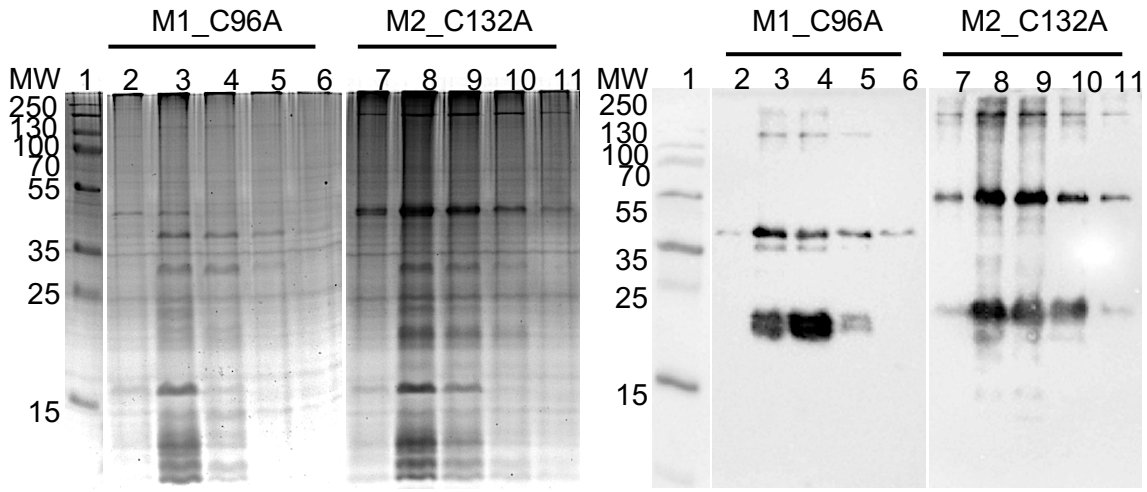

Figure 17: Purification of mutant variants of MRAP1/2. (A) SDS-PAGE of cysteine mutants M1_C96A, M2_C132A. Displayed is the performed gel electrophoresis of the elution fractions during MRAP protein purification. The gel shows the purified protein. **(B) Western blot of cysteine mutants M1_C96A, M2_C132A.** To confirm the presence of the correct target protein, a Western blot was performed. The elution fractions contain the the target protein sample. Primary antibody: anti-His antibody, secondary antibody: GAMPO antibody. 1: Marker *PageRuler Plus Prestained*, 2-6: elution fractions MRAP1, 7-11: elution fractions MRAP2. The molecular weight of the marker ranges from 15 kDa to 250 kDa.

After successful purification, and confirmation by SDS-PAGE and Western blot, the EAS of all isolated proteins was recorded (Figure 18). As a control, PLpro (papain-like protease), a protein that exhibits no distinct absorbance peak in the spectrum, was measured in 3 M urea buffer (Figure 18, black spectrum). Shown is an overview of the EAS spectra for MRAP1 and MRAP2, along with a close-up of the spectrum. The wild-type form of MRAP1 and MRAP2 both exhibit an absorbance peak at 410 nm, while the control sample does not show a peak in intensity at 410 nm. This concludes, that

the introduced mutation in the predicted metal binding site of both proteins, did not have an influence on the EAS.

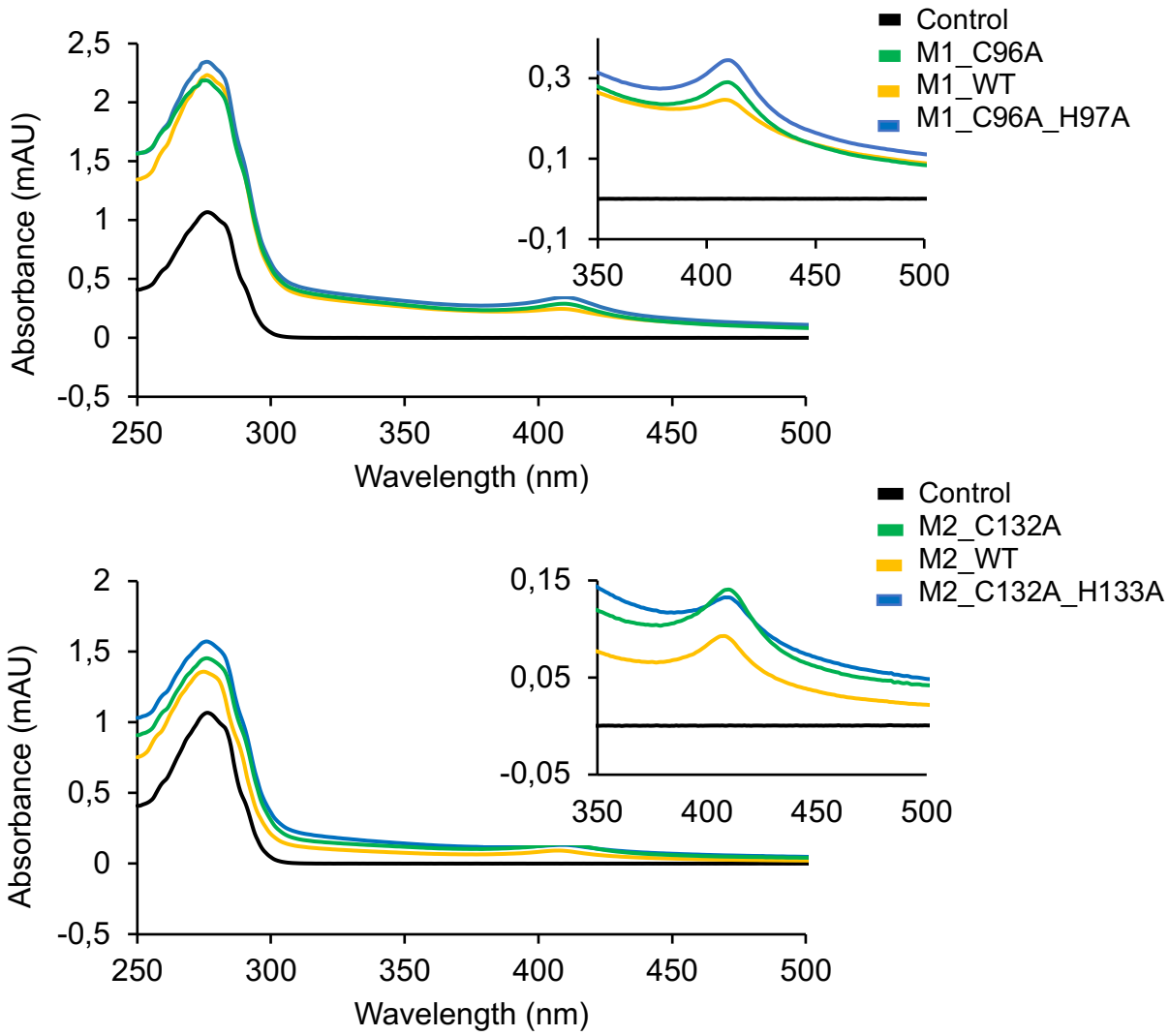

Figure 18: Characterization of MRAP electronic absorption spectrum. Plotted is the absorbance (mAU) against the wavelength (nm). As baseline, buffer containing 20 mM NaPi, 50 mM NaCl and 6 M urea was used. Both figures show a peak in intensity at 410 nm. **(A) EAS of MRAP1.** Shown, is an overview of the spectrum of MRAP1 cysteine mutant (M1_C96A, green), MRAP1 cysteine-histidine mutant (M1_C96A_H97A, blue), MRAP1 wild-type (M1_WT, yellow) and a control sample (PLpro papain-like protease, black). As a control, a protein with no visible electronic spectrum was used. **(B) EAS of MRAP2.** MRAP2 cysteine mutant (M2_C132A, green), MRAP2 cysteine-histidine mutant (M2_C132A_H133A, blue), MRAP2 wild-type (M2_WT, yellow) and a control sample (PLpro papain-like protease, black).

Taken together, the cloning, protein expression and purification of the MRAP mutants was successful. Despite modifications to the predicted metal-binding motifs (CYS-LEU-PRO-CYS-HIS in MRAP1 and ALA-LYS-ALA-CYS-HIS in MRAP2), no significant differences were observed in either cell growth (Figure 16) or EAS analysis (Figure 18). Since we substituted the metal coordinating amino acids, CYS and HIS, in the

predicted iron-binding motif, the absorbance peak should be absent in the mutant samples. However, as this could not be confirmed in the electronic spectrum, the peak could originate from MRAP itself or from an *E. coli* protein capable of metal binding. Additionally, since this is only a predicted metal-binding site and mutations were only introduced at this location, the involvement of other amino acids in metal coordination cannot be excluded.

To gain further insights into MRAP2 and exclude the possibility that the metal spectrum originates from an *E. coli* protein, the next step was to recombinantly express MRAP2 in *Sf*9 insect cells using the baculovirus expression system.

4.5. Recombinant Protein Production of MRAP in *Sf*9 cells

The baculovirus expression system (BVE) is widely used for protein expression, in insect and mammalian cells.[90] Within this work, the BVE protein expression system was utilized for two target proteins.

To determine whether protein expression could be improved and to investigate, if the EAS of MRAP2 isolated from insect cells would also exhibit the absorbance peak at 410 nm, different MRAP2 constructs were generated (Figure 19). The constructs, that were generated both contained a Twin-Strep-Tag and a 10xHis-Tag for protein purification to improve protein purity. The second construct contained two copies of the MRAP2 genes, to allow in and out orientation of the protein and therefore the formation of an antiparallel homodimer.

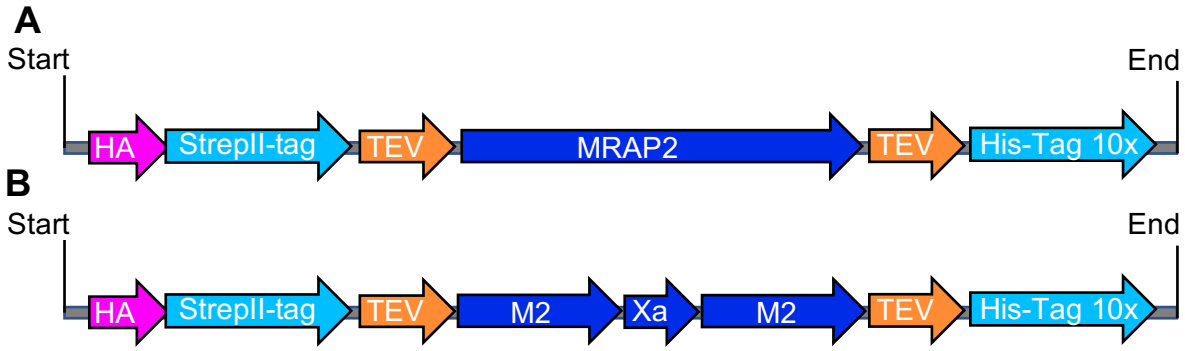

Figure 19: Design of constructs of MRAP2 for *Sf*9 insect cells. Depicted are the components of the two MRAP constructs, which were used for recombinant protein expression in *Sf*9 insect cells (A: MRAP2, B: MRAP2_2). Both constructs consist of a HA-signal (pink), a twin-strep-tag (cyan), a TEV cleavage site (orange), one copy or two copies of the MRAP2 gene (blue), followed by a second TEV cleavage site (orange) and 6xHistidin-tag (cyan). For MRAP2_2, the two copies of the gene are separated by factor Xa (blue). Plasmid design was carried out by using *SnapGene.*

After cloning, the correct sequence was confirmed by sanger sequencing and the bacmid prepared. The correct bacmid was analyzed by agarose gel electrophoresis. Subsequently, the virus was prepared. Cells were transfected with the bacmid and incubated for 4 days. The viral infection process was documented through microscopic imaging of the cells (Figure 20). At the initial stage of virus infection, the cells appear large and round, displaying the typical shape of *Sf*9 cells. After 48 hours of incubation with the virus, the cells begin to lose their shape. By 72 hours post-infection, the cells have visibly lost their typical morphology and have become significantly enlarged. After 4 days of incubation with the baculovirus, the cells are clearly infected, and harvesting was carried out. The supernatant, containing the virus, was used for further infection of *Sf*9 with baculovirus for recombinant protein production of MRAP2 and MRAP2_2.

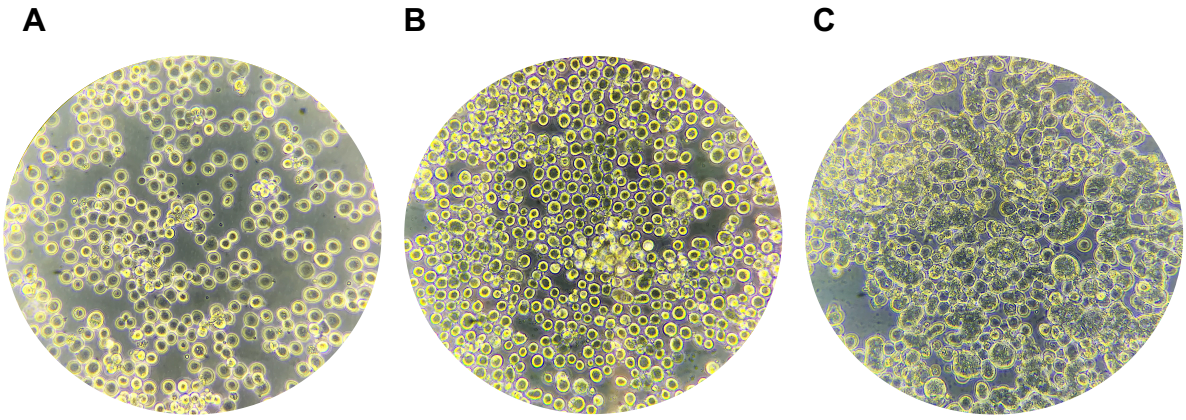

Figure 20: Microscope images of *Sf*9 cells during baculovirus infection. During different stages of virus infection, images were taken of the *Sf*9 cells with a 20x magnification. **(A) *Sf*9 cells at initial stage (T=0)**. The image shows the cells immediately after the addition of baculovirus. The cells have the typical characteristics of insect cells, displaying a large and rounded morphology. **(B) *Sf*9 cells 24 h post infection (T=24).** After 24 h of incubation, the cell morphology looks different as compared to the beginning. **(C) *Sf*9 cells 72 h post infection (T=72).** The image shows, that most of the cells lost their conventional cell shape and have increased in size.

After virus preparation, expression tests were carried out with different ratios of baculovirus to *Sf*9 cells. Cells were harvested after 2 days of incubation with the baculovirus and a sample of the cell pellet analyzed by gel electrophoresis as well as Western blot analysis. The results show that MRAP2 is present in all loaded samples, however, MRAP2_2 could not be detected (Figure 21). Therefore, protein expression was further carried out with MRAP2 construct and not MRAP2_2.

4.6. Protein Purification of MRAP2 by Strep-tag

The next step was to solubilize the protein, as it was still present in the cell pellet. For protein purification or solubilizing the protein, the same protocol as for MRAP2 *E. coli* expression was used. Therefore, the harvested cell pellet was resuspended in NaPi Buffer with 6 M of urea and loaded onto the SDS-PAGE.

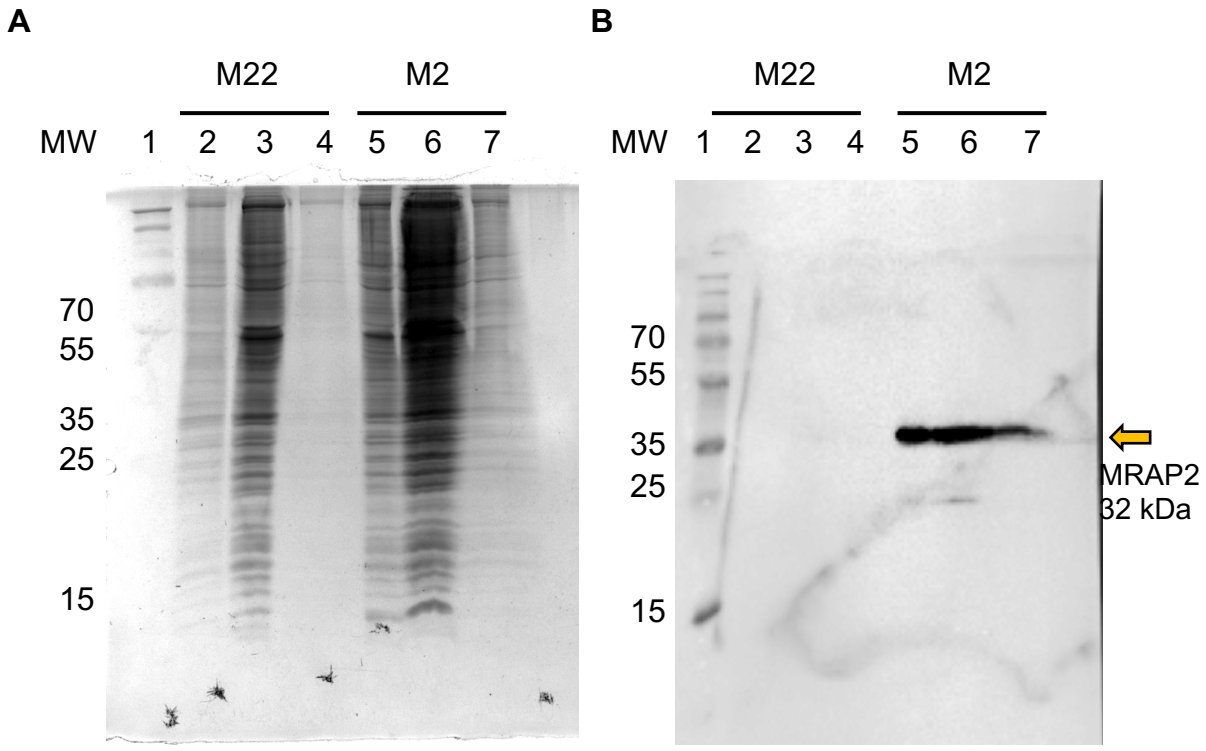

Figure 21: Detection of MRAP2 in *Sf*9 cells. The gel electrophoresis (A) as well as the Western blot (B) shows the MRAP2_2 samples (2-4) and the MRAP2 samples (5-7). The cell culture was harvested after protein expression, and the cell pellet was tested for the target protein. The cell pellet was resuspended in buffer and different dilutions loaded onto the SDS-PAGE. Primary antibody: anti-His antibody, secondary antibody: GAMPO antibody. 1: *PageRuler Plus Prestained,* 2-4: MRAP2_2 cell pellet resuspended in buffer, 5-7: MRAP2 cell pellet resuspended in buffer.

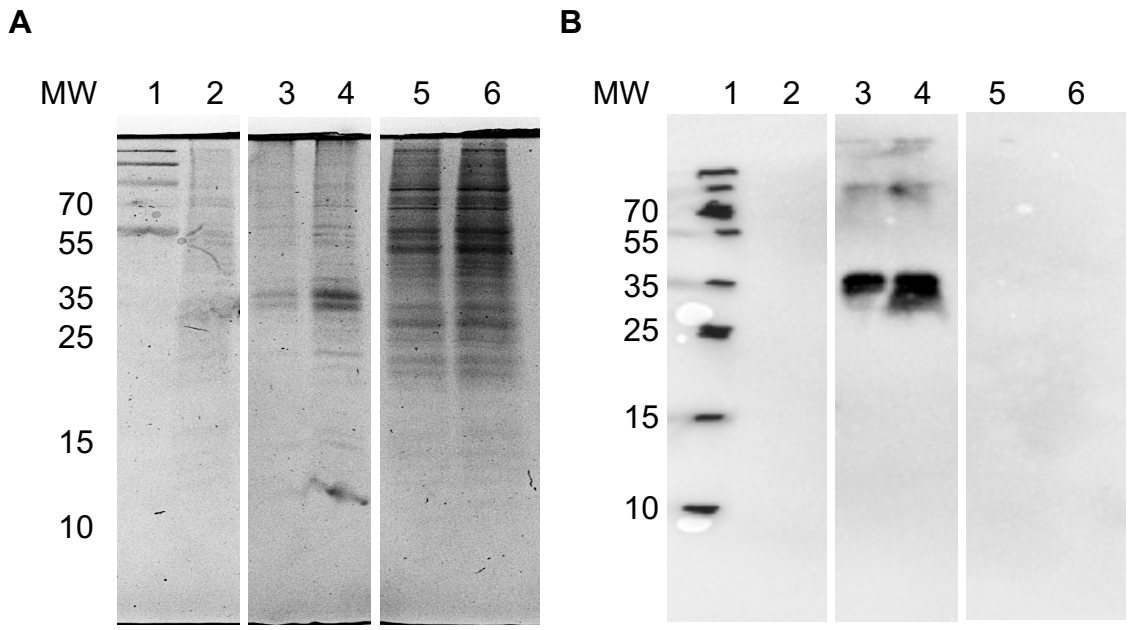

Figure 22: Solubilization of MRAP2. The SDS-PAGE and the Western blot analysis (B) show the result of solubilization of the MRAP2 protein in comparison to empty insect cells as a control (band 2). The Western blot shows a distinct band in both cell pellet samples of MRAP2 at 35 kDA (3,4) and no detected antibody signal in the supernatant (5,6). The cell culture was harvested at 4 °C and 500 × g, and the resulting cell pellet was resuspended in urea buffer (20 mM NaPi, 50 mM NaCl, 6 M urea) before being lysed by sonication. The lysate was then centrifuged at 40,000 × g for 45 minutes, and both the cell pellet and the supernatant (soluble fraction) were analyzed for MRAP2. 1: *PageRuler Plus Prestained*, 2: control, 3/4: MRAP2 cell pellet, 5/6: MRAP2 supernatant. Primary antibody: anti-His antibody, secondary antibody: GAMPO antibody.

The results show, that MRAP2 could be detected in both loaded samples (different dilutions) in the cell pellet. However, MRAP2 was not detected in the supernatant, which concluded that solubilizing the protein with 6 M urea was not successful.

Protein expression was performed again, and this time a Strep-tag was used for purification, following a Strep-tag-specific purification protocol. The obtained cell pellet was resuspended in luciferase cell culture lysis buffer (Tris-HCl pH 7.4 - 8.0, NaCl 150 mM, 1% v/v Triton X-100, 1,2-Diaminocyclohexane-N,N,N′,N′-tetraacetic acid CDTA 1 mM, 10% v/v Glycerol, protease inhibitor). The result of the strep-tag purification is displayed in Figure 23.

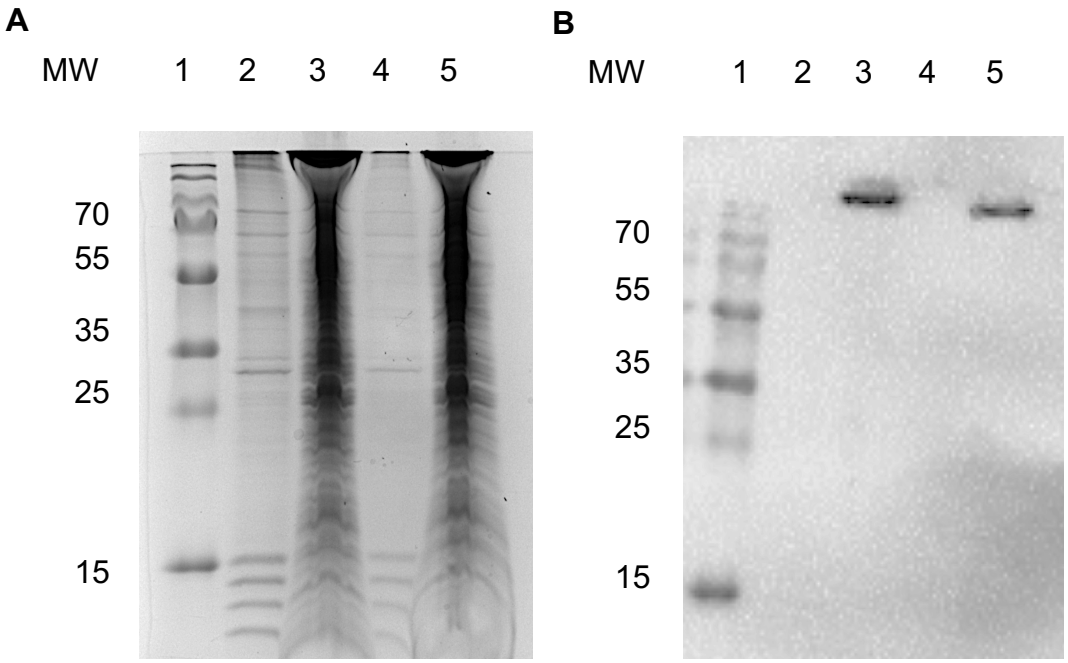

Figure 23: Analysis of MRAP2 from *Sf*9 cells. (A) SDS PAGE of MRAP2 and Western blot (B). The cell pellet was resuspended in lysis buffer Tris-HCl (pH 7.4 - 8.0), NaCl 150 mM, 1% v/v Triton X-100, 1,2-Diaminocyclohexane-N,N,N′,N′-tetraacetic acid CDTA 1 mM, 10% v/v Glycerol, Protease inhibitor) and incubated for 20 min at RT. Subsequently, the lysate was clarified by centrifugation at 40.000xg for 45 min. The cell pellet (2,4) as well as the supernatant (3,5) was evaluated by gel electrophoresis. 1: *PageRuler Plus Prestained*, 2/4: MRAP2 cell pellet, 3/5: MRAP2 supernatant. Primary antibody: anti-His antibody, secondary antibody: GAMPO antibody.

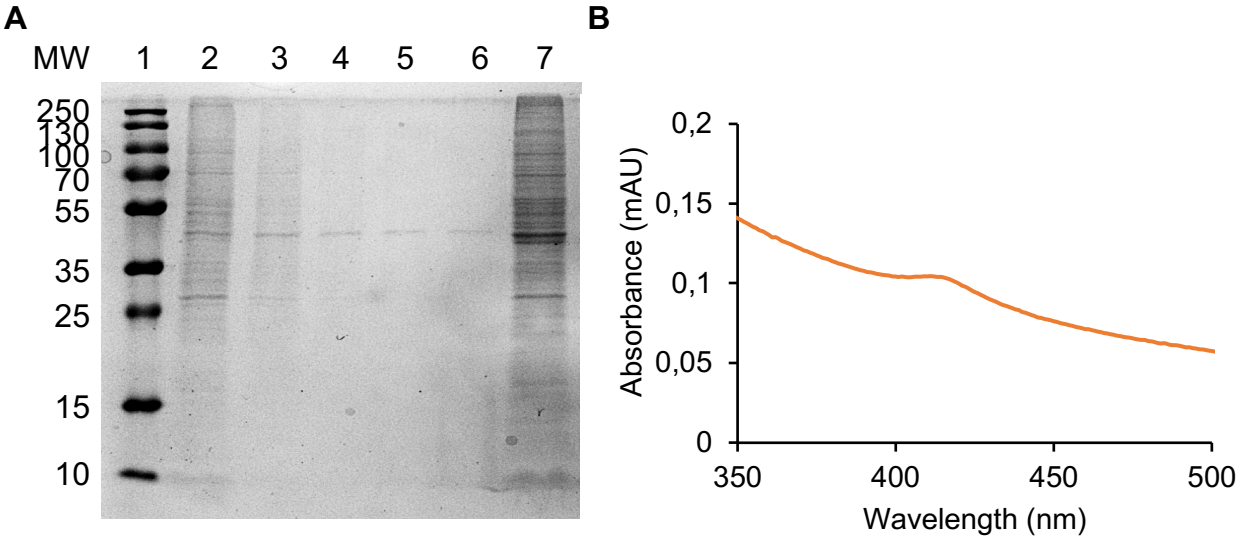

Figure 24: Characterization of MRAP2 from *Sf*9 cells. (A) SDS PAGE of *Sf*9 MRAP2 purification using strep-tag. The image shows the elution fractions (2-6), collecting during protein purification. Band 7 shows the concentrated samples of Sf9 MRAP2 after dialysis. As a marker the *PageRuler Plus Prestained* was used, which ranges from 10-250 kDa in this figure. **(B) EAS of *Sf*9 MRAP2.** Plotted is the absorbance (mAU) against the wavelength (nm). As baseline, strep tactin buffer was used. The spectrum shows an intensity peak at 410 nm.

Taken together, the bacmid and baculovirus preparation for MRAP2 were successful. The cells were visibly infected, and the expression test showed a positive Western blot signal for MRAP2, but not for MRAP2_2. Comparing the cell pellet to the supernatant can be challenging, as the cell pellet is typically much more concentrated. Furthermore, the protein was still stuck in the cell pellet and remained insoluble (Figure 23B). The attempt to solubilized the protein with luciferase cell culture lysis buffer seem to be successful (Figure 23B). The lysis buffer contains 1% v/v Triton X-100 as a detergent to solubilize the membrane fraction.

However, the protein sample was still stuck in the pocket of the SDS-PAGE, which could be caused by aggregation of the protein or formation of oligomers. Since the lysis buffer additionally contained glycerol, this could also lead to higher viscosity of the loaded sample and therefore the sample is stuck in the gel pockets. The MRAP protein being stuck in the gel pockets is commonly problem which occurred with this protein due to the formation of oligomers. After the Strep-tag purification, the SDS-PAGE showed several bands. However, when comparing the SDS-PAGE in Figure 24 to the Western blot in Figure 22B, the size of the purified MRAP2 proteins differs from the expected size. The construct has a size of 31.5 kDa, but no band could be detected at this size on the SDS-PAGE. Still, it is difficult to visualize the protein directly on the gel due to the relatively low yield, which may be insufficient for detection by gel electrophoresis alone. It is possible, that the protein is present, but in very low quantities. Therefore, a Western blot, which is more sensitive, should be performed.

Interestingly, the recorded EAS in Figure 24B closely resembles the EAS of *E. coli* MRAP2. This suggests that the peak in intensity at 410 nm is not caused by other impurities, but rather by MRAP2 itself. To further analyze this outcome, the purified MRAP2 protein from Figure 24B should be sent for MS measurement.

4.7. Recombinant Protein Production of hNET in *Sf*9 cells

The human Norepinephrine Transporter (hNET) is responsible for the recycling of Norepinephrine in the synaptic cleft. A dysregulation leads to cardiovascular diseases, making the transporter an interesting pharmaceutical target.[48] Since hNET is a protein with several posttranslational modifications the Baculovirus Expression System (BVE) was chosen for recombinant protein production. This part of this thesis was part of a joined research project with the group of Dr. Aldino Viegas from the *NOVA School of Science and Technology* in Lisbon.

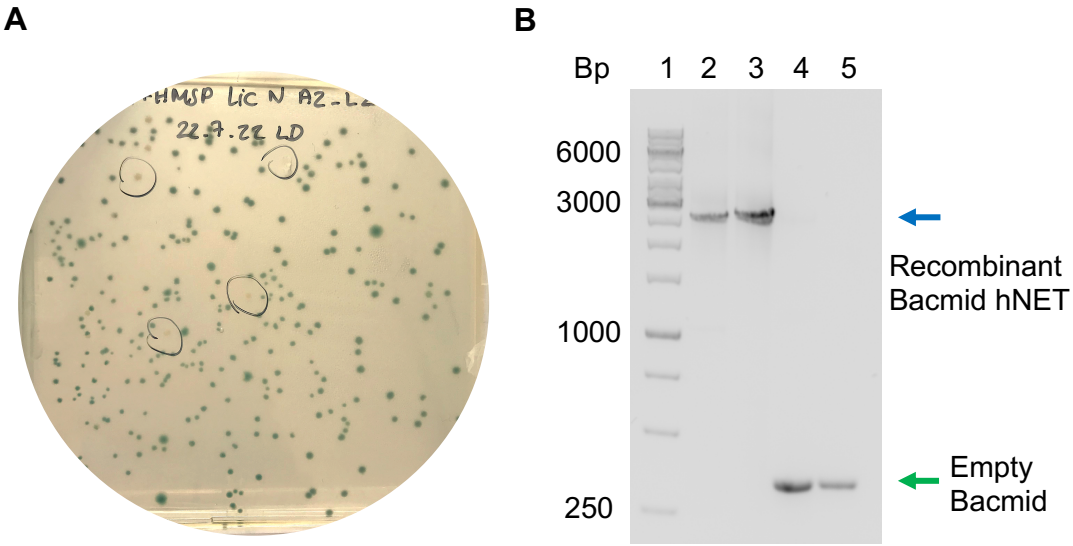

Figure 25: Bacmid preparation of hNET. (A) X-gal screening of recombinant colonies. The hNET DNA was transformed using DH10Bac chemical competent cells and plated out onto agar plates containing IPTG, X-gal, tetracycline and kanamycin. Plates were incubated for 3-4 days at 37 °C. Subsequently, the Bacmid DNA from the positive white colonies was isolated. The blue colonies contain no recombinant Bacmid DNA. **(B) Agarose gel of Bacmid.** The isolated Bacmid DNA was analyzed using gel electrophoresis. The recombinant Bacmid DNA (blue arrow) was loaded as well as empty Bacmid (green arrow). 1: DNA Ladder GeneRuler 1 kb, 2/3: hNET Bacmid, 4/5: empty Bacmid. The marker ranges from 250 bp to 6000 bp.

Different constructs were generated in advance by the group of Dr. Aldino Viegas and the plasmid DNA provided for us. In total 6 different constructs were generated, which included different truncated versions of hNET. The initial approach involved transforming all hNET constructs into Bac10 *E. coli* chemically competent cells. However, subsequent experiments were carried out only with the full-length hNET construct. The protocol for preparing the bacmid and baculovirus was the same as in

the expression of MRAP in *Sf*9 cells. Figure 25 shows the results of the generation of bacmid. After successful transformation of the plasmid into chemical competent cells, the cells were plated out for blue-white screening. The image of the agar plate is displayed in Figure 25A. The white colonies, containing the recombinant bacmid, were isolated and analyzed by agarose gel electrophoresis. The agarose gel shows two samples of the purified recombinant bacmid (blue arrow) and two samples of empty bacmid (green arrow). The target bacmid has the correct molecular weight of 2756 bp. Subsequent to bacmid preparation, the baculovirus was prepared as describe in the methods. After virus preparation, expression tests were carried out and Western blot analysis performed to detect the target protein. Besides the sample possible containing the target protein, a negative control (*Sf*9 cells) and positive control (His-tagged protein) were loaded. The results show, no detection of hNET in the loaded sample on the Western Blot, but a clear signal for the positive control, concluding that the target protein was not present in the sample.

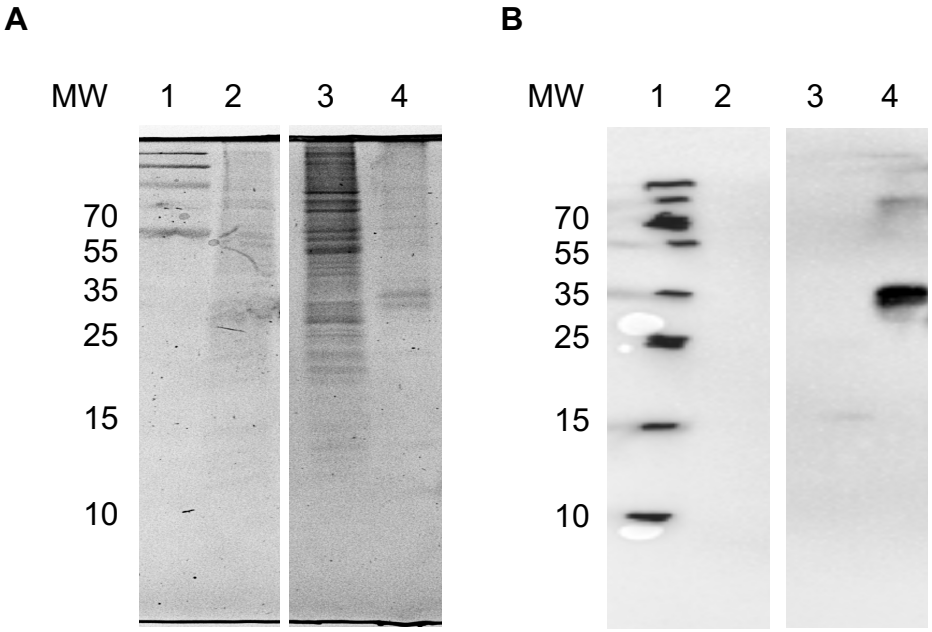

Figure 26: Detection of hNET. hNET protein expression in *Sf*9 cells was performed and the cell culture harvested by centrifugation. The resulting cell pellet was tested for the target protein and analyzed by gel electrophoresis and Western blot. *Sf*9 cells were used as a negative control, while a His-tagged protein served as a positive control. 1: PageRuler Plus Prestrained, 2: negative control (*Sf*9 cells), 3: hNET cell pellet, 4: positive control (His-tagged protein). **(A) SDS PAGE of hNET. (B) Western blot of hNET.** The analysis shows a signal for the positive control, whereas no signal was detected in the hNET cell pellet (band 3).

Taken together, the Bacmid was successfully prepared, as confirmed by agarose gel analysis. However, when the Bacmid DNA was sent for Sanger sequencing, the samples could not be sequenced, due to its large size. Despite this, since the Bacmid

DNA appeared at the correct molecular weight, the baculovirus preparation and protein expression were further proceeded with. Ultimately, after performing several Western blots and expression tests, hNET could not be detected in any sample, leading to the conclusion that recombinant protein expression in Sf9 cells was unsuccessful with the construct used. Since expression with our construct did not work out, a next step could be to use a different vector, such as the original pFASTBac vector that was successfully used in this thesis for MRAP2 production in *Sf*9 cells. For our approach, the pFHMSP-LIC-N was used with an N-terminal HIS-tag. The vector is suitable for insect cell expression. The vector is a derivative of the pFASTBac vector, with an additional honeybee melittin signal sequence placed before the His-tag. Further optimization could be incorporating different affinity tags, like a FLAG-tag or Strep-tag, could improve protein purification and detection. Before optimization could be carried out, the cryo-EM structure of hNET was published by Tan et al. in 2024 (Figure 27).[91]

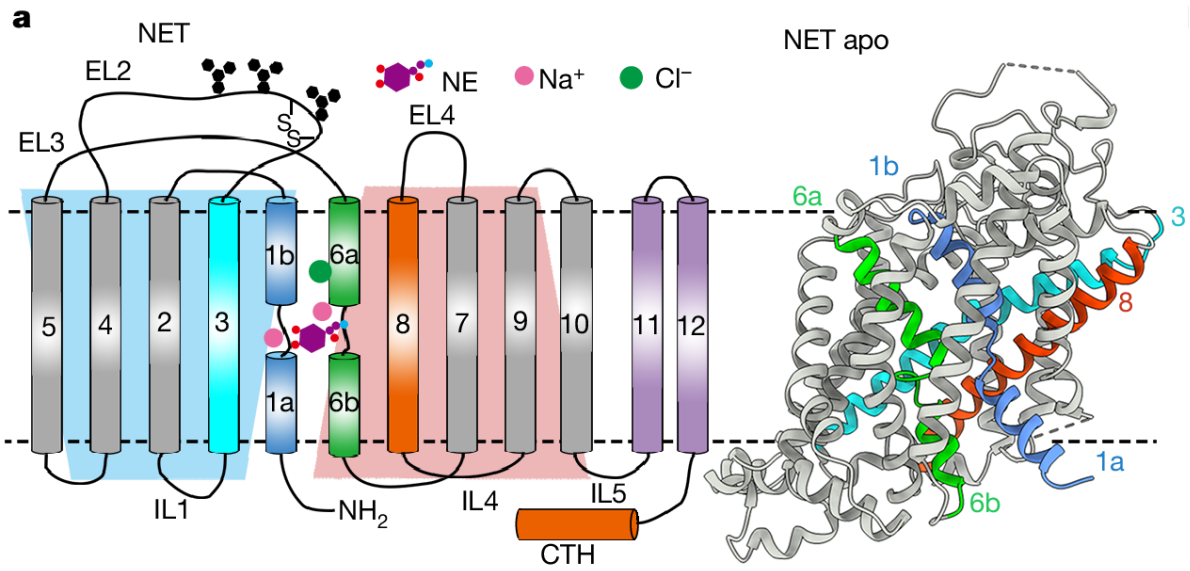

Figure 27: Structure of hNET.[91] The structure of hNET in its apo-state is presented. As previously known, hNET is a 7-transmembrane (7-TM) protein featuring multiple post-translational modifications. The protein displays a pseudo-twofold symmetry, formed by transmembrane helices 1–5 (TM1–5) and TM6–10. Within this structure, TM1, TM3, TM6, and TM8 create a cavity that serves as the primary substrate-binding pocket (S1) (EL, extracellular loop; IL, intracellular loop). Taken from Tan et al., 2024.

The approach taken by the research group was similar to ours, involving the generation of constructs with affinity tags, protein production in eukaryotic cells, and purification via affinity chromatography. The group generated the NET construct with an N-terminal FLAG-tag and used HEK293F cells for protein production. For plasmid amplification,

they used the same E. coli strain, DH5α, as we did. However, the main difference was that they used HEK293F cells, which are commonly employed for the expression of recombinant proteins, resulting in high yields of purified protein. This cell line is a variant of the human embryonic kidney 293 cell line, adapted for rapid cell growth, and is widely used in the production of viral vectors.[92] For cloning of the NET expression constructs, the human wild-type, full-length NET cDNA (UniProt ID: P23975) was used and cloned into the pCAG vector with an N-terminal FLAG-tag. The pCAG vector, containing the CAG promoter known for the stable expression for viral vectors.[92] For lysis of the cells, lysis buffer (20 mM Tris-HCl (pH 8.0), 150 mM NaCl or 150 mM KCl), was used. The cell membrane was solubilized at 4 °C for 2 h in lysis buffer containing 2% DDM and different protease inhibitors (aprotinin, pepstatin and leupeptin), followed by centrifugation at 20,000g at 4 °C for 1 h. The supernatant was loaded onto an anti-FLAG resin and the target protein purified by gravity flow. The elution fractions were pooled and purified by SEC.

Overall, the group's approach was similar to ours, but ultimately, the protein production in insect cells in this thesis was unsuccessful, or the yield was too low to be detectable. Since the expression worked in HEK cells, these cells may be a better host organism, as they are widely used for the expression of human proteins. However, insect cells are also a common choice for expressing human proteins. Another difference was that they used a FLAG-tag for protein purification. FLAG-tags are often more stable compared to His tags, making them a better choice for protein purification when low protein yield is anticipated.[93,94] Additionally, FLAG-tags are less likely to interfere with other proteins than His tags. It is known that many proteins other than the target protein are purified when using a His-tag. Therefore, the FLAG-tag may result in a purer purification. However, the His-tag remains widely used and is still the first choice for affinity chromatography due to its cost-effectiveness and reliability in purifying recombinant proteins.

4.8. Nanodiscs – as a platform to study molecular interactions

A part of this work involved the preparation of membrane mimetics (nanodiscs) and their use in interaction studies with respective binding partners. In the first approach, the interaction between DNAzymes and nanodiscs were analyzed using Microfluidic diffusional sizing (MDS). In the second approach, Nanodiscs were used to analyze whether an inhibitory compound (IC1), affects membrane binding of Glutathione peroxidase 4 (GPX4) using bio-layer interferometry (BLI). Figure 28 shows exemplary data for the used nanodiscs preparations.

DNAzymes are small molecules that perform their function inside the cell, suggesting the potential for interactions with the cell membrane. To explore possible interactions, nanodiscs, composed of model lipids, and MDS was used. In the setup the Fluidity One-M measures molecular size (hydrodynamic radius) of a sample by evaluating its diffusion in a microfluidic chamber.

The measurements were performed with the *Fluidity one-m* instrument by Fluidic analytics at room temperature by using a fluorescent labeled DNAzyme (DNAzyme Cy5') and two different types of nanodiscs.

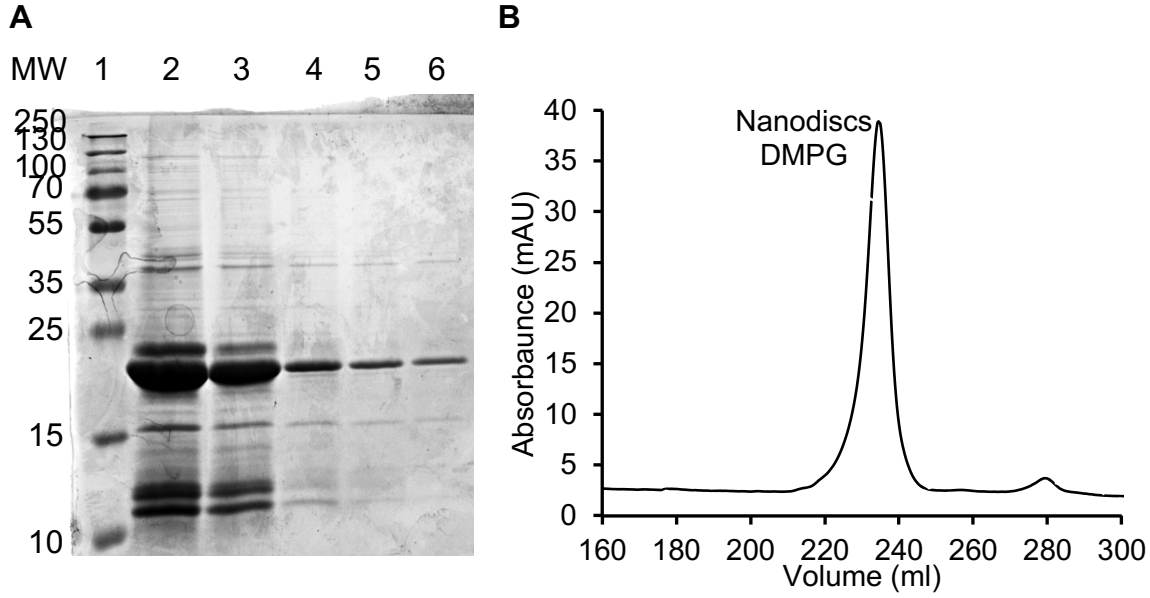

Figure 28: Nanodiscs preparation. (A) MSP1D1 purification. For nanodiscs assembly, MSP1D1 was purified beforehand using gravity flow and Ni-NTA agarose. The image shows the SDS-PAGE of the elution fractions (MSP1D1 23 kDa, band 2-6), collected during purification. 1: *PageRuler Plus Prestained*, 2-6: MSP1D1 elution fractions. **(B) Chromatogram of nanodiscs purification.** The assembled Nanodiscs, were purified by SEC. Plotted is the

absorbance in mAU against the retention volume in ml. The chromatogram of nanodiscs assembled with DMPG lipids is shown as an example.

The first step in nanodiscs preparation, was the recombinant protein production of the membrane scaffold protein MSP1D1. Results of the successful protein purification can be seen in Figure 28A. The scaffold protein has a molecular weight of 23 kDa and can be detected on the SDS gel (yellow arrow). Subsequently, nanodiscs were successful prepared and purified using SEC. The peak fractions were combined and the sample concentrated and further used for MDS and BLI measurements.

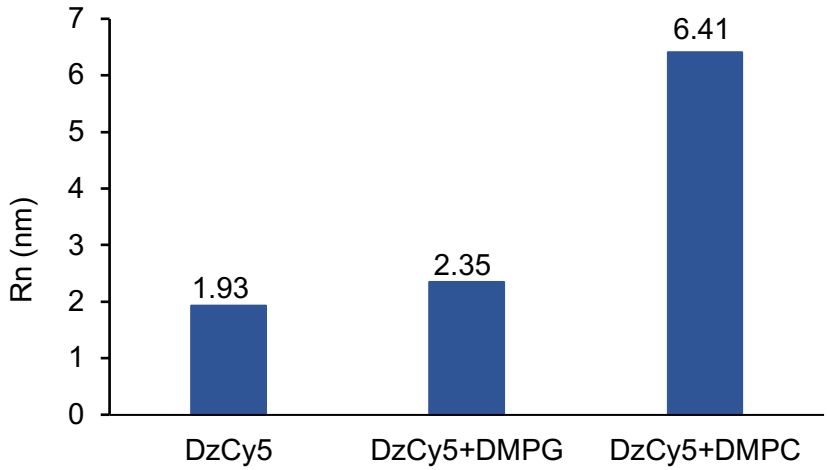

Figure 29: Results of nanodiscs DNAzyme interaction study. The Figure displays the results of the MDS measurement, showing the interaction study between DNAzymeCy5 and DMPG-Nanodiscs as well as DMPC-Nanodiscs. For these measurements, the Fluidity One-M from Fluidic Sciences Ltd was used. Rn (nm) represents the hydrodynamic radius.

For MDS measurements, Cy5-labeled DNAzymes were used and incubated for 30 minutes with the respective nanodiscs prior to use. The results show different hydrodynamic radius (Rn in nm) for the two types of lipid nanodiscs. The Rn value for the DzCy5+DMPC sample is 6.41 nm, while the hydrodynamic radius of the DzCy5+DMPG is 2.35 nm. This suggests that the DzCy5 and the DMPC nanodiscs interact more strongly, leading to a larger hydrodynamic radius. This result is consistent with expectations, as the phosphate backbone of the DNA is negatively charged, while DMPC nanodiscs are zwitterionic due to their phosphocholine headgroup, which does not carry a net charge. On the other hand, DMPG is negatively charged due to its phosphate group, which suggests that there would be no interaction with the negatively

charged DNAzyme. The data presents, for the first time, a potential interaction of DNAzymes with lipid bilayers.

In the next step, the prepared nanodiscs, composed of POPG lipids, were used in a study employing BLI. This experiment was conducted in collaboration with Dr. Carsten Berndt's group at the University Hospital in Düsseldorf. The study aimed to investigate the potential inhibition of GPX4 binding to a membrane by the inhibitory compound (IC1). The results are presented below in Figure 30.

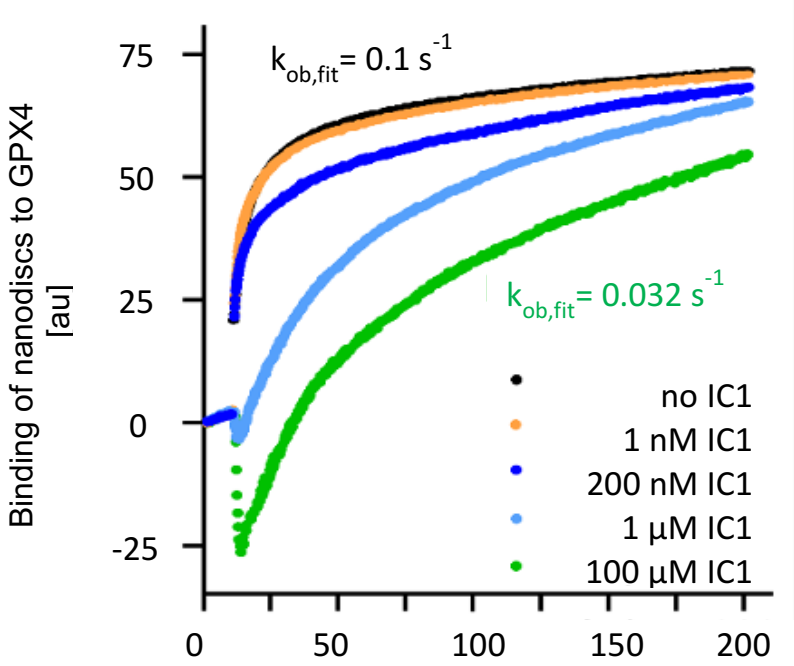

Figure 30: IC1 inhibits lipid binding of GPX4. Bio-Layer Interferometry (BLI) following association of nano discs loaded with negatively charged 1-Palmitoyl-2-oleoyl-sn-glycero-3-phosphoglycerol (POPG) to GPX4 in presence of indicated concentrations of IC1. The observed rates of GPX4-POPG interaction (kob) indicate no effects of the presence of ATM up to 1 nM and considerably slower binding at ATM concentrations of 1 µM and similarly at 100 µM.

As shown in Figure 30, 1 µM IC1 strongly reduces binding of GPX4 to negatively charged unsaturated lipids. While unspecific contributions of nanodiscs binding and/or changes induced by the presence of IC1 prevent deduction of exact association rates or binding affinities, the observed rate of GPX4-POPG interaction (kob) is considerably slower in presence of 1-100 µM IC1.

Overall, the produced nanodiscs were successfully used in both interaction studies, highlighting that nanodiscs are a promising tool for research with a wide range of applications.

5. Conclusion and Outlook

Membrane proteins (MP) are crucial for various vital biological processes, such as providing structural support, facilitating signal transduction, enabling cell-to-cell communication, supporting energy production and contributing to immune responses. MP research is of significant importance to the pharmaceutical industry, as a wide range of drugs target membrane proteins. Consequently, continuous improvement in this field is crucial for enhancing our understanding of diseases and paving the way for the development of new therapeutic drugs. Within membrane research, GPCRs are one of the main areas of focus. The melanocortin system, consisting of various ligands, accessory proteins, and GPCR receptors, offers an ideal model system for studying the interactions between these components and gaining insights into receptor function. This system serves as a perfect platform for applying diverse biophysical techniques for both structural and functional analysis.

Studying membrane proteins in vitro is particularly challenging because of their hydrophobic properties and instability when extracted from the lipid bilayer. To address these issues, specific techniques are necessary. Furthermore, producing these proteins in large quantities and ensuring sample purity is often a complex task. As a result, optimizing both protein production and purification is a key initial step toward enabling structural analysis.

The main achievements obtained in this work were:

- Recombinant protein production of MRAPs in *E. coli* and protein purification
- Cloning of MRAP mutants to further analyze the metal-binding characteristics of MRAP
- First successful production of MRAP2 in *Sf*9 cells
- Expression of hNET in *Sf*9 cells
- Application of nanodiscs to study membrane binding

This dissertation focuses on the recombinant protein production and characterization of the accessory proteins MRAP1 and MRAP2, with particular emphasis on the newly postulated metal-binding site by our group. Both MRAP1 and MRAP2 were successfully expressed in bacterial cells. The correct target protein sequence was

confirmed by sanger sequencing. Moreover, it was confirmed by Western blot analysis, that the purified protein is MRAP2.

The EAS of all MRAP proteins was characterized and the characteristic Fe spectrum was in alignment with results previously obtained by our group. Additionally, the obtained samples were analyzed using mass spectrometry (MS), and after comparison with the database, a sequence coverage of over 80% was obtained for MRAP2. To further assess the aspect that MRAP2 might be a metal-binding protein, mutants of MRAP were successfully cloned and purified and their EAS further analyzed. The MS data suggest that the characteristic Fe spectrum could originate from *E. coli* protein impurities.

Eukaryotic expression of membrane systems was established in this work. MRAP2 was recombinantly expressed in *Sf*9 cells taking advantage of the BVE. The bacmid preparation of MRAP2 was successful as well as the subsequent protein expression. MRAP2 showed a positive Western blot signal in the analyzed cell pellet sample. The protein was solubilized and purified via Step-Tag. The final results did not fully confirm the successful purification of MRAP2; however, its expression was achieved. Further optimization of the purification process is required, for example, by using different detergents such as n-Dodecyl-β-D-maltoside (DDM) for solubilization.

The BVE system was further utilized for the recombinant expression of hNET. The bacmid was prepared, and expression tests were conducted. However, the Western blot did not show a positive signal for the target protein. Ultimately, the structure and successful expression and purification of hNET was published by Tan et al., 2024. Therefore, further optimization of the expression was not attempted.

Moreover, nanodiscs were prepared and successfully used in membrane binding studies, demonstrating the versatile application of membrane mimetics. The first part presented an initial interaction study of DNAzymes with lipid bilayers. Showing, for the first time, that DNAzymes interact with zwitterionic phospholipids. The second part introduced a new inhibitory compound (IC1), which affected the membrane binding of Glutathione peroxidase 4 (GPX4), resulting in a slower binding rate of the protein to the lipid bilayer.

The outcome of this work provides a foundation for future advancements in membrane protein research and offers valuable insights into the challenges of recombinant protein production, purification, and biophysical characterization.

6. Supporting Material

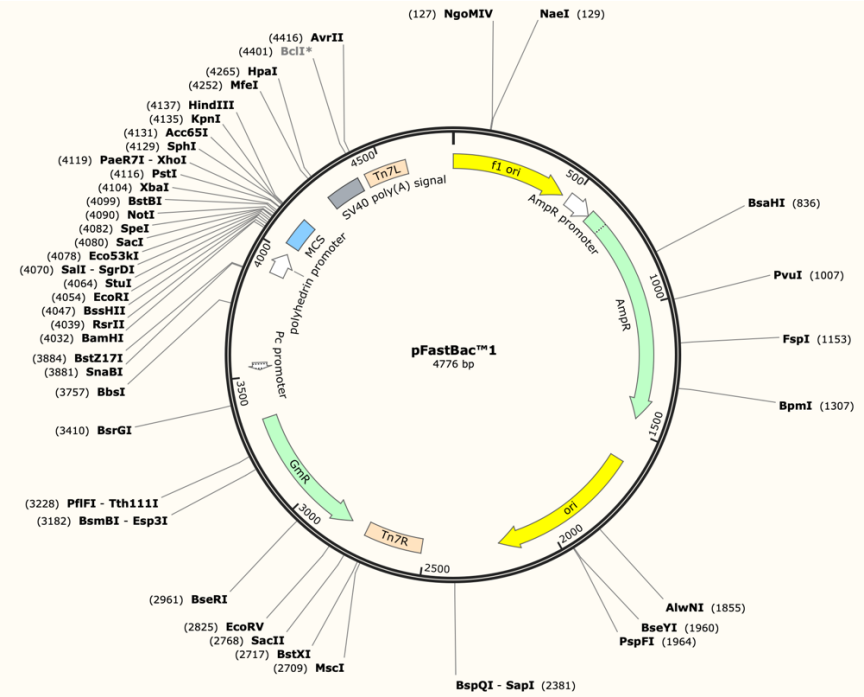

Figure 31: Vector map of pFASTBac1. Vector used for recombinant protein production of MRAP in *Sf*9 cells.

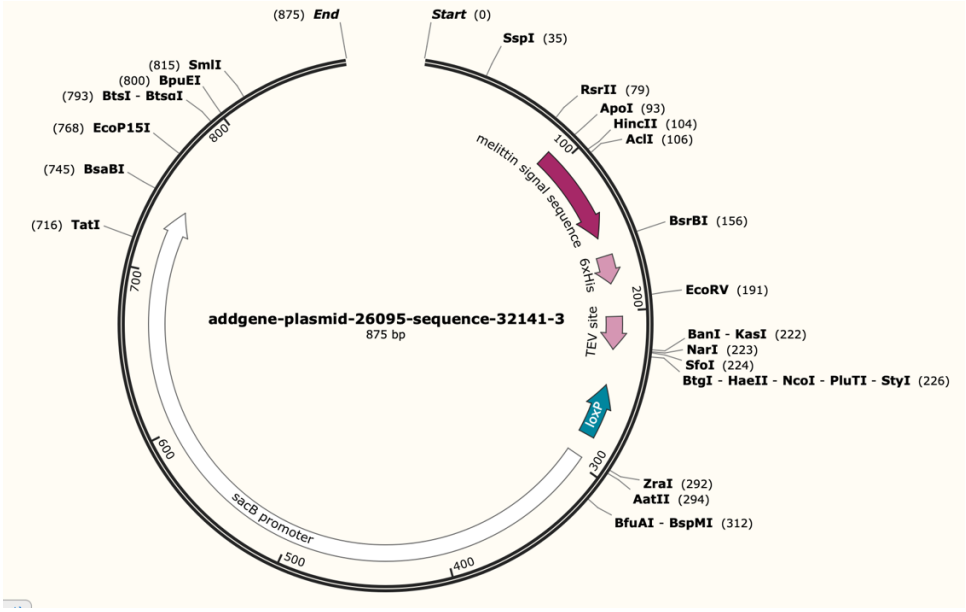

Figure 32: Vector map of pFHMSP-LIC-N. Vector used for recombinant protein production of hNET in *Sf*9 cells.

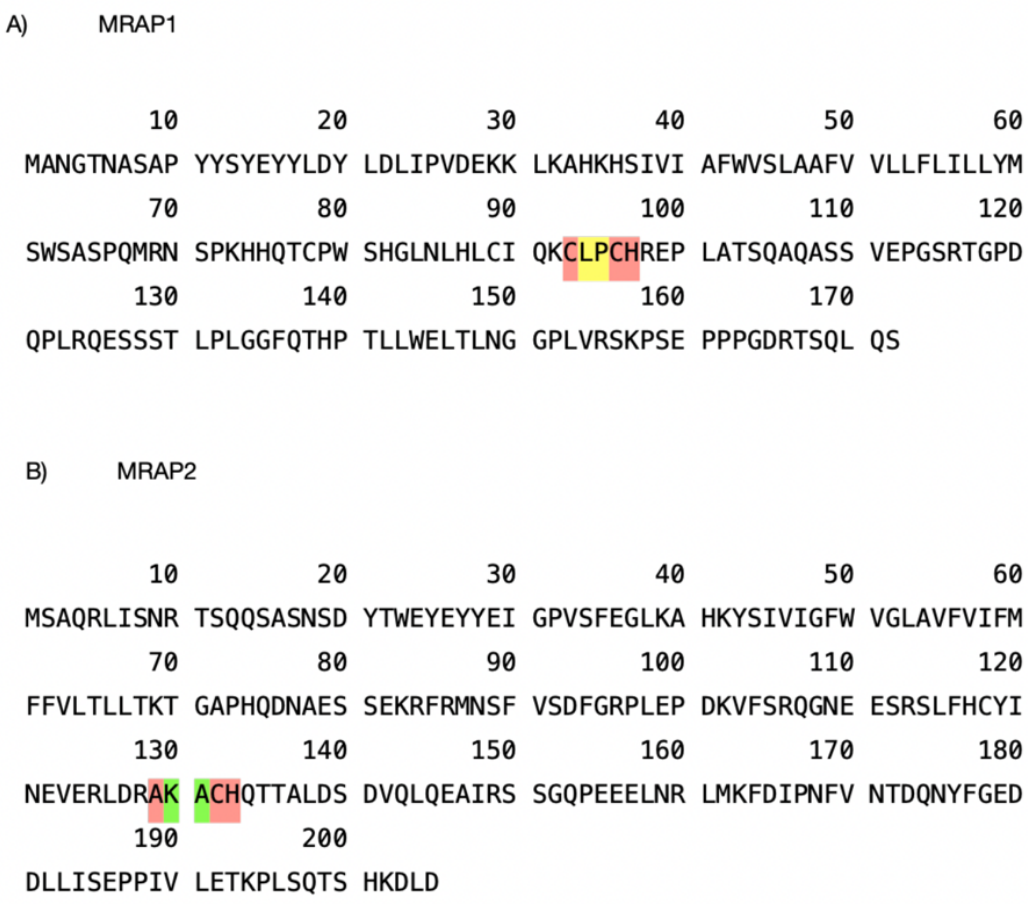

Figure 33: Predicted metal-binding site. (A) MRAP1 amino acid sequence (B) MRAP2 amino acid sequence. Taken from Escobedo et al., 2023.

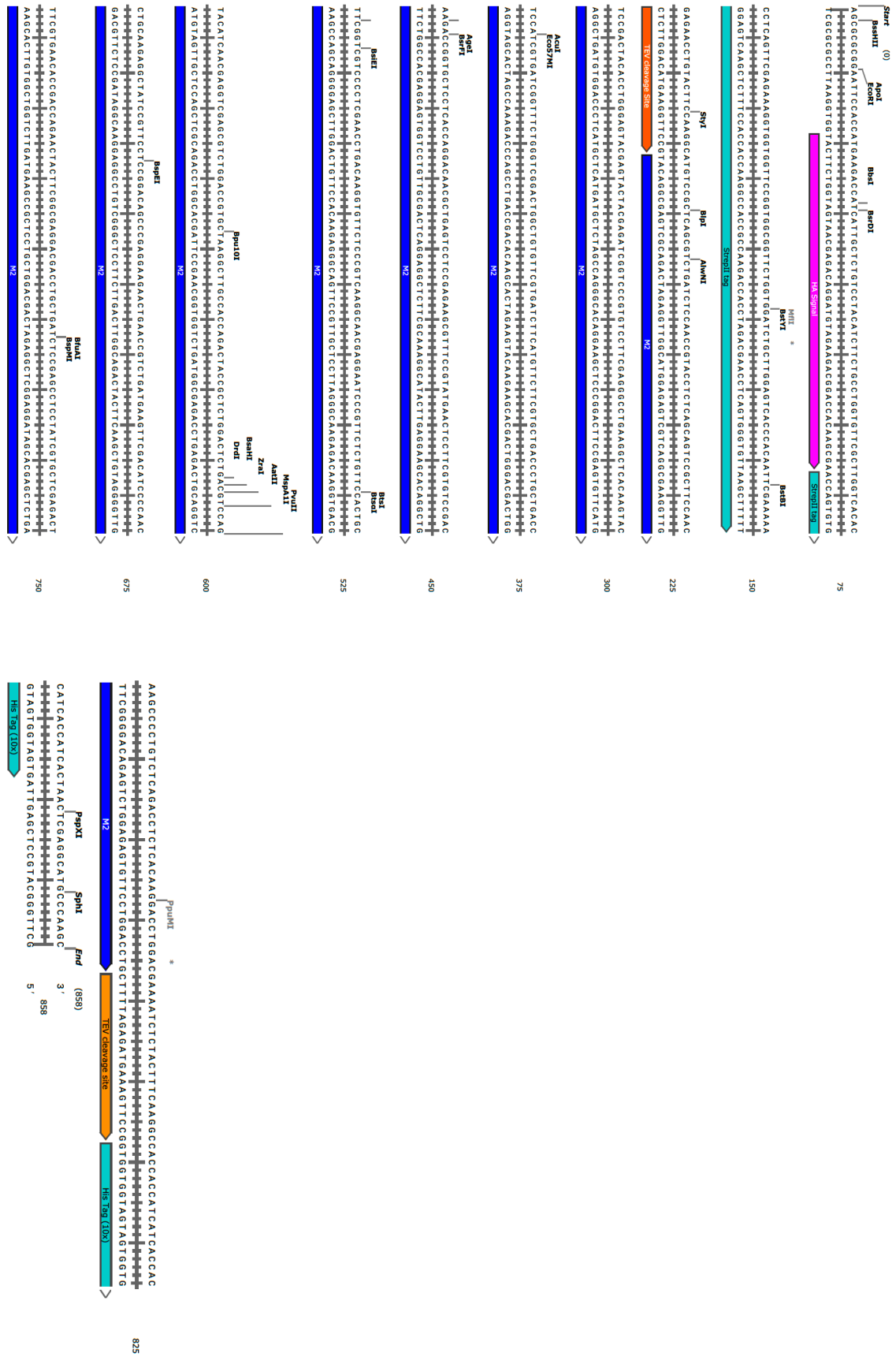

Figure 34: DNA Sequence of MRAP2 for *Sf*9 cell expression.

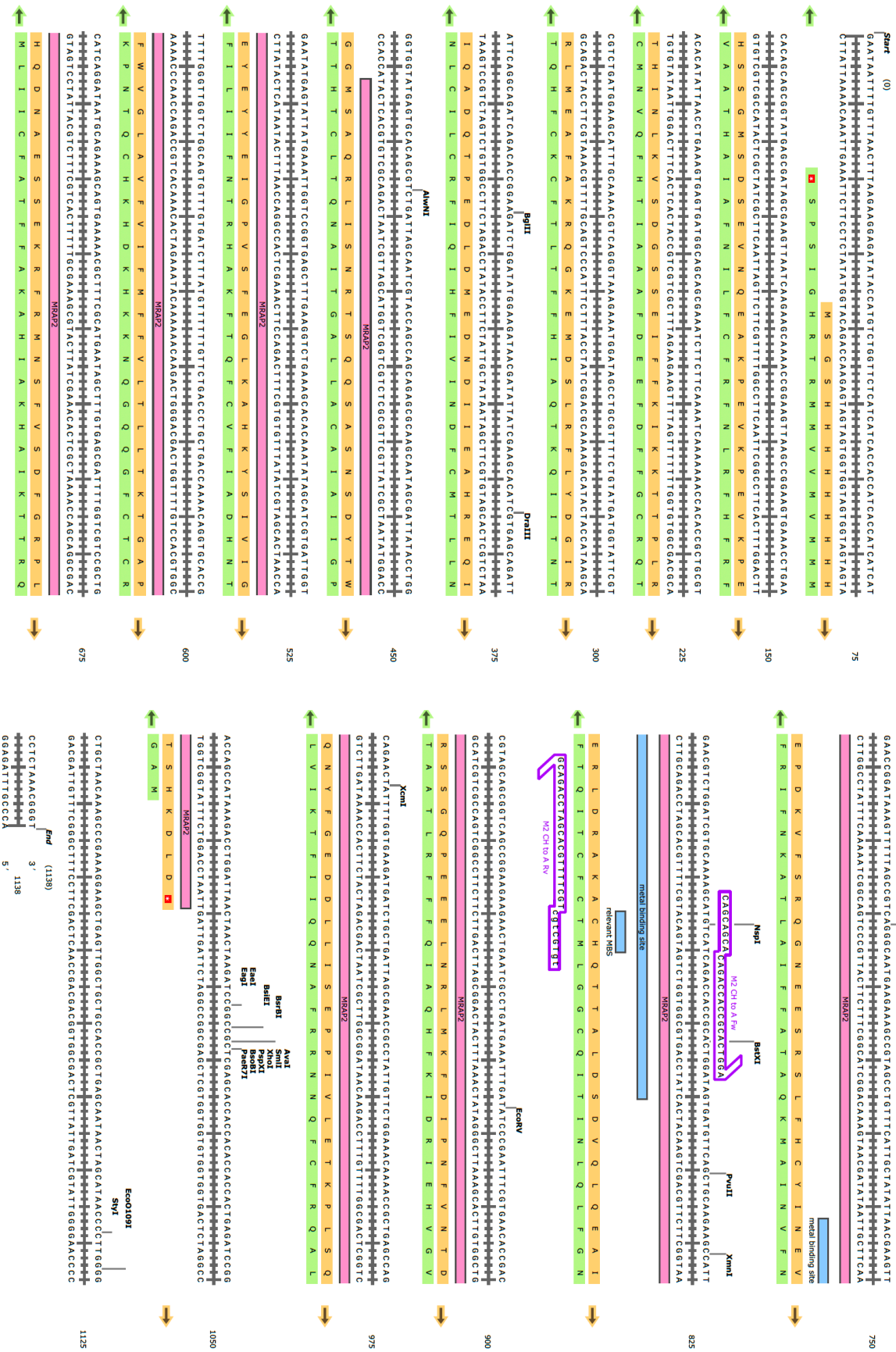

Figure 35: DNA Sequence of MRAP2_C132A_H133A.

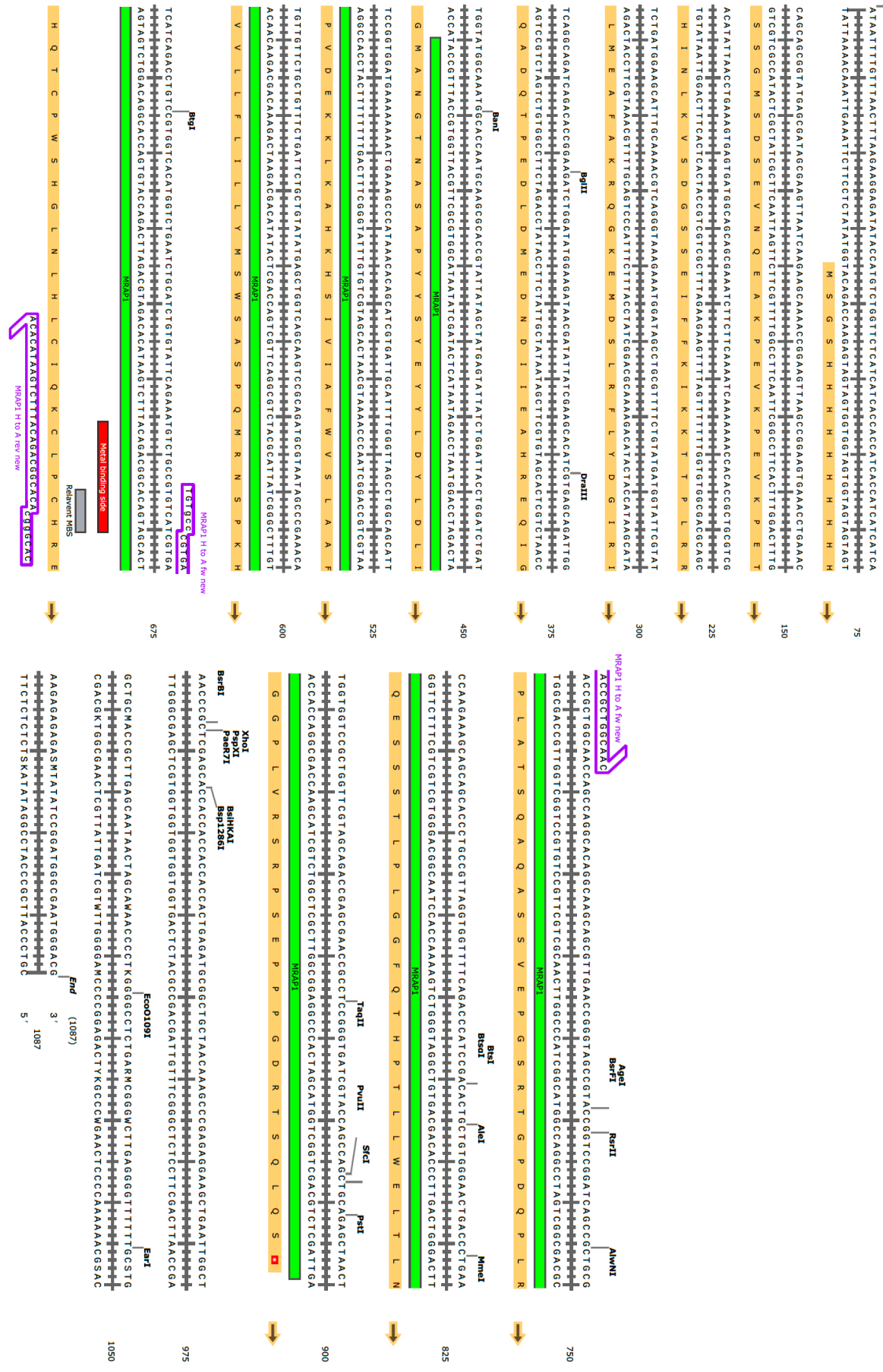

Figure 36: DNA Sequence of MRAP1_H97A.

7. References

[1] C. S. Gandhi, E. Y. Isacoff, *Trends Neurosci* **2005**, *28*, 472–479.
[2] S. Tan, H. T. Tan, M. C. M. Chung, *Proteomics* **2008**, *8*, 3924–3932.
[3] Y. Zhu, S. D. Yun, T. Zhang, J.-Y. Chang, L. Stover, A. Laganowsky, *Chem Sci* **2023**, *14*, 14243–14255.
[4] C. Kruse, *Ann. NY Acad. Sci.* **1982**, *386*, 499–501.
[5] E. de Jong, A. Kocer, *Membranes (Basel)* **2023**, *13*, 409.
[6] D. M. Boes, A. Godoy-Hernandez, D. G. G. McMillan, *Membranes (Basel)* **2021**, *11*, 346.
[7] Y. Lee, S. Basith, S. Choi, *J Med Chem* **2018**, *61*, 1–46.
[8] Q. Zhou, D. Yang, M. Wu, Y. Guo, W. Guo, L. Zhong, X. Cai, A. Dai, W. Jang, E. I. Shakhnovich, *Elife* **2019**, *8*, e50279.
[9] S. Basith, M. Cui, S. J. Y. Macalino, J. Park, N. A. B. Clavio, S. Kang, S. Choi, *Front Pharmacol* **2018**, *9*, 128.
[10] N. Liu, Y. Wang, T. Li, X. Feng, *Int J Mol Sci* **2021**, *22*, 5260.
[11] A. J. Venkatakrishnan, **2017**.
[12] W. I. Weis, B. K. Kobilka, *Annu Rev Biochem* **2018**, *87*, 897–919.
[13] S. Liu, P. J. Anderson, S. Rajagopal, R. J. Lefkowitz, H. A. Rockman, *Circ Res* **2024**, *135*, 174–197.
[14] L. Cheng, F. Xia, Z. Li, C. Shen, Z. Yang, H. Hou, S. Sun, Y. Feng, X. Yong, X. Tian, *Molecular Biomedicine* **2023**, *4*, 46.
[15] M. N. Davies, A. Secker, M. Halling-Brown, D. S. Moss, A. A. Freitas, J. Timmis, E. Clark, D. R. Flower, *BMC Res Notes* **2008**, *1*, 1–5.
[16] P. Sweeney, L. E. Gimenez, C. C. Hernandez, R. D. Cone, *Nat Rev Endocrinol* **2023**, *19*, 507–519.
[17] M. Ricart-Ortega, J. Font, A. Llebaria, *Mol Cell Endocrinol* **2019**, *488*, 36–51.
[18] S. Zorman, M. Botte, Q. Jiang, I. Collinson, C. Schaffitzel, *Curr Opin Struct Biol* **2015**, *32*, 123–130.
[19] I. G. Denisov, S. G. Sligar, *Chem Rev* **2017**, *117*, 4669–4713.
[20] T. H. Bayburt, S. G. Sligar, *Protein science* **2003**, *12*, 2476–2481.
[21] M. T. Marty, *Int J Mass Spectrom* **2020**, *458*, 116436.
[22] T. H. Bayburt, Y. V Grinkova, S. G. Sligar, *Nano Lett* **2002**, *2*, 853–856.
[23] T. H. Bayburt, S. G. Sligar, *FEBS Lett* **2010**, *584*, 1721–1727.
[24] G. S. H. Yeo, D. H. M. Chao, A.-M. Siegert, Z. M. Koerperich, M. D. Ericson, S. E. Simonds, C. M. Larson, S. Luquet, I. Clarke, S. Sharma, *Mol Metab* **2021**, *48*, 101206.
[25] A. G. Gravina, R. Pellegrino, T. Durante, G. Palladino, G. Imperio, G. D'Amico, M. C. Trotta, M. Dallio, M. Romeo, M. D'Amico, *Cells* **2023**, *12*, 1889.
[26] Y. Yang, *Eur J Pharmacol* **2011**, *660*, 125–130.
[27] D. D. Markov, O. V Dolotov, I. A. Grivennikov, *Int J Mol Sci* **2023**, *24*, 6664.
[28] R. D. Cone, *Endocr Rev* **2006**, *27*, 736–749.
[29] J. E. S. Wikberg, *Eur J Pharmacol* **1999**, *375*, 295–310.
[30] A. P. Ross, A. Ben-Zacharia, C. Harris, J. Smrtka, *Front Neurol* **2013**, *4*, 21.
[31] I. Gantz, T. M. Fong, *American Journal of Physiology-Endocrinology and Metabolism* **2003**, *284*, E468–E474.

[32] L. F. Chan, T. R. Webb, T.-T. Chung, E. Meimaridou, S. N. Cooray, L. Guasti, J. P. Chapple, M. Egertová, M. R. Elphick, M. E. Cheetham, *Proceedings of the National Academy of Sciences* **2009**, *106*, 6146–6151.
[33] A. E. Moscowitz, H. Asif, L. B. Lindenmaier, A. Calzadilla, C. Zhang, M. Mirsaeidi, *Front Med (Lausanne)* **2019**, *6*, 145.
[34] S. S. Negus, *Biochem Pharmacol* **2006**, *71*, 1663–1670.
[35] A. A. J. Rouault, D. K. Srinivasan, T. C. Yin, A. A. Lee, J. A. Sebag, *Biochimica et Biophysica Acta (BBA)-Molecular Basis of Disease* **2017**, *1863*, 2462–2467.
[36] M. Wang, X. Wang, B. Jiang, Y. Zhai, J. Zheng, L. Yang, X. Tai, Y. Li, S. Fu, J. Xu, *Clin Transl Med* **2022**, *12*, e1091.
[37] J. A. Sebag, P. M. Hinkle, *Proceedings of the National Academy of Sciences* **2007**, *104*, 20244–20249.
[38] S. Malik, T. M. Dolan, Z. J. Maben, P. M. Hinkle, *Journal of Biological Chemistry* **2015**, *290*, 27972–27985.
[39] N. N. A. Berruien, C. L. Smith, *Gene* **2020**, *757*, 144949.
[40] M. Asai, S. Ramachandrappa, M. Joachim, Y. Shen, R. Zhang, N. Nuthalapati, V. Ramanathan, D. E. Strochlic, P. Ferket, K. Linhart, *Science (1979)* **2013**, *341*, 275–278.
[41] R. Wei, D. Li, S. Jia, Y. Chen, J. Wang, *Adv Biol* **2023**, *7*, 2300035.
[42] V. Chen, A. E. Bruno, L. L. Britt, C. C. Hernandez, L. E. Gimenez, A. Peisley, R. D. Cone, G. L. Millhauser, *Journal of Biological Chemistry* **2020**, *295*, 16370–16379.
[43] A. Bernard, I. O. Naharros, F. Bourgain-Guglielmetti, J. Ciprin, X. Yue, S. Zhang, E. McDaid, M. Nachury, J. F. Reiter, C. Vaisse, *bioRxiv* **2020**, 2011–2020.
[44] W. Zhou, J.-D. Li, W.-P. Hu, M. Y. Cheng, Q.-Y. Zhou, *Regul Pept* **2012**, *179*, 84–90.
[45] A. L. Chaly, D. Srisai, E. E. Gardner, J. A. Sebag, *Elife* **2016**, *5*, e12397.
[46] I. Sohail, S.-A. Laurin, G. Kleinau, V. Chunilal, A. Morton, Z. C. U. Kagiali, J. A. Tello, M. J. Lohse, P. Scheerer, M. Bouvier, *bioRxiv* **2024**, 2024.
[47] T. Pacholczyk, R. D. Blakely, S. G. Amara, *Nature* **1991**, *350*, 350–354.
[48] C. Schroeder, J. Jordan, *American Journal of Physiology-Heart and Circulatory Physiology* **2012**, *303*, H1273–H1282.
[49] D. Luo, Y. Zhang, Y. Li, Z. Liu, H. Wu, W. Xue, *J Phys Chem B* **2024**, *128*, 8651–8661.
[50] H. Bönisch, F. Runkel, C. Roubert, B. Giros, M. Brüss, *J Auton Pharmacol* **1999**, *19*, 327–333.
[51] H. E. Melikian, S. Ramamoorthy, C. G. Tate, R. D. Blakely, *Mol Pharmacol* **1996**, *50*, 266–276.
[52] H. Bönisch, R. Hammermann, M. Brüss, in *Adv Pharmacol*, Elsevier, **1997**, pp. 183–186.
[53] P. Mandela, G. A. Ordway, *J Neurochem* **2006**, *97*, 310–333.
[54] R. D. Blakely, L. J. De Felice, H. C. Hartzell, *Journal of Experimental Biology* **1994**, *196*, 263–281.
[55] T. Pacholczyk, R. D. Blakely, S. G. Amara, *Nature* **1991**, *350*, 350–354.
[56] T. T. Nguyen, S. G. Amara, *J Neurochem* **1996**, *67*, 645–655.
[57] S. Apparsundaram, A. Galli, L. J. DeFelice, H. C. Hartzell, R. D. Blakely, *Journal of Pharmacology and Experimental Therapeutics* **1998**, *287*, 733–743.
[58] L. D. Jayanthi, D. J. Samuvel, S. Ramamoorthy, *Journal of Biological Chemistry* **2004**, *279*, 19315–19326.

[59] A. Kesidis, P. Depping, A. Lodé, A. Vaitsopoulou, R. M. Bill, A. D. Goddard, A. J. Rothnie, *Methods* **2020**, *180*, 3–18.
[60] G. F. X. Schertler, *Curr Opin Struct Biol* **1992**, *2*, 534–544.
[61] J. Kubicek, H. Block, B. Maertens, A. Spriestersbach, J. Labahn, in *Methods Enzymol*, Elsevier, **2014**, pp. 117–140.
[62] B. Miroux, J. E. Walker, *J Mol Biol* **1996**, *260*, 289–298.
[63] H. Tegel, S. Tourle, J. Ottosson, A. Persson, *Protein Expr Purif* **2010**, *69*, 159–167.
[64] D. Linke, in *Methods Enzymol*, Elsevier, **2014**, pp. 141–148.
[65] D. L. Jarvis, in *The Baculoviruses*, Springer, **1997**, pp. 389–431.
[66] T. A. Kost, J. P. Condreay, D. L. Jarvis, *Nat Biotechnol* **2005**, *23*, 567–575.
[67] R. S. Felberbaum, *Biotechnol J* **2015**, *10*, 702–714.
[68] T. P. Loisel, H. Ansanay, S. St-Onge, B. Gay, P. Boulanger, A. D. Strosberg, S. Marullo, M. Bouvier, *Nat Biotechnol* **1997**, *15*, 1300–1304.
[69] G. E. Smith, M. D. Summers, M. J. Fraser, *Mol Cell Biol* **1983**, *3*, 2156–2165.
[70] R. J. Clem, A. L. Passarelli, *PLoS Pathog* **2013**, *9*, e1003729.
[71] J. L. Vaughn, R. H. Goodwin, G. J. Tompkins, P. McCawley, *In Vitro* **1977**, *13*, 213–217.
[72] C. I. Murphy, H. Piwnica-Worms, *Curr Protoc Neurosci* **2000**, *10*, 4–18.
[73] D. S. Dimitrov, *Nat Rev Microbiol* **2004**, *2*, 109–122.
[74] T. A. Kost, C. W. Kemp, *Advanced technologies for protein complex production and characterization* **2016**, 187–197.
[75] V. A. Luckow, S. C. Lee, G. F. Barry, P. Olins, *J Virol* **1993**, *67*, 4566–4579.
[76] Z. Xie, Z. Zhang, Z. Cao, M. Chen, P. Li, W. Liu, H. Qin, X. Zhao, Y. Tao, Y. Chen, *Appl Microbiol Biotechnol* **2017**, *101*, 3811–3820.
[77] S. Sadeghi, N. Ahmadi, A. Esmaeili, F. Javadi-Zarnaghi, *RSC Adv* **2017**, *7*, 54835–54843.
[78] M. Hong, T. Li, W. Xue, S. Zhang, L. Cui, H. Wang, Y. Zhang, L. Zhou, Y. Gu, N. Xia, *Front Bioeng Biotechnol* **2022**, *10*, 994743.
[79] C. Ono, T. Okamoto, T. Abe, Y. Matsuura, *Viruses* **2018**, *10*, 510.
[80] A. Jungbauer, R. Hahn, in *Methods Enzymol*, **2009**.
[81] S. N. Cooray, A. J. L. Clark, *Mol Cell Endocrinol* **2011**, *331*, 215–221.
[82] S. Ramachandrappa, R. J. Gorrigan, A. J. L. Clark, L. F. Chan, *Front Endocrinol (Lausanne)* **2013**, *4*, 9.
[83] A. A. J. Rouault, D. K. Srinivasan, T. C. Yin, A. A. Lee, J. A. Sebag, *Biochim Biophys Acta Mol Basis Dis* **2017**, *1863*, 2462–2467.
[84] L. Schonnop, G. Kleinau, N. Herrfurth, A. Volckmar, C. Cetindag, A. Müller, T. Peters, S. Herpertz, J. Antel, J. Hebebrand, *Obesity* **2016**, *24*, 1976–1982.
[85] C. L. Bianco, C. S. Schneider, M. Santonicola, A. M. Lenhoff, E. W. Kaler, *Ind Eng Chem Res* **2011**, *50*, 85–96.
[86] A. Soloaga, J. M. Ramírez, F. M. Goñi, *Biochemistry* **1998**, *37*, 6387–6393.
[87] S. Soulié, L. Denoroy, J.-P. Le Caer, N. Hamasaki, J. D. Groves, M. le Maire, *The journal of biochemistry* **1998**, *124*, 417–420.
[88] U. Consortium, *Nucleic Acids Res* **2015**, *43*, D204–D212.
[89] A. Passerini, M. Punta, A. Ceroni, B. Rost, P. Frasconi, *Proteins: Structure, Function, and Bioinformatics* **2006**, *65*, 305–316.
[90] S. N. Beljelarskaya, *Mol Biol* **2011**, *45*, 123–138.

[91] J. Tan, Y. Xiao, F. Kong, X. Zhang, H. Xu, A. Zhu, Y. Liu, J. Lei, B. Tian, Y. Yuan, *Nature* **2024**, *632*, 921–929.
[92] G. P. Subedi, R. W. Johnson, H. A. Moniz, K. W. Moremen, A. Barb, *J Vis Exp* **2015**, 53568.
[93] A. Einhauer, A. Jungbauer, *J Biochem Biophys Methods* **2001**, *49*, 455–465.
[94] K. Pajęcka, C. W. Nielsen, A. Hauge, I. Zaganas, L. K. Bak, A. Schousboe, A. Plaitakis, H. S. Waagepetersen, *Neurochem Res* **2014**, *39*, 487–499.